



FRAGILITY CURVES FOR DIKES IN THE WESTERN SCHELDT

ASSESSING THE APPLICABILITY OF TYPOLOGY-BASED FRAGILITY CURVES IN ASSESSING DIKE REINFORCEMENT COST FOR COASTAL DIKES

MSc THESIS

J.M. VAN WOUDEBERG

Fragility Curves for Dikes in the Western Scheldt

Assessing the Applicability of Typology-Based Fragility Curves in Assessing Dike Reinforcement Cost for Coastal Dikes

by

J.M. van Woudenberg

to obtain the degree of Master of Science

at the Delft University of Technology,

to be defended publicly on Friday July 7, 2023 at 15:00 PM.

Thesis committee:	Prof. dr. ir. M. Kok,	TU Delft
	Dr. ir. C. Mai Van,	TU Delft
	Dr. ir. M. M. Rutten,	TU Delft
	Ir. M. L. Drost,	Witteveen+Bos
	Ir. D. G. Fiolet,	Witteveen+Bos

An electronic version of this thesis is available at <http://repository.tudelft.nl/>.

Preface

Before you lies the master thesis "Fragility curves in the Western Scheldt: assessing the applicability of typology-defined fragility curves in assessing dike reinforcement cost for coastal dikes". It has been written to achieve the Master of Science degree in Hydraulic Engineering at the Faculty of Civil Engineering and Geosciences of the Delft University of Technology. This research was carried out in cooperation with Witteveen+Bos.

First and foremost, I express my gratitude to Margot Drost and Daniel Fiolet, who welcomed me to Witteveen+Bos and guided me through the project with their knowledge and kindness. Without your expertise, weekly meetings with feedback and tips, I would not have been able to conduct this research.

I would like to express my gratitude towards Prof. Dr. Ir. Matthijs Kok for his positivity, guidance and feedback during the committee meetings as chairman of the thesis committee. Furthermore, I like to thank Dr. ir. Cong Mai Van for his kindness, advice and valuable knowledge on probabilistic-, risk based design approach of coastal flood defences. Also, I would like to thank Dr. ir. Martine Rutten for the valuable feedback she offered, particularly on the structuring of the thesis.

In addition, I would like to thank water board Scheldestromen, and especially Samantha van Schaick, for providing the necessary data and answering my questions. Also, I would like to thank Witteveen+Bos and all its colleagues for their interest, input and ideas on this research, making this graduation internship an enjoyable journey.

Furthermore, I would like to thank my family for supporting me all the way and providing all these amazing opportunities. Besides my girlfriend, who encouraged me and helped me throughout the process, I am especially grateful to my roommates for making my study time memorable.

*J.M. van Woudenberg
Delft, July 2023*

Summary

The sea level is rising, possibly by one meter, by the end of this century. The Netherlands is preparing for this scenario through Kennisprogramma Zeespiegelstijging (KP-ZSS). One of the goals is to determine the hydraulic effects of sea level rise (SLR) on the current system. For the flood risk analysis within KP-ZSS, the current strength of the flood defences needs to be described. A set of typology-defined fragility curves based on river dikes in river areas describes the current strength of all the primary flood defences in the Netherlands. However, it is unknown if these fragility curves are applicable to sea dikes due to shorter high water and differences in soil parameters in sea/tidal areas. The research described in this thesis aims to evaluate if site-specific fragility curves for sea dikes result in significantly different predictions of future reinforcement cost for sea dikes compared to the typology-defined fragility curves. The analysis is centred around three dike sections in trajectories 29-3, 30-3 and 32-4 in the Western Scheldt. Initially, an evaluation is conducted on the fragility curves related to the geotechnical failure mechanisms of macro-instability and backward erosion piping. Subsequently, the height requirement is taken into account during the cost calculation.

The typology-defined fragility curves underestimate the strength of macro-stability in two out of three cases with a factor 10^4 and factor 10^2 , while underestimating it for one section with a factor 10^5 . For the piping failure mechanism the typology-defined fragility curves overestimate the strength in two out of the three cases with a factor 10^3 and factor 10^2 , but underestimates it for one section with a factor 10^3 . The pre-overburden pressure appeared to be the most important factor influencing the failure probability of the macro-stability failure mechanism, with higher occurring values for the sections in the Western Scheldt. The failure mechanism of piping was influenced most by the hydraulic conductivity, where the encountered soil in the Western Scheldt consisted of finer soils with lower hydraulic conductivity.

From the results, it can be concluded that the use of site-specific fragility curves resulted in a decrease of 13% in net present value, averaging over all SLR scenarios for an analysis until 2200. Considering the most probable SLR scenario resulted in a 12% decrease. If the height requirement is included in the cost calculation, the use of site-specific fragility curves results in a 7% decrease in net present value on average and a 12% decrease for SLR scenario low. For the low SLR scenario, the cost of relocating the road infrastructure in and around the expansion zone of the dike is dominant. With increasing SLR scenarios, the increase in crest height becomes the most important factor, with the revetment the dominating factor cost-wise, leading to minimal differences in reinforcement cost between the fragility curve approaches.

Contents

1	Introduction	1
1.1	Motivation	1
1.2	Problem definition	2
1.3	Study objective	2
2	Literature	4
2.1	Flood safety standards	4
2.2	Reliability analysis for failure mechanisms	4
2.2.1	Failure probability	4
2.2.2	Reliability method and influence coefficients	6
2.3	Concept of fragility curves	7
2.4	Considered failure mechanisms	8
2.4.1	Failure process of macro-instability	8
2.4.2	Failure process of backward erosion piping	9
2.5	Differences between sea dikes and river dikes	10
2.5.1	Hydraulic loads	10
2.5.2	General dike dimensions	11
2.5.3	Subsoil	11
2.6	Methodology Kennisprogramma Zeespiegelstijging	12
2.6.1	Typologies and fragility curves macro-stability	13
2.6.2	Typologies and fragility curves piping	14
3	Framework for developing the fragility curves and estimating cost	15
3.1	Western Scheldt study area	15
3.2	Constructing fragility curves	16
3.3	Modelling approach macro-stability	17
3.3.1	Fragility points	17
3.3.2	Schematization pore water pressures	17
3.3.3	Shear strength models	18
3.3.4	Limit equilibrium model	20
3.4	Modelling approach piping	21
3.5	Hydraulic loads	23
3.6	Cost calculation with OKADER	26
4	Fragility curves in the Western Scheldt	29
4.1	Fragility curves for macro-stability	29
4.2	Factors of influence macro-stability	31
4.2.1	Influence coefficients	31
4.2.2	Comparison river dike sections	32
4.3	Fragility curves for piping	33
4.4	Factors of influence piping	35
4.4.1	Influence coefficients	35
4.4.2	Comparison river dike sections	36
5	Results cost calculation	38
5.1	Cost of reinforcement	38
5.1.1	Cost comparison	39
5.1.2	Present value	40
5.2	Inclusion height requirement	40
5.2.1	Cost comparison	41

5.2.2 Present value	42
5.3 Cost analysis	43
5.3.1 Strength increase in OKADER	43
5.3.2 Factors determining reinforcement cost	44
6 Discussion	50
7 Conclusion and recommendations	52
7.1 Conclusion	52
7.2 Recommendations	53
A Importance factors FORM method	57
B Uplift and strength reduction	58
C Design cycle for calculating reinforcement cost	60
D Water level frequency lines and HBN	64
E Applied input variables	66
E.1 Macro-stability	66
E.1.1 Schematization cross-sections.	66
E.1.2 Soil parameters for macro-stability	68
E.1.3 POP-value	69
E.2 Backward erosion piping	69
E.2.1 DP745.	70
E.2.2 DP399.	70
E.2.3 DP167.	71
F Additional results reliability analysis	72
F.1 Macro-stability	72
F.2 Backward erosion piping	73
G Phreatic line	74
H Additional OKADER results	76
H.1 Reinforcements	76
H.2 Discount rate	93
H.3 Time step	94

Nomenclature

List of Abbreviations

CDF	Cumulative distribution function
CoV	Coefficient of variation
DP	Dike pole
FORM	First Order Reliability Method
FoS	Factor of safety
IPCC	Intergovernmental Panel on Climate Change
KNMI	Koninklijk Nederlands Meteorologisch Instituut
KP-ZSS	Kennisprogramma Zeespiegelstijging
NAP	Normaal Amsterdams Peil (reference level)
NPV	Net present value
PDF	Probability density function
POP	Pre-overburden pressure
SLR	Sea level rise
WBI	Wettelijk beoordelings instrumentarium

List of Symbols

α	Influence coefficient
β	Reliability index
η	Drag factor coefficient
γ_{sat}	Saturated volumetric weight soil
γ_{sub}	Volumetric weight sand submerged
γ_w	Volumetric weight water

λ	Damping factor
μ	Mean of a probability distribution
ν	Kinematic viscosity
Φ	Cumulative distribution function of the standard normal distribution
ϕ	Friction angle
σ	Standard deviation of a probability distribution
θ	Bedding angle
D	Thickness of the aquifer
d	Thickness blanket
d_{70m}	Reference value for d70 in revised Sellmeijer model
d_{70}	70th -percentile of the grain size distribution
h	Water level
h_p	Hinterland phreatic level
$i_{c,h}$	Critical heave gradient
k	Hydraulic conductivity aquifer
kD	Transmissivity
L	Seepage length
m	Strength increase exponent
m_p	Model factor Sellmeijer
m_u	Model factor uplift
P_f	Probability of failure
S	Shear strength ratio

Introduction

1.1. Motivation

The Intergovernmental Panel on Climate Change (IPCC) 2021 report shows that the global mean sea level increased by 0.20 m between 1901 and 2018 (IPCC, 2021). The Koninklijk Nederlands Meteorologisch Instituut (KNMI) has released an interpretation of the report with implications for the Netherlands. Based on different climate scenarios for the years 2050 and 2100, the sea level rise and the rate of sea level rise have been predicted. This report states that the sea level will rise 30 cm by 2100 in the most favourable case. However, this will be two meters in the most unfavourable situation (KNMI, 2021a).

For flood defences, the most relevant loads are water levels and waves. When designing or evaluating a flood defence system, various methods are available to assess its safety. One of the key factors that these methods often consider is the concept of risk. Risk is typically defined as the chance of an undesirable event occurring and its potential impact. The probability of failure, potential consequences, and the associated costs and benefits of risk-reducing measures are necessary to address risk effectively (Vergouwe, 2014). The safety of flood defences is given by the probability of failure (P_f), which denotes the likelihood that the load is greater than the resistance and is expressed in units of time. In the Netherlands, a flood defence is considered safe if the failure probability is smaller than the legal safety standards.

Within the Delta programme, the effect of sea level rise until 2050 is considered for assessing dike safety. However, there is still a great deal of uncertainty in these predictions. Questions about flood protection, freshwater availability and land use arise. To reduce some of these uncertainties, Kennisprogramma Zeespiegelstijging (KP-ZSS)¹ has been initiated. Under this programme, government authorities, research institutes, businesses, planners, and NGOs are pursuing new expertise on the potential rise in sea level (Ministerie van Infrastructuur en Waterstaat, 2021). The programme consists of five research lines, each exploring signalling methods, long-term solutions and the expected sea level rise. Research line II investigates which measures effectively strengthen the current Delta Programme strategies. This analysis tries to gain insight into the effects of different magnitudes of sea level rise on the primary flood defences in the Netherlands after 2050. The analysis is based on climate-independent scenarios, with sea level rise of 0.5, 1, 2, 3, and 5 meters combined with land subsidence and increased river discharge (Rijkswaterstaat, 2022).

An increase in sea level directly influences the hydraulic loads acting on the flood defences since water levels and wave heights increase. Due to the higher loads, reinforcements of the flood defences are needed to comply with the maximum allowable probability of flooding. The effect of the changing hydraulic loads on the design, use of land and cost are assessed within research line II. Also, the impact on flood risk and probability of flooding is reevaluated. For the water safety system analysis within KP-ZSS, the current strength of the flood defences should be described. Since the knowledge programme is a policy study, assumptions and uncertainties must be dealt with. This report will look at a different approach to describe the current strength of the primary flood defences in the Netherlands and tries to gain insight into the most dominant factors determining dike reinforcement cost under sea level rise.

¹English: *the Knowledge Programme on Sea Level Rise*

1.2. Problem definition

As mentioned in Section 2.6, Kennisprogramma Zeespiegelstijging (KP-ZSS) is a policy study and due to the high level of abstraction, many simplifications are necessary. A set of typology-defined fragility curves for the failure mechanisms macro-stability and piping have been drawn up, describing the strength (resistance) of the majority of the Dutch primary flood defence system. Fragility curves have been set up for the river region (Kolen et al., 2021) and have been used to compose this nationwide set of fragility curves. In KP-ZSS, these curves are used to calculate the cost of future flood defence reinforcement.



Figure 1.1: Trajectories in the river area (green) and trajectories sea/tidal areas (black) (Fiolet et al., 2022)

One of the primary concerns is in the understanding of the potential alteration of fragility curves when applying them to dike sections in sea/tidal areas, as they were originally derived for river areas in the Netherlands. It is not verified whether the typology-defined curves are suitable for these locations. Soil parameters used in assessing geotechnical mechanisms like piping differ in tidal areas compared to riverine areas. It is unknown what the effect of typology-defined fragility curves is on estimating the failure probability of dike sections in sea/tidal areas and, consequently, the approximation of dike reinforcement cost.

1.3. Study objective

The study objective is to investigate, analyze, and provide insights into the problem of assessing flood defence systems for future reinforcements, with a specific focus on tidal areas, within the framework of the KP-ZSS. This research addresses uncertainties, assumptions related to fragility curves and the impact of various parameters. Doing so, it aims to understand the reliability of flood defences in sea/tidal areas better, helping to make better-informed decisions on future flood defence investments.

Probabilistic calculations for dike sections in the Western Scheldt will be performed to assess the influence of different failure mechanisms and their corresponding parameters. Three sections are considered to get a representative picture of the research area. The research aim is formulated as follows:

"Does the use of site-specific fragility curves result in a significantly different assessment of future reinforcement cost for sea dikes compared to typology-defined fragility curves in the Western Scheldt?"

To reach this objective, the following sub-questions will be addressed:

- How do site-specific fragility curves for dikes in the Western Scheldt differ from the assigned typology-defined fragility curves?

- Which strength and load variables significantly influence the failure probability of a dike section in the Western Scheldt?
- What are the dominant factors in predicting future dike reinforcement cost under sea level rise?

While the Kennisprogramma Zeespiegelstijging (KP-ZSS) considers three failure mechanisms: macro-stability, piping, and wave overtopping/overflow, this research focuses on macro-stability and piping. It should be noted that the impact of choices regarding overtopping/overflow is considered out of the scope of this research. Since the load statistics have been derived more specifically for different locations in the Netherlands and are therefore considered representative, the load statistics from KP-ZSS will be adopted in this research.

2

Literature

Understanding this research's key concepts is necessary to develop well-defined and relevant research objectives. To create clear and appropriate research goals, one must first understand the fundamental principles that form the core of the research topic. This chapter provides an overview of the basic concepts essential for formulating the research objectives. The Dutch flood risk assessment is briefly explained first. Second, reliability analysis for failure mechanisms is elaborated on. Next, the concept of fragility curves is described, followed by an introduction to the relevant failure mechanisms. Finally, the concept of typology-defined fragility curves used in Kennisprogramma Zeespiegelstijging (KP-ZSS) is introduced.

2.1. Flood safety standards

Approximately 59% of the land surface in the Netherlands is susceptible to flooding, with 26% of it situated below sea level (see Figure 2.1). Floods are considered one of the most severe disasters that can impact the country, leading to significant consequences. Floods in the densely populated country can cause many thousands of casualties and hundreds of thousands more would be affected in some way (PBL, 2023).

Since 2017, new safety standards for flood protection have been implemented to help protect the Netherlands. These standards are defined as the maximum allowable probability of flooding due to a dike segment failing. The new standards are derived based on potential damage, total protection costs, and individual- and group risk. The standards guarantee that the probability of a person passing away due to flooding is less than 10^{-5} per year. Also, potentially large economic damages and infrastructure were considered (Kok et al., 2017). The resulting norms per dike trajectory can be seen in Figure 2.2.

Any dike section, dune or hydraulic structure can fail due to different failure mechanisms. The probability of flooding equals the probability that at least one of these mechanisms occurs. The extent to which a dike section conforms to the standard can be determined by calculating the probability of flooding at that section and comparing it to the standard.

Different assessment types exist in the WBI2017, to check if a dike section complies with the standards; simple, detailed and custom assessment. Within the detailed assessment, the distinction is made between probabilistic and semi-probabilistic assessments. The following section provides an introduction to how failure probabilities can be calculated using a probabilistic method.

2.2. Reliability analysis for failure mechanisms

2.2.1. Failure probability

The failure probability is defined in general as the probability that the solicitation (the load) S exceeds the resistance (the strength) R . This can be expressed in the reliability function Z , also known as the limit state function:

$$Z = R - S \quad (2.1)$$

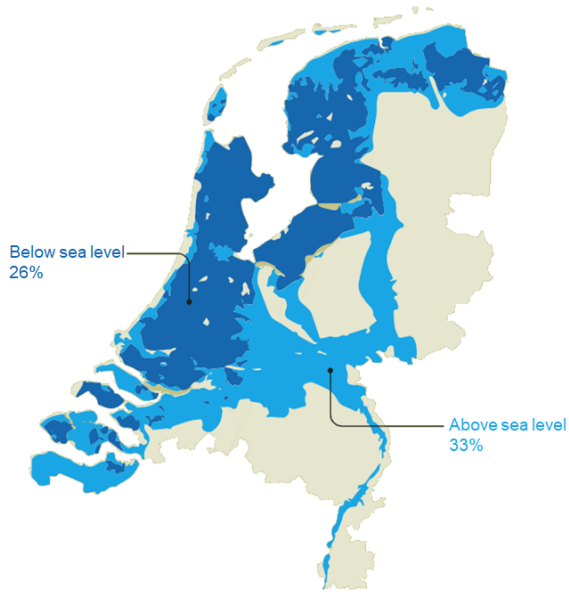


Figure 2.1: Flood-prone areas in the Netherlands (PBL, 2023)



Figure 2.2: Safety standards per dike trajectory in the Netherlands (Informatiehuis Water, 2022)

Positive values of Z correspond to non-failure and negative values to failure. Hence, the probability of failure is denoted as $P\{Z < 0\}$.

$$P_f = P(R < S) = P(Z < 0) \tag{2.2}$$

If the limit state function contains more than one solicitation and resistance variable, the failure probability is defined as the limit state function $Z(\mathbf{X})$ being less than zero. In this function, \mathbf{X} denotes the vector of all stochastic variables and $f_{\mathbf{X}}(\mathbf{x})$ the joint probability density function:

$$P(Z(\mathbf{X}) < 0) = \int_{Z(\mathbf{X}) < 0} f_{\mathbf{X}}(\mathbf{x}) d\mathbf{x} \tag{2.3}$$

The failure probability is determined by all stochastic variables in the failure domain (defined as $Z(\mathbf{X}) < 0$), or stated otherwise, the probability of all parameter combinations leading to failure. An illustration of the failure domain can be seen in Figure 2.4.

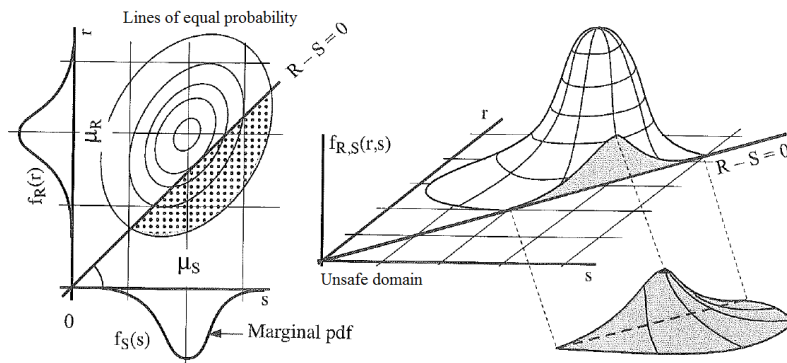


Figure 2.3: Joint probability density solicitation and resistance (Jonkman et al., 2018)

2.2.2. Reliability method and influence coefficients

Several different reliability methods can be used to compute the probability of failure of a structure. Each method has its strengths and limitations and the choice of method depends on the specific application and the level of accuracy required. In this research, a so-called level II method is applied, which is based on the approximation that all variables are normally distributed. The parameters are modelled by the mean values and the standard deviations. This means that the joint probability density is simplified. The limit state function is linearized, typically using a method known as the First Order Reliability Method (FORM), which simplifies the joint probability density function and reduces the computational effort.

FORM is a widely used reliability analysis method for assessing the probability of failure of a structure. As aforementioned, the FORM method is based on the assumption that the limit state function, which defines the boundary between the safe and failure regions in the space of the input variables, can be approximated by a linear function around a design point (see Figure 2.4). The design point is chosen to minimise the probability of failure. The linear approximation is obtained by taking the first-order Taylor series expansion of the limit state function (Jonkman et al., 2018).

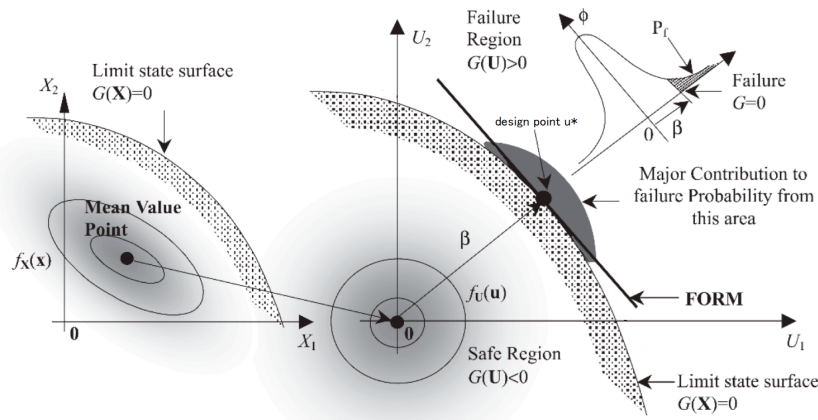


Figure 2.4: First Order Reliability Method (Mahmood et al., 2022)

The reliability index is the shortest distance between the design point and the limit state function. This index is often denoted by β , and the probability of failure can be calculated from the standard normal distribution as the complement of the reliability index.

$$P_f = 1 - \Phi(\beta) \quad (2.4)$$

where:

Φ = the cumulative distribution function of the standard normal distribution

Knowing that the design point is the combination of parameters having the highest probability density for $Z = 0$, the linearized and normalized limit state function that results from the FORM analysis can be written as:

$$Z = \beta - \sum_{i=1}^n \alpha_i u_i \quad (2.5)$$

with:

β = reliability index

α_i = influence coefficient stochastic variable X_i

i = normalized stochastic variable involved in the limit state function

The relative significance of the uncertainty surrounding a stochastic variable is measured by the influence coefficient α . The squared value of an influence coefficient is equal to the percentage of a stochastic variable's variance that can be attributed to the linearized and normalised limit state function. The sum of all the influence coefficients squared should add up to 1 (Kanning et al., 2016). More details on the reliability index and influence coefficient are provided in Appendix A.

The FORM method has several advantages, including its ability to handle complex models and sensitivity to input parameters and assumptions. This sensitivity allows a more comprehensive analysis of the system's behaviour under different conditions. It is computationally efficient compared to other methods, such as the Monte Carlo simulation method, which can be time-consuming and computationally intensive (Diermanse, 2016).

2.3. Concept of fragility curves

Fragility curves are commonly used to assess a dike's failure probability. A fragility curve of a dike section results from the cumulative distribution function of the resistance (the strength) of the section, which expresses the relationship between the solicitation (the load) and the failure probability given this solicitation. The failure probability of a flood defence can be calculated using a reliability method as discussed before (van der Meer et al., 2008). The (water-side) water level h is used as the reference solicitation for dikes. Figure 2.5 gives an example of a fragility curve. On the x-axis, the water level h is displayed, and on the y-axis, the cumulative distribution of the resistance F_R , also known as the conditional failure probability P_f . The resistance properties of the dike determine the shape of the fragility curve. The greater the uncertainty in the properties, the less steep the fragility curve is (Casati & Faravelli, 1991).

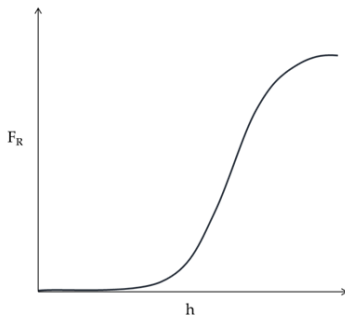


Figure 2.5: Fragility curve

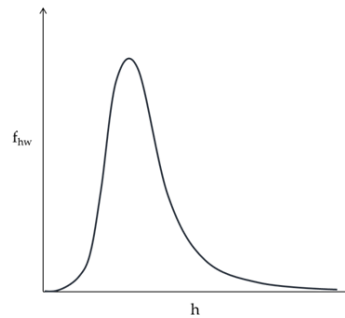


Figure 2.6: Probability density function

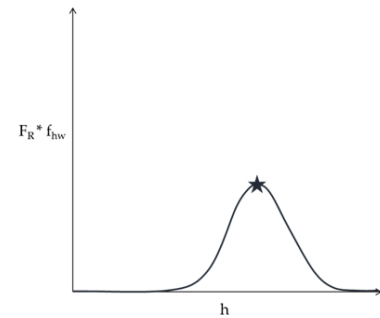


Figure 2.7: Failure contribution

The use of fragility curves for flood defences is particularly useful given the complexity of flood events and the potential for damage to occur in different ways. For example, a dike may fail due to overtopping, internal erosion, or slope instability. Each of these failure modes has its own set of physical characteristics and requires different mitigation measures. To compute the total failure probability, the fragility curve is multiplied by the probability density function (PDF) of the solicitation (see Figure 2.6). This multiplication leads to the failure contribution per water level. The resulting graph represents the contribution to the yearly probability of failure for different water levels. The yearly failure probability equals the area under the graph depicted in Figure 2.7. In mathematical terms, the yearly failure probability can be written as:

$$P_f = \int_{-\infty}^{\infty} f_{hw}(h_w) \cdot F_R(h_w) dh_w \quad (2.6)$$

where:

$f_{hw}(h_w)$ = probability distribution function of the water level
 $F_R(h_w)$ = cumulative distribution function of the strength

One main advantage of fragility curves is the decoupling of the solicitation and resistance, allowing a better understanding of the different factors contributing to the failure probability. Figure 2.8 demonstrates the influence of an increase in the water level. The water level in situation (b) increases compared to the situation (a), while the fragility curve remains the same. Comparing the failure contribution graphs of both cases (graphs on the right), the red area underneath the graph for situation (b) increases, indicating a larger failure probability than situation (a).

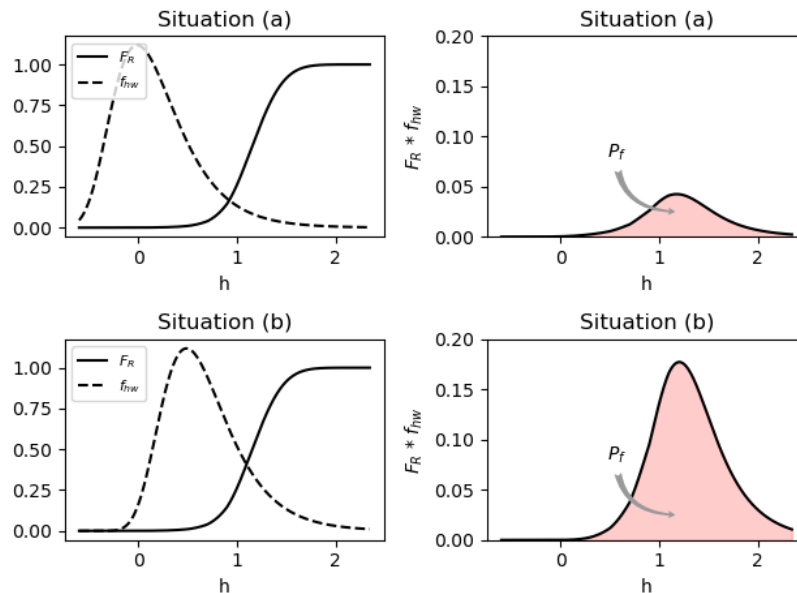


Figure 2.8: Shifting of the probability density function of the water level and increasing failure contribution

Using this relation between the fragility curve, water level PDF and failure probability, the effect of sea level rise becomes clear. When sea level rises, higher water levels are more likely to appear. This means that the water level PDF is shifting towards the higher water levels, in the case of Figure 2.8 to the right. When the effect of sea level on the water level PDF for a specific location is known, the impact of sea level rise on the failure probability can be found.

2.4. Considered failure mechanisms

Understanding the entire cost of reinforcing the primary flood defences in the Netherlands is one topic of interest in KP-ZSS. The knowledge program's main objective is to provide information on the financial implications of strengthening the primary flood defences in the Netherlands. The programme aims to help decision-makers by offering insights into the associated costs. Looking at the reinforcement cost of a dike section, the profile and dimensions of the dike are governing. Macro-stability and backward erosion piping are the dominant geotechnical failure mechanisms determining a dike's dimensions. They, therefore, are alongside wave wave overflow/overtopping, the most important mechanisms to consider when determining dike reinforcement cost. A brief introduction to macro-stability and backward erosion piping is given in the following sub-sections, while more detailed information about modelling choices is provided in Section 3.3 and Section 3.4.

2.4.1. Failure process of macro-instability

The failure mechanism macro-instability deals with the sliding of large soil masses along straight or deep circular slip planes, as shown in Figure 2.9. The cause of this sliding is the loss of equilibrium of the soil mass. Water infiltration into the dike body increases the pore water pressure, decreasing shear-strength capacity and causing loss of equilibrium. Increased pore water pressures can occur due to high water levels, precipitation or deformations. Furthermore, the equilibrium can be disturbed by an increase in the driving moment due to external forces such as traffic ('t Hart, 2018).

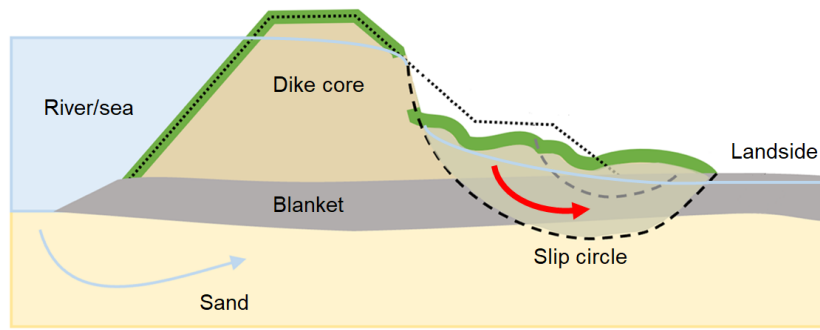


Figure 2.9: Macro-instability inner slope ('t Hart, 2018)

Different sliding planes can lead to slope instability of the inner slope. The critical sliding plane can be identified using the factor of safety (FoS). The most critical plane has the least resistance against sliding, thus, the lowest safety factor. The factor of safety is defined as the resistance divided by the driving moment.

$$FoS = \frac{M_R}{M_d} \quad (2.7)$$

The weight of the core material plays a critical role in determining the driving moment of the slip circle, as indicated by Equation 2.7. This parameter reflects the force exerted by the weight of the core material, contributing to the overall stability of the slope. On the other hand, the moment of resistance is influenced by the frictional characteristics of the soil particles and the pore water pressure in the dike. The friction between the soil particles acts as a resisting force against the driving moment, contributing to the overall stability of the slip circle.

2.4.2. Failure process of backward erosion piping

Backward erosion piping, or just piping, is a phenomenon that can occur caused by a substantial difference between the water levels outside and inside the structure. Sand transport due to receding erosion under a cohesive blanket layer will take place and an open channel will be created. As a result of receding erosion, sand boils occur ('t Hart, 2018). Figure 2.10 illustrates the process of backward erosion piping.

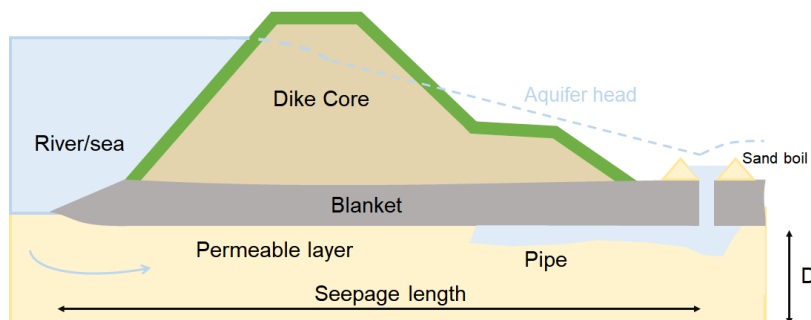


Figure 2.10: Process of backward erosion piping (Pol, 2022)

In the Netherlands, piping is assessed by an average gradient-based criterion based on the revised Sellmeijer model and piping, heave and uplift are considered a parallel system. The latter means all three (sub-)mechanisms must occur for failure to happen (Rijkswaterstaat, 2016). Uplift occurs when the pore pressures in the permeable layer under the dike (aquifer) increase due to an increase in the outside water level. If the upward pressure under the blanket layer exceeds the weight of the layer, it is lifted and ruptured. When the gradient at the exit point of the dike exceeds a critical gradient, sand particles start eroding. When erosion progresses, a pipe can form and, if large enough, can lead to a collapse (TAW, 1999).

Two crucial factors in assessing piping in dikes are the gradient of the hydraulic head and the transmissivity. The hydraulic head gradient is influenced by the difference in water levels between the outer and inner sides of the dike, as well as the length of the seepage path.

The ability of soil to transport water is known as hydraulic conductivity, and the thickness of the permeable layer tells us how deep the water-conducting zone is within the dike. The hydraulic conductivity and the permeable layer's thickness determine the dike's transmissivity. These variables directly affect the amount and rate of seepage through the dike body, which affects the likelihood of piping.

2.5. Differences between sea dikes and river dikes

In order to gain a better understanding of the applicability of typology-defined fragility curves in the Western Scheldt, it is important to highlight the key differences between river dikes and sea dikes. This section briefly highlights the key aspects, such as load duration, general dimensions and encountered subsoils.

2.5.1. Hydraulic loads

Hydraulic loads play a crucial role in determining the dimensions of flood defences. The major difference in hydraulic loading between the two areas is the duration of high water. Due to greater discharge, higher water levels in rivers might last for days, whereas high tides only last a few hours. Where sea water levels depend on tide and storm duration, river water levels depend on discharge, changing bathymetry and the presence of obstacles. Figure 2.11 show the difference in flood duration measured in the North Sea and at Lobith. In general, sea dikes are dominated by storms, which include high water levels. Rivers are dominated by the discharge, with high water levels as the most important load.

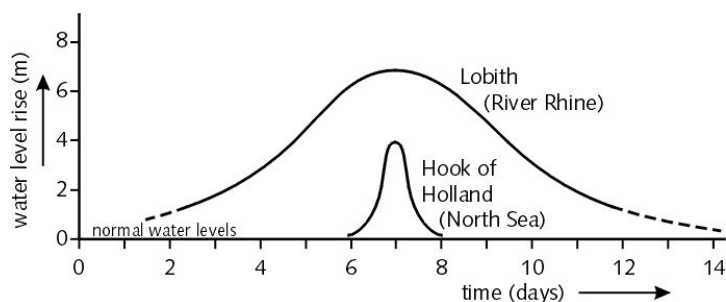


Figure 2.11: Difference in flood duration in rivers and at sea (Jonkman et al., 2021)

The duration of high water influences the pore water pressure, which is an essential part of a stability analysis of dikes since the phreatic line has more time to adjust. With non-stationary conditions (short flood duration), the pore water pressure will be lower in and under the dike compared to stationary conditions. The same holds for piping, where the duration of the flood event determines whether or not a pipe will form and create piping issues. The influence of time on the phreatic line is shown in Figure 2.12, where the transient case is compared to the steady state one.

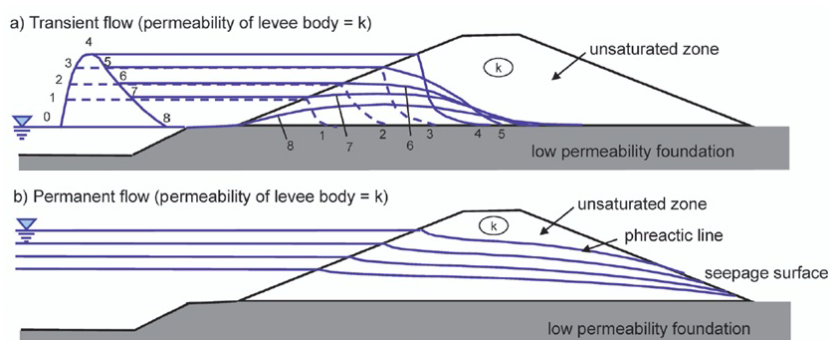
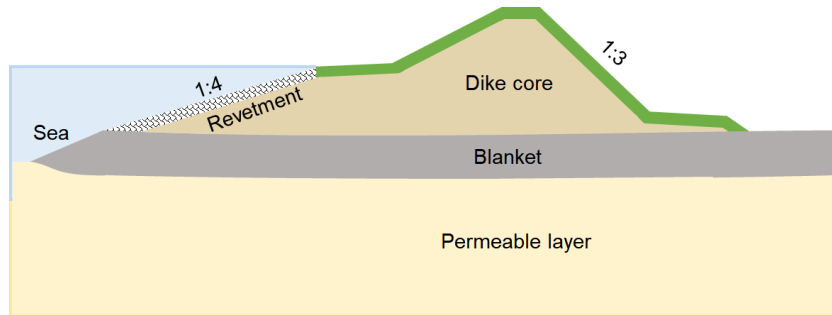


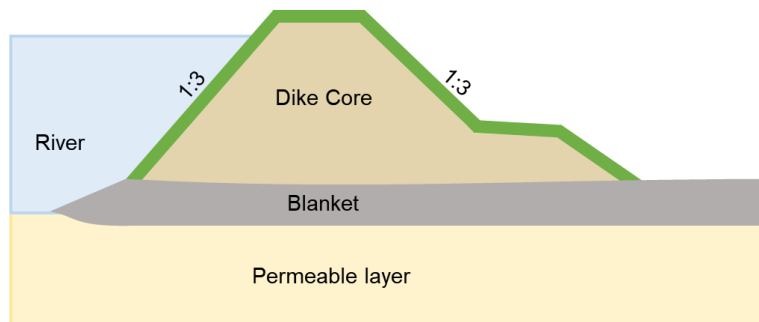
Figure 2.12: Positions of the phreatic surface for transient states during high water (a) and for steady states (b) (CETMEF et al., 2007)

2.5.2. General dike dimensions

The design loads have a significant impact on the dike's chosen dimensions. Because of the large waves that are formed during a storm, sea dikes often have a shallower outer slope and an outer berm. Also, revetments in the form of stones or asphalt are used. The shallower outer slope leads to a larger footprint of the dike. Figure 2.13a gives an example of a typical cross-section for a sea dike in the Netherlands. For river dikes, the use of an outer berm is not common since the waves along a river are often smaller. An inner berm or shallow slope is generally applied to prevent macro-instability during long periods of high water. In Figure 2.13b, a schematization of a river dike is depicted.



(a) Cross-section of a sea dike



(b) Cross-section of a river dike

Figure 2.13: Schematization of cross-sections of a sea dike and river dike in the Netherlands

2.5.3. Subsoil

Another difference between dikes in the river area and those along the coast is the subsoil beneath the dike, which is a crucial aspect when assessing the failure mechanism of piping. In 2.14, the prevalent subsoil types in the Netherlands are presented. When comparing the coastal area to the river area, it is noticeable that there is a higher presence of clay-like soil along the coast, whereas more sandy soil is found in the river area. Generally, the subsoil in the river area has a higher permeability compared to the coastal area, this implies that piping is more of an issue for river areas. Also, as mapped by “Dijken op getijdenzand: veel sterker dan gedacht” (2023), coastal areas also have more deposits of tidal sand. Generally, this tidal sand contributes to a lower permeability of the soil. This implies that the probability of flooding due to piping is considerably lower along the coast.

Table 2.1: Overview difference dike characteristics based on

Type	Characteristics		Loads					
	Hydraulic conditions	Subsoil characteristics	Water level River discharge	Water level tide	Water level wind	Wave wind	Storm oscillation	Precipitation
Coastal dike	Short tidal duration	Sand dike on clay layer	-	+	+	+	+	+/-
River dike	Long flood duration	Clay dike on clay layer	+	-	-	+/-	-	+

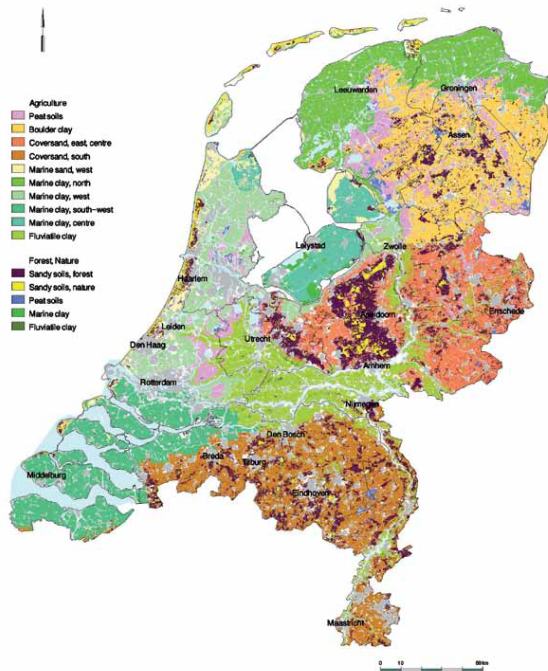


Figure 2.14: Distribution of the main soil types in the Netherlands (Brus et al., 2009)

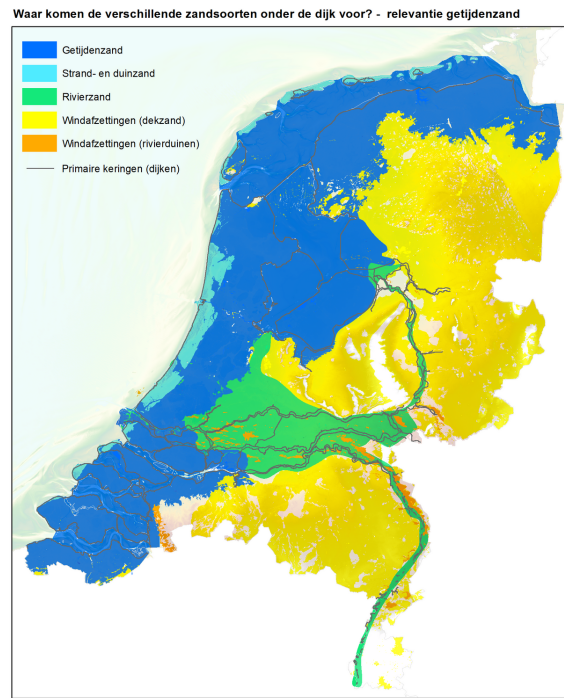


Figure 2.15: Different sand types underneath the dikes in the Netherlands (“Dijken op getijdenzand: veel sterker dan gedacht”, 2023)

2.6. Methodology Kennisprogramma Zeespiegelstijging

The primary flood defence system in the Netherlands consists of approximately 3,500 kilometers of dikes, dams, and other structures designed to protect against storm surges, high tides, and river flooding (Rijkswaterstaat, 2023). A simplified approach characterised the system’s strength of the extensive kilometres of flood defences outlined in the Kennisprogramma Zeespiegelstijging (KP-ZSS). This simplified method was used to approximate the total reinforcement cost.

Typology-defined fragility curves are used for the water safety analysis within KP-ZSS. The typologies are set up based on relevant physical characteristics of the flood defences for each failure mechanism. A fragility curve is constructed for every typology based on a representative location. This means that a typology is assigned based on the characteristic properties of a dike section. A limited number of typologies that give a representative distribution of the Netherlands are used (Kolen et al., 2021). Based on a set of fragility curves set up for Programma Integraal Riviermanagement (2021) in the river region of the Netherlands, a nationwide set of curves is created. The curves are defined with respect to ground level behind the flood defence and can be applied to various dike sections at different elevations.

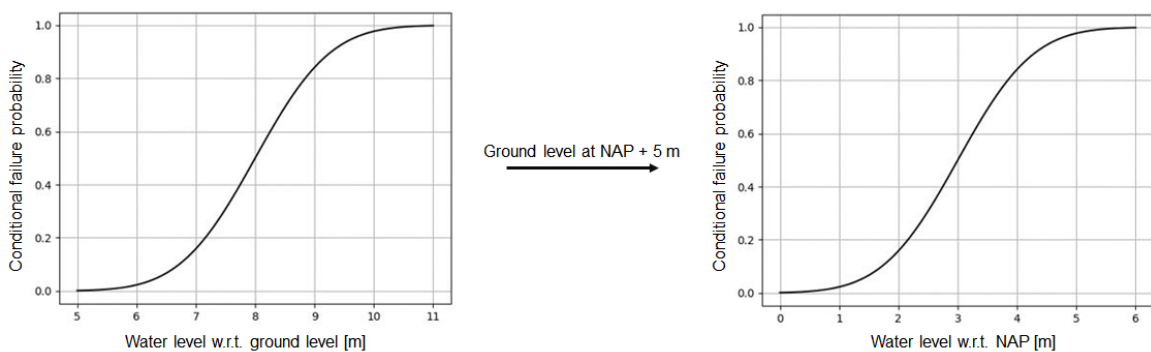


Figure 2.16: Scaling of fragility curve from ground level to NAP with fictional ground level at NAP + 5 m

The piping failure mechanism has been found to have several common characteristics, such as differences in the thickness of the blanket layer, transmissivity, and seepage length. Regarding macro-stability, factors like the core material, presence of a berm, blanket layer thickness, and the extent of wave overtopping are all considered. The following subsections discuss the typologies for each failure mechanism in more detail, where it becomes clear that all combinations of characteristic properties lead to a different typology.

The strength of the fragility curves is determined by the (un)drained shear strength of (un)drained materials. The Uplift-Van model is used to define the critical slip circle, resulting in the fragility curves depicted in Figure 2.17

2.6.1. Typologies and fragility curves macro-stability

In Table 2.2, the defined typologies for the failure mechanism inner slope stability are given. The typologies are separated based on the core material, presence of a berm, blanket layer thickness and significant wave overflowing/overtopping.

Table 2.2: Typologies for the failure mechanism inner slope stability

Typology STBI	Thin blanket layer (<4 m)	Thick blanket layer (>4 m)	
Sand core	Very sensitive (type 0)	Type 2	With overflow / overtopping
	Type 3	Type 4	Without overflow / overtopping
Clay core	Very sensitive (type 0)	Type 6	With overflow / overtopping
	Type 7	Type 8	Without overflow / overtopping
Sand core with inner berm	Type 9	Type 10	With overflow / overtopping
	Type 11	Insensitive (type 999)	Without overflow / overtopping
Clay core with inner berm	Type 13	Type 14	With overflow / overtopping
	Type 15	Insensitive (type 999)	Without overflow / overtopping

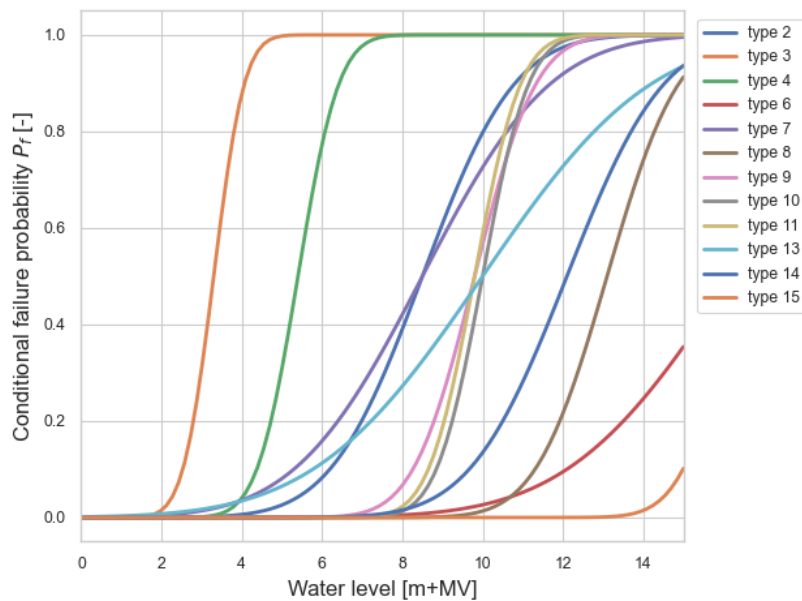


Figure 2.17: Fragility curves typologies STBI

2.6.2. Typologies and fragility curves piping

For the failure mechanism piping, each section is categorised into a typology according to the blanket layer thickness, transmissivity, and seepage length for the failure mechanism piping (depicted in Figure 2.10). The transmissivity indicates the rate at which groundwater is flowing through the permeable layer. Where the seepage length indicates the shortest distance at which water can flow underneath the dike. The different typologies are listed in Figure 2.18.

Sellmeijer's revised rule is used to express the strength in the fragility curves as shown in Figure 2.18. The typologies are based on Beoordelingsinstrumentarium (WBI 2017), calibration research and experience applying this rule.

Table 2.3: Typologies for the failure mechanism piping and heave

Typology STPH	Transmissivity (kD) <250 m ² /day	Transmissivity (kD) 250 - 1250 m ² /day	Transmissivity (kD) >1250 m ² /day	
Thin blanket layer (<2 m)	Type 1	Type 2	Very sensitive (0)	seepage length <50 m
	Type 4	Type 5	Type 6	seepage length >50 m
Thick blanket layer (>2 m)	Type 7	Type 8	Type 9	seepage length <50 m
	Insensitive (999)	Type 11	Type 12	seepage length >50 m

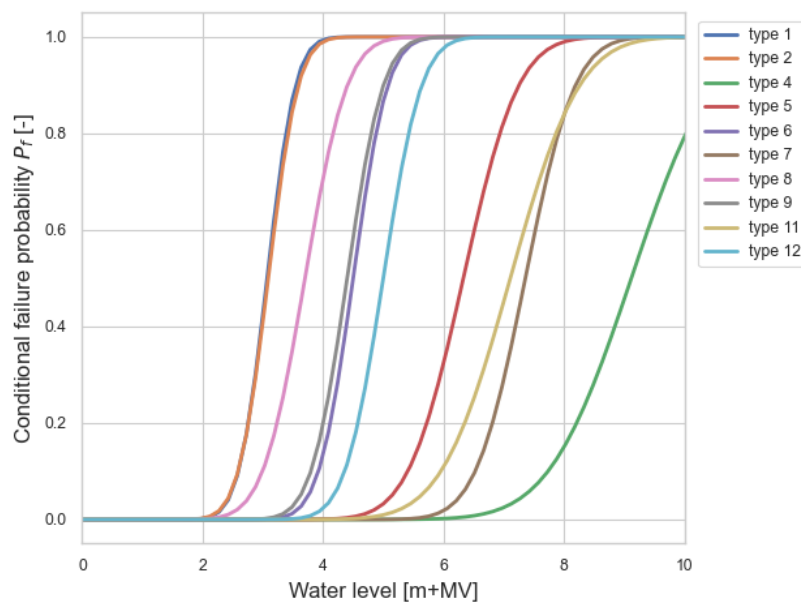


Figure 2.18: Fragility curves typologies STPH

Framework for developing the fragility curves and estimating cost

This chapter focuses on the development of new fragility curves. First, the case study area and the chosen dike sections are introduced. Then, assumptions and modelling approaches for both macro-stability and piping are described. In general, the model approach of the water board Scheldestromen outlined in *WBI2017 Basisrapport* (2022) is used in combination with *Schematiseringshandleiding macrostabiliteit* (2021a) and *Schematiseringshandleiding piping* (2021b). This chapter describes the most important principles used to set up the models for the reliability analysis and construction of the fragility curves. Also, an introduction to the cost calculation software OKADER is given.

3.1. Western Scheldt study area

The data available in this research is provided by the waterboard Scheldestromen (WS), which is used to schematize the cross-sections to draw up new fragility curves of the primary flood defences in the Western Scheldt. Three different sections in different dike trajectories (29-3, 30-3, 32-4) will be studied; this way the influence of the typology-defined fragility curves can be portrayed better, and some degree of coincidence can be excluded.

In the subsequent sections of this research, the specific dike section under investigation will be referred to as DP (Dike Pole), indicating the location of the dike cross-section. Figure 3.1 depicts the dike sections that are examined in this study. The figure provides an overview of the studied dike sections within the study area. Each dike section is labelled with its corresponding DP number, allowing for easy reference throughout the research. The dike following dike sections correlate with the dike trajectories: DP745 lies in trajectory 29-2, DP399 in trajectory 30-3 and DP167 within trajectory 32-4.

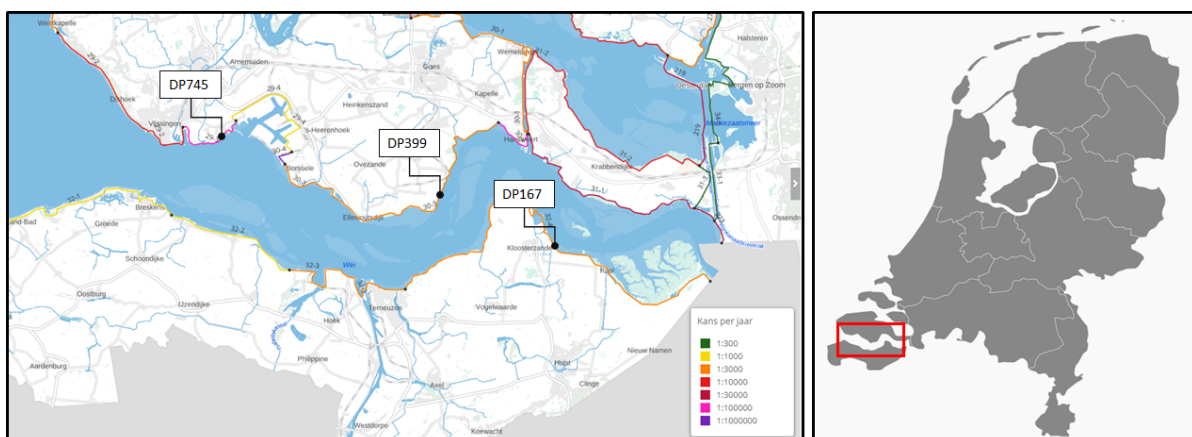


Figure 3.1: Overview of the study area (Informatiehuis Water, 2022; “Map of the Netherlands with Provinces”, 2023)

These locations are selected based on multiple criteria. Firstly, the respective dike sections had to be assigned a typology for macro-stability and piping (meaning they are not considered insensitive). In Figure 3.2, the typologies for macro-stability and piping are shown. It should be noted that this classification pertains to the OKADER sections (refer to Section 3.6 for an explanation of the OKADER sections). The dike sections were selected based on their individual classification. For example, DP745 appears to be located in an area classified as typology 999 (insensitive). However, when considering only this particular section, it falls under type 4. For this study, it was assumed that the typology of the considered dike section represents the entire OKADER section.

Secondly, the current assessments of the flood defences were considered (van Schaick, 2021, 2022; van Schaick & van Sabben, 2021). This involved identifying cross-sections that have the highest possible probability of failure in terms of either macro-stability or piping. In conjunction with the first criterion, these three dike sections were selected for investigation.

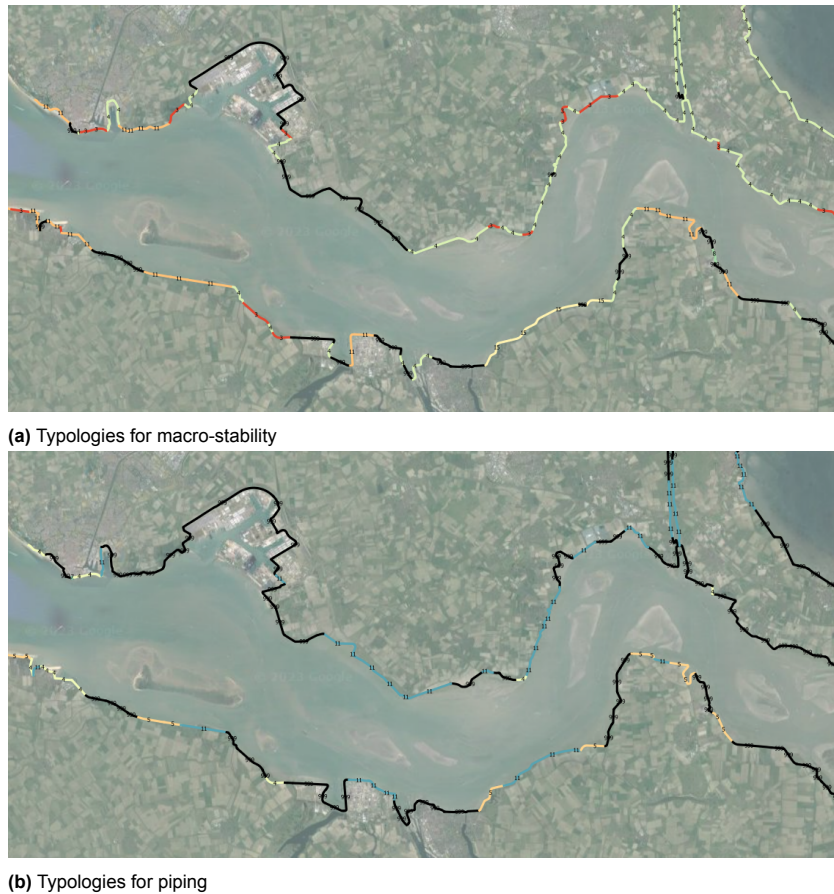


Figure 3.2: Typologies for macro-stability (a) and piping (b) for the Western Scheldt

3.2. Constructing fragility curves

Constructing a fragility curve is a systematic process involving several steps. First, a range of relevant water levels to the structure is determined. Next, the probability of failure is estimated for each water level based on calculations. The water level is discretized, while other parameters are implemented as stochastic variables with a probability distribution conform to the guideline of the so-called Wettelijk Beoordelingsinstrumentarium 2017 (WBI2017). The result of a single reliability calculation is a conditional failure probability with corresponding reliability index β and is called a fragility point. When this process is repeated for several water levels, multiple combinations of β and water levels are found. Inter- and extrapolation between these points gives a curve as in Figure 3.3. Using the relation between β and the probability of failure:

$$P(Z < 0|h) = \Phi[-\beta(h)], \quad (3.1)$$

the (β, h) -curve can be transformed into a fragility curve (Figure 3.4). This transformation is used since β -values are more suitable for interpolation. However, suppose the interval between fragility points is very small. In that case, many water levels and failure probabilities are considered, and the fragility curve can be constructed directly because little to no interpolation is required. This last method is more accurate but requires greater computational effort because the number of computations increases. Applying this more accurate method is more feasible for the failure mechanism of backward erosion piping, where computational time is minimal, in contrast to macro-stability, which has longer computational times (van Montfoort et al., 2020).

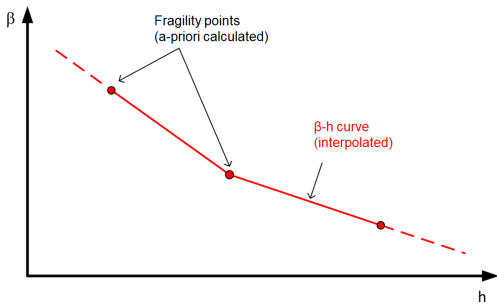


Figure 3.3: (β, h) -curve: The fragility points represent the reliability indices corresponding to the conditional probabilities of failure derived for discrete water levels (Schweckendiek & Kanning, 2017)

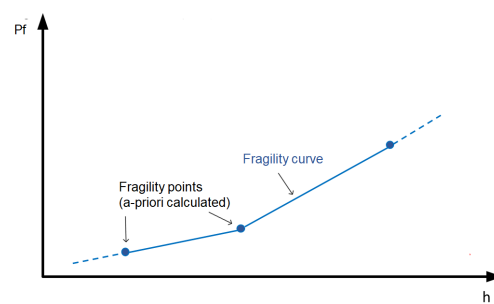


Figure 3.4: Fragility curve: The fragility points represent the failure probabilities corresponding to the reliability indices

3.3. Modelling approach macro-stability

Introduced in section 2.4, macro-stability is the failure mechanism dealing with the sliding of soil masses. For the probabilistic analysis of macro-stability, the modelling procedure is followed as described in *Handreiking Faalkansanalyse Macrostabilliteit* (2017). This section describes assumptions and choices that have been made regarding the modelling of macro-stability for the construction of fragility curves.

3.3.1. Fragility points

As discussed in Section 3.2, only a limited amount of water levels is used to construct the fragility curve for macro-stability due to the long computational time. A standardized approach is used to compute the fragility points so they can be applied at the various cross-sections. Selecting five distinct levels for calculating the fragility points is considered sufficient for fitting the curve. In situations where uplift plays a role, there is generally a discontinuity in the fragility curve. Since using fragility curves involves interpolating between fragility points, these discontinuities must be modelled with sufficient accuracy (Teixeira, 2021).

The first two points are chosen just before uplift and right after rupture of the blanket because this process is non-linear and thus crucial to capture for the interpolation of the fragility points. Detailed explanation about the uplift condition and how it is handled in this study is provided in Appendix B. The other two points are taken around the outer berm of the dike. One is at the lower part of the berm and the other on the upper part because these points are easily identified for every dike section. The last point is arbitrarily 30 cm below the dike section's crest. All points for the reliability analysis are illustrated in Figure 3.5.

3.3.2. Schematization pore water pressures

In dike stability analysis, the phreatic line is an important factor that must be carefully chosen to ensure reliable results. The phreatic line represents the pore water pressure within the dike and can significantly impact the structure's stability. For schematization, the pore water pressure is divided into two kinds, the phreatic line (in the dike) and the head in the permeable layer (also known as the aquifer).

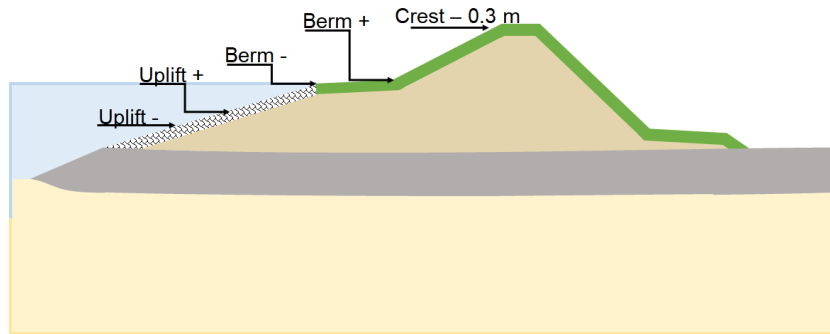


Figure 3.5: Chosen points for reliability analysis macro-stability

Daily conditions

The daily phreatic line's reference point is the hinterland's ground level minus half a meter of dewatering. For locations with a groundwater monitoring well, the average value of the measurement is used. The daily water pressure is needed to describe the yield stress of the soil. For the pore water pressure in the permeable layer, a value of the average outside water level minus half a meter is used. If the groundwater monitoring wells are present, the average value of the wells is taken.

Norm conditions

In the calculation of this research, the pore water pressure in the dike and permeable layer schematized are schematized according to TAW, 2004 (2004). As can be seen in Figure 3.6a, the phreatic line drops half the water level measured at the outer toe of the dike. After that, it moves gradually to the inner toe of the dike, where it intersects at a height equal to a quarter of the water level referenced to the hinterland.

For the schematization of the pore water pressure in the permeable layer, groundwater level measurements are used if available. If not, a combination of Figure 3.6b and the reduction table in Table 3.1 is used. This reduction table gives the head reduction at the outer berm with respect to the outside water level. The rows in Table 3.1 under the standard represent the return period of the considered outside water level.

Table 3.1: Reduction of pore water pressure in the permeable layer from the outer berm/crest (van Sabben et al., 2022)

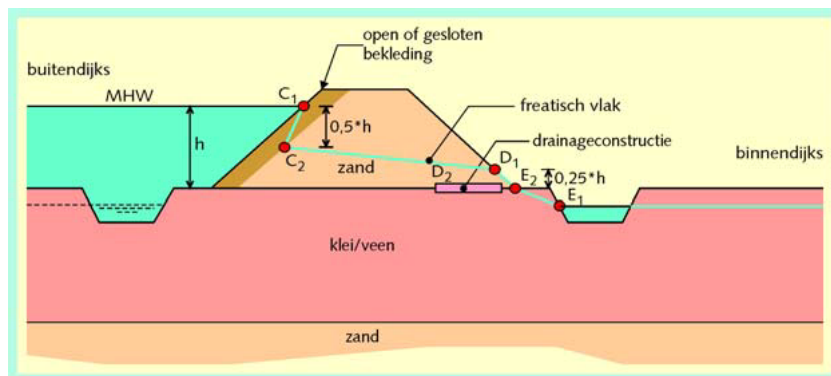
Reduction in m w.r.t. outside water level	Standard			Course head Cotan:	
	1/1000	1/10000	1/100000	Outer berm - Inner toe	Inner toe - Ditch
Very unfavourable	1.00	1.25	1.50	50	100
Unfavourable	1.50	1.75	2.00	50	100
Average	2.00	2.25	2.50	100	150
Favourable	2.50	2.75	3.00	100	150
Very favourable	3.00	3.50	4.00	150	150

Wave overtopping

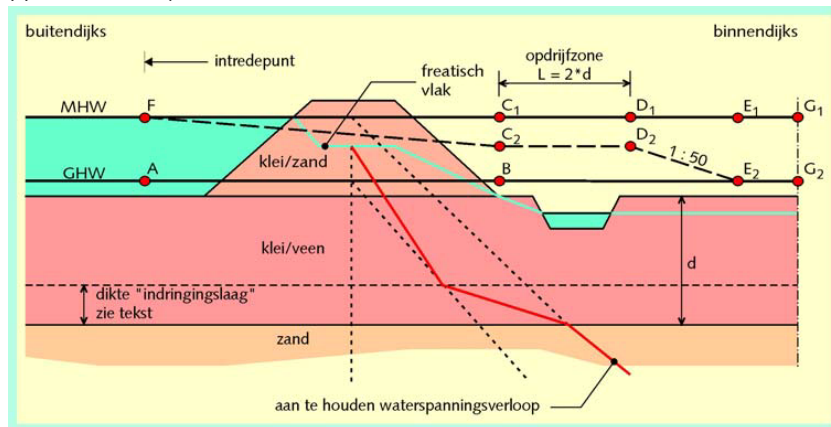
In the classification of fragility curves in Kennisprogramma Zeespiegelstijging for the Western Scheldt, it has been reasoned that no significant wave overtopping occurs. Therefore, all assigned typologies for macro-stability are classified without wave overtopping. In this study, the same assumption is made, and this phenomenon is disregarded and no correction on the phreatic line is made.

3.3.3. Shear strength models

There are two types of soil shear strength: drained and undrained. The choice of condition will determine how to calculate the shear strength. Using the appropriate condition depends on several variables, including the kind of soil and grain size, the saturation level, the degree of consolidation, and the loading rate. While the soil cannot drain in an undrained environment, the pore water can quickly exit under drained conditions. The state influences the soil's equilibrium reaction. If the soil's effective stress reduces as a result of this reaction, there will be a decrease in its shear capacity (Verruijt, 2001).



(a) Schematization phreatic line



(b) Schematization pore water pressure aquifer

Figure 3.6: Schematization of the pore water pressure in the dike body and in the permeable layer according to TR-26 (2004)

MohrCoulomb model drained conditions

For drained soil response, the Mohr-Coulomb strength model is typically used. In terms of effective stresses, the shear strength is often approximated by Equation 3.2 (Terzaghi, 1942). The ϕ values for the drained layers have been adopted from the schematization manual (Rijkswaterstaat, 2021a).

$$\tau = c' + \sigma' \tan(\phi') \quad (3.2)$$

where:

- τ = shear stress [kN/m²]
- c' = cohesion [kN/m²]
- σ' = effective normal stress [kN/m²]
- ϕ' = effective friction angle [°]

SHANSEP for undrained conditions

In the undrained situation, the shear strength is based on the SHANSEP model following WBI2017 (Rijkswaterstaat, 2021a). The SHANSEP formulation of undrained shear strength uses two material parameters (S and m) and one state parameter (σ'_y). The history of the soil is included when calculating the effective vertical stress. We assume that the soil retains the maximum effective stress (also known as yield stress) per location in the subsoil, which is denoted by y' (R. van der Meij, 2020). The pre-overburden pressure (POP) parameter defines the relationship between the yield stress and the effective stress:

$$\sigma'_y = \sigma'_v + POP \quad (3.3)$$

where:

- σ'_y = vertical yield stress [kN/m²]
- σ'_v = vertical effective stress [kN/m²]
- POP = pre-overburden pressure [kN/m²]

Using Equation 3.3, the shear strength along the slip plane is calculated using the following equation:

$$\tau = s_u = \begin{cases} \sigma'_v > 0 & \sigma'_v \cdot S \cdot \left(\frac{\sigma'_y}{\sigma'_v}\right)^m \\ \sigma'_v = 0 & 0 \end{cases} \quad (3.4)$$

where:

- S = ratio between the undrained shear strength s_u and the yield stress [-]
- m = strength increase exponent [-]

From the water board, a regional set of soil parameters is available. It includes characteristic values and average values for the strength parameters ϕ , S , m , and POP values. The values of S and m are based on (Spoorenberg, 2019). All the used soil parameters can be found in Appendix E

3.3.4. Limit equilibrium model

For the calculations of macro-stability, the software D-stability is used. The standard model to assess the slope stability of a dike, according to the WBI2017, is the Uplift-Van model. This model allows for a non-circular slip circle, which is often the case in uplift conditions. Increased pore water pressures in the aquifer (permeable layer) can significantly reduce the effective stresses under the blanket, which can cause the lifting of the blanket layer (Van et al., 2005).

The slip circle of the Uplift-Van model is an elongated one, described by two circular slip circles connected by a horizontal slip line. Depicted in Figure 3.7, one circle is on the active zone and another on

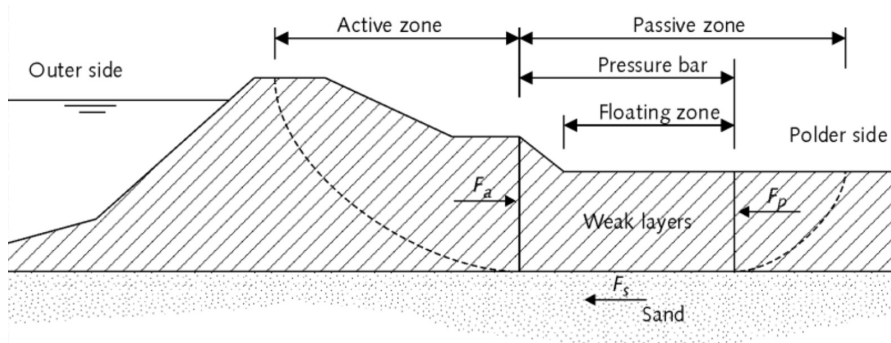


Figure 3.7: Sliding plane of the Uplift-Van method (Jongejan, 2017).

the passive zone linked by the horizontal line lying at the bottom of the weak soil layer. If the horizontal line approaches zero, the slip circle reduces to a single circle. The safety factor is defined as the ratio of the resisting moment to the driving moment, where the resistance is determined by the soil shear strength (Simanjuntak et al., 2018).

The probabilistic calculation includes the model factor as a stochastic with a mean of 1.005 and a standard deviation of 0.033. This complies with *Schematiseringshandleiding macrostabiliteit* (2021a). According to WBI2017 only the slip surfaces that enter from the waterside to halfway the inner slope are relevant.

3.4. Modelling approach piping

Piping occurs under the dike due to seepage flow causing continuous transport of soil. Section 2.4.2 a description of the failure mechanism was given. In the analysis of piping, the revised Sellmeijer model is used for this study. The limit state functions and computations for uplift, heave and piping are briefly described in this section following *Ontwerpinstrumentarium 2014* (Rijkswaterstaat, 2016). The groundwater model shown in Figure 3.8 is a schematic representation to illustrate the different parameters corresponding to the sub-mechanisms. The used parameters for the calculations can be found in Appendix E.

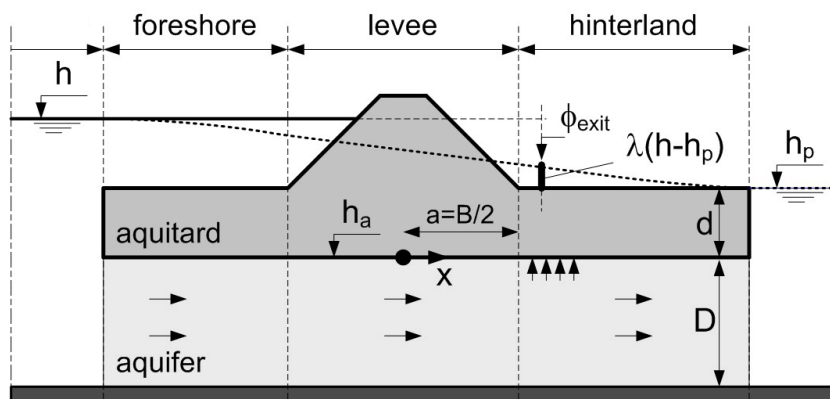


Figure 3.8: Groundwater flow model (TAW, 2004)

Uplift

Based on a comparison of pore pressures at the upper boundary of the aquifer with the weight of the blanket layer, the uplift model used in safety evaluations and design in the Netherlands was developed.

The result is the limit state function shown below:

$$Z_u = m_u \cdot d \frac{\gamma_{sat} - \gamma_w}{\gamma_w} - \lambda \cdot (h - h_p) \quad (3.5)$$

where:

- m_u = model factor [-]
- γ_{sat} = saturated volumetric weight blanket (aquitar in Figure 3.8) [kN/m³]
- γ_w = volumetric weight water [kN/m³]
- h = outside water level [m]
- h_p = polder level [m]
- d = thickness of the blanket layer (aquitar in Figure 3.8) [m]
- λ = damping factor exit point [-]

Heave

Heave takes into account the beginning of sand erosion, whereas uplift is concerned with the rupture of the cohesive, low-permeability blanket. It is thought that exceeding a critical heave gradient is a necessary (but not sufficient) condition. In the literature, there are many methods for determining the critical heave gradient, including the popular one of Terzaghi:

$$Z_h = i_{c,h} - \frac{(h - h_p) \cdot \lambda}{d} \quad (3.6)$$

where:

- $i_{c,h}$ = critical heave gradient blanket layer

Sellmeijer

Sellmeijer developed a hypothesis on piping stability based on the flow pattern produced by the head difference between the waterside and the landside water level. This is the primary cause of internal erosion and the sand grains' resistance to erosion in partially constructed piping channels. Physical models and tests have led to the revision of the model (Sellmeijer et al., 2011). This leads to the following limit state function:

$$Z_p = m_p \cdot H_{c,p} - (h - h_p - 0.3 \cdot d) \quad (3.7)$$

with:

$$\begin{aligned} H_{c,p} &= L * F_{resistance} \cdot F_{scale} \cdot F_{geometry} \\ F_{resistance} &= \frac{\gamma'_p}{\gamma_w} (\eta \cdot \tan(\theta)) \\ F_{scale} &= \frac{d_{70m}}{\sqrt[3]{\kappa L}} \left(\frac{d_{70}}{d_{70m}} \right)^{0.4} \\ F_{geometry} &= 0.91 \cdot \left(\frac{D}{L} \right)^{\frac{0.28}{\left(\frac{D}{L} \right)^{2.8} - 1} + 0.04} \end{aligned} \quad (3.8)$$

where:

m_p	= model factor [-]
H	= head difference [m]
h	= water level entry point (water side) [m]
h_p	= phreatic level exit point (land side) [m]
d	= thickness blanket layer (aquitar in Figure 3.8) [m]
L	= seepage length [m]
γ_s	= volumetric weight of sand grains (=26.5 [kN/m ³])
γ_w	= volumetric weight of water (=10 [kN/m ³])
θ	= bedding angle [deg]
D	= thickness of the aquifer [m]
η	= drag factor coefficient [-]
ν	= kinematic viscosity of water (=1.33·10 ⁻⁶ [m ² /s])
d_{70}	= 70%-fractile of the grain size distribution [m]
d_{70m}	= reference value for d70 [m]
g	= gravitational constant (=9.81 [m ² /s])
κ	= specific conductivity [m/s]

Parallel system

Backward erosion piping can only occur if all three (sub-)mechanisms take place. Regarding reliability, the system is considered parallel, meaning all three (sub-)mechanisms must occur for the system to fail. The failure probability for a parallel system is given as follows:

$$P_f = P(Z_u < 0 \cap Z_h < 0 \cap Z_p < 0) \quad (3.9)$$

Considering the system as fully dependent, the failure probability for backward erosion piping is the minimum of the three failure probabilities because the system is parallel (see 3.9).

System type	failure probability of dependent events	failure probability of independent events	failure probability of mutually exclusive events
series system	$\max_{i=1,n} P_i$ lower bound	$1 - \prod_{i=1}^n (1 - P_i)$	$\sum_{i=1}^n P_i$ upper bound
parallel system	$\min_{i=1,n} P_i$ upper bound	$\prod_{i=1}^n P_i$	0 lower bound

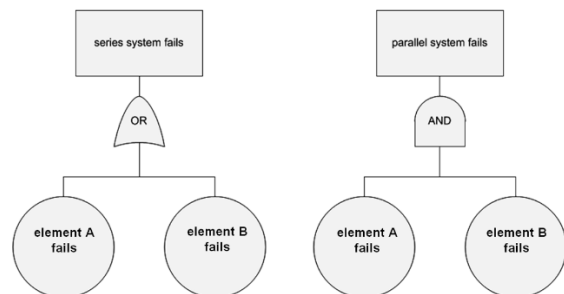


Figure 3.9: Failure probability and fault tree for series and parallel system (Jonkman et al., 2018)

3.5. Hydraulic loads

As previously stated, this research focuses on a different approach to describe the strength of the failure mechanisms macro-stability and piping. However, for the overall picture of reinforcement costs, the height requirement is included. In this research, the derived water level statistics for Kennisprogramma Zeespiegelstijging (KP-ZSS) are used for a fair comparison between the two fragility curve approaches. This section briefly discusses on the water level frequency lines and the required crest heights derived for KP-ZSS.

KP-ZSS uses four scenario timelines describing the sea level rise from 2023 to 2200. The timelines are: low, medium, extreme and very extreme. These timelines depicted in Figure 3.10 are used to calculate the water levels and required crest heights for the coming years. These scenarios are based on the predictions made by the KNMI (2021b).

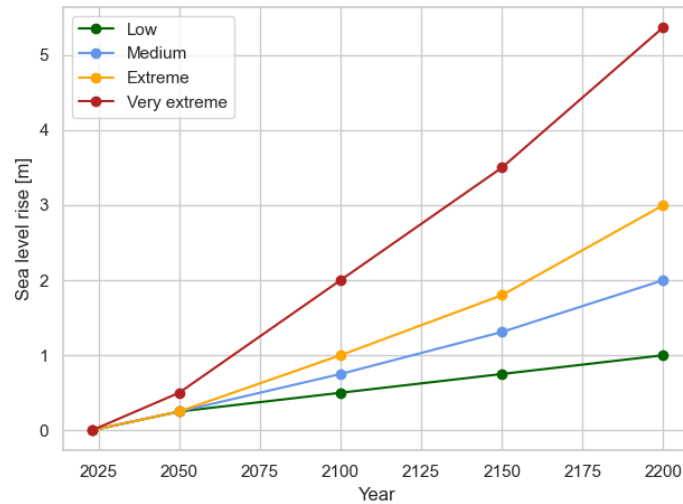


Figure 3.10: Sea level rise timelines for different scenarios (Rijkswaterstaat, 2021c)

Hydraulic loads under sea level rise

Calculating hydraulic loads is done by determining the main hydraulic boundary conditions. This can include wind (waves and set-up), lake level, river discharge and failing storm surge barriers. Often combinations of these are governing. The required heights and strengths are calculated by combining these events and probabilities of the events and translating these combinations into hydraulic loads on flood defences.

KP-ZSS calculates the hydraulic loads for 173 different dike sections in the Western Scheldt, using 173 output locations from the Hydra-NL and WBI2017 databases with different amounts of sea level rise. The year 2023 is used as a reference year, meaning the amount of sea level rise in this year is set to zero (Duits, 2021). Wave conditions are determined with SWAN-2D computations using 21 different conditions of wind speed, wind direction and local water level. For every scenario of sea level rise, the water level is corrected. This gives the wave conditions per scenario for every output location. If the foreshore affects the wave conditions, the SWAN-2D conditions are used as input for SWAN-1D computations (Zethof et al., 2022).

In the Western Scheldt, the water levels at the toe of the dike are directly influenced by sea level rise since it has an open connection to the sea. Therefore it is assumed that the water levels increase evenly with the amount of sea level rise. Examples of water level frequency lines for each scenario are shown in Figure 3.11 till Figure 3.14. The y-axis displays the occurring water level, and the x-axis the occurring frequency (or returning period). The water level frequencies for the years 2023, 2100 and 2200 are computed. For the water levels, the following return periods have been analyzed: 10, 30, 100, 300, 1.000, 3.000, 10.000, 30.000, and 100.000 years (Oerlemans et al., 2022). The effect of the sea level is visible in the graphs because, for each reference year, the line has shifted linearly up, indicating this rise in sea level.

These water level frequency lines play a crucial role in determining the reinforcement needed. They serve as input for evaluating whether the dike satisfies the specified requirements at each time step and help identify the specific reinforcements that are necessary. Section 3.6 delves further into how these reinforcements and associated costs are calculated.

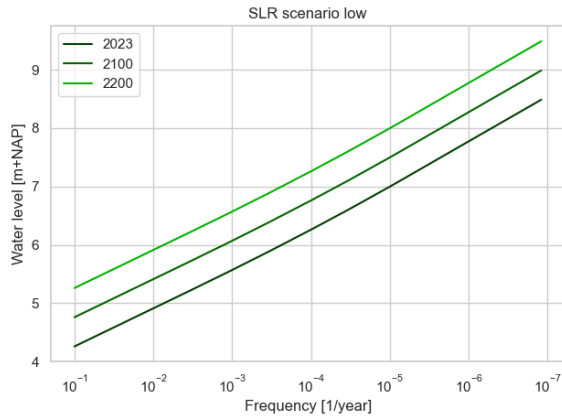


Figure 3.11: Water level frequency lines section DP399 for scenario low

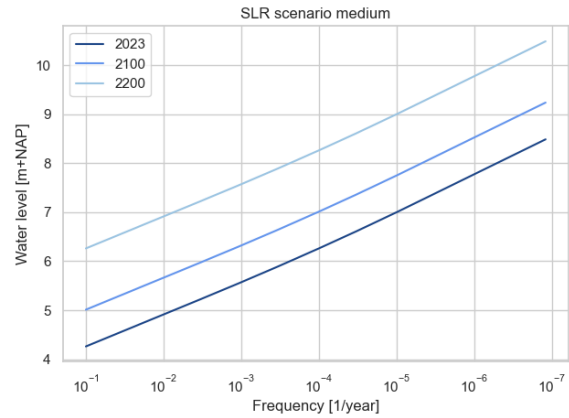


Figure 3.12: Water level frequency lines section DP399 for scenario medium

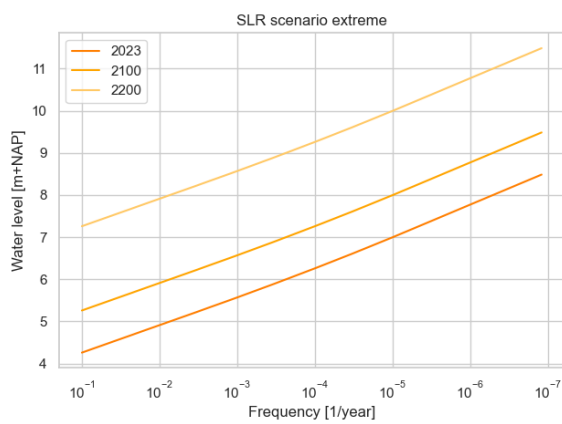


Figure 3.13: Water level frequency lines section DP399 for scenario extreme

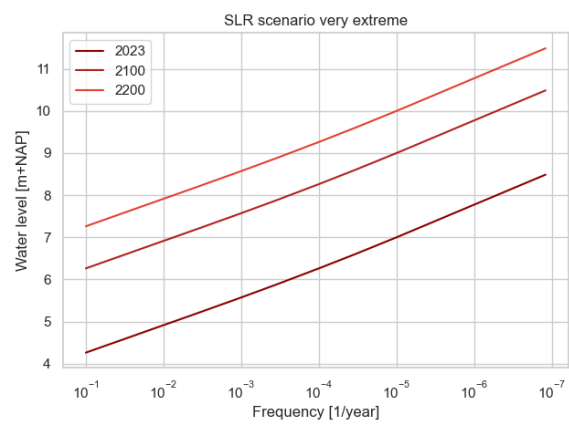


Figure 3.14: Water level frequency lines section DP399 for scenario very extreme

HBN

In this report, the approach used in KP-ZSS for the height calculation is adopted, as it is more location-specific due to the load statistics and height calculations. While new fragility curves will be derived for macro-stability and piping, no new fragility curves will be derived for the height calculation. To determine the required height, the calculated Hydraulic Load Level computed for KP-ZSS is used.

The Hydraulic Load Level, or *Hydraulisch Belasing Niveau* (HBN) in Dutch, is a concept widely used to determine the required crest height probabilistically and is defined as: "The minimum required crest height at which water and waves can be safely retained." (Helpdesk Water, 2017). The Hydraulic Load Level is based on the critical overtopping discharge and can be computed with software like Hydra-NL. Using the calculated wave conditions and water levels, the crest heights are determined with the Hydraulic Load Level. In determining the HBNs, a critical discharge of 5 l/ms/ is used (Duits, 2022). For all four timelines, the evolution of the HBN is made. An example of this HBN evolution for dike section DP399 can be found in Figure 3.15. Please see Appendix D for the additional water level frequency lines and HBNs of the other considered dike sections.

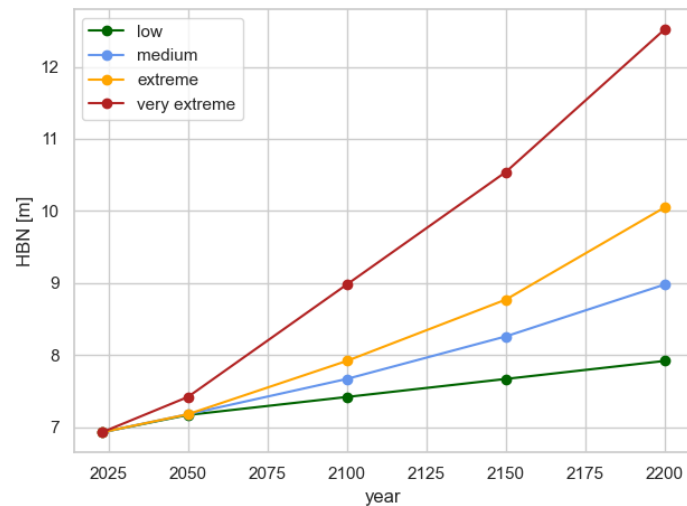


Figure 3.15: HBN development lines for section DP399

3.6. Cost calculation with OKADER

In this research, the software package OKADER (Opgave en Kosten Analyse Dijkversterking en Rivierverruiming)¹ is used to calculate costs. In 2021, OKADER was modified by the Integrated River Management (2021) program to allow calculations in areas beyond just the upper rivers. This modification considers river discharge and downstream water levels, at sea or in the IJsselmeer, as contributing factors.

In OKADER, each dike section is assessed at various time steps to determine if dike reinforcement is necessary under the current hydraulic conditions. The dimensions of a dike reinforcement measure primarily depend on three failure mechanisms: overflow/overtopping (height), macro-stability, and piping (width of the dike base). The failure probabilities for macro-stability and piping are determined by combining the water level statistics with the associated fragility curves.

OKADER uses the standard failure probability budgeting prescribed in WBI2017. In this case, 24% of the failure probability space is allocated for overtopping/overflow, 24% for piping, and 4% for inner slope stability. The remaining 48% is distributed among revetment, structures, and others (Knoeff, 2016). The failure probability requirement of each norm trajectory is translated to the dike cross-section using length effects. OKADER analyses are conducted with a time step of 5 years, this means that the dike is assessed every 5 years and can be reinforced if necessary. When reinforcement is required, the dike is designed for a standard lifetime of 50 years.

The failure probability is compared with the legal requirement. For overflow/overtopping, the hydraulic load level obtained from Hydra-NL is used. If a dike section fails to meet the requirements, reinforcements are needed. OKADER completes the following steps (de Grave, 2021):

1. Determining the failure probability per mechanism from local water level statistics and fragility curves.
2. Determine the maximum allowable probability of failure based on legal requirements.
3. Assessment: if a dike meets the requirements, go back to step 1 for a later time step. If it does not meet the requirements, go to step 4.
4. Design: determine the new dike dimensions to comply with the requirements for the design lifetime.
5. Determine reinforcement cost using the cost database KOSWAT.

¹English: *Specification and Cost Analysis of Dike Reinforcement and River Widening*

OKADER determines the dike reinforcement requirements over time based on the development of hydraulic scenarios (low, moderate, extreme, and very extreme timelines, as mentioned in the previous section). OKADER stores the failure probability progression per dike section and calculates the dike reinforcement requirements (dimensions) along with the corresponding reinforcement costs. Several reinforcement measures are implemented in the KOSWAT database and are shown in Figure 3.16. The measure of choice depends on the required space to implement the actual measure versus the actual available space. As the available space decreases or the required space increases, it becomes necessary to switch to combinations of structural (or innovative piping measure) and ground measures with decreasing spatial requirements. The 'most expensive' measures are found in situations with the least available space (or no space at all). More detailed information about the cost database KOSWAT, available reinforcement methods and the design cycle of OKADER can be found in Appendix C.

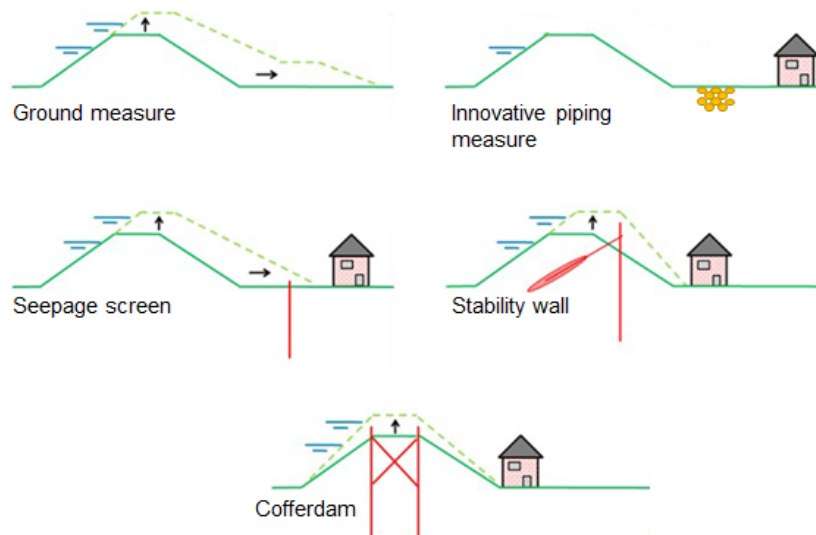


Figure 3.16: Mix of the possible reinforcement measures in KOSWAT

Reinforcements for OKADER

OKADER requires fragility curves for macro-stability and piping for different berm lengths to determine the amount of reinforcement (extra berm length) needed to meet the standard. For this, new fragility curves need to be computed, including these reinforcements. For the piping calculations, it is assumed that an increase in seepage length equals the added berm length. If a fragility curve for the situation with a 10 m berm is constructed, the seepage length is increased by 10 m. For each section, new fragility curves will be constructed for a berm of 10, 20, 50, 100 and 200 meter length.

For the failure mechanism piping, it is relatively easier to develop new fragility curves, while it takes more time for macro-stability. In D-stability, new calculations are performed by adding a berm. A new fragility curve is constructed for all dike sections in the case of a 5-meter-long berm and a 10-meter-long berm. An example of how this is taken into account can be seen in Figure 3.17. As indicated in the figure, the height of the berm is chosen as 1/3 of the height between the inner toe and crest of the dike.

OKADER sections

In the databases, the division of the study area into dike sections is predefined. The initial classification is based on the VNK (National Flood Risk Assessment) section division, which has section lengths typically less than 1 kilometer. Along the Western Scheldt, there are 173 OKADER sections based on the VNK sections (Figure 3.18). For each section, boundary conditions are determined. The midpoint of each section is selected as the output location for the hydraulic loads. The reinforcement costs are calculated for each OKADER section. In this study, the strength of the considered dike sections describes the strength of the OKADER section in which the respective cross-sections are located.

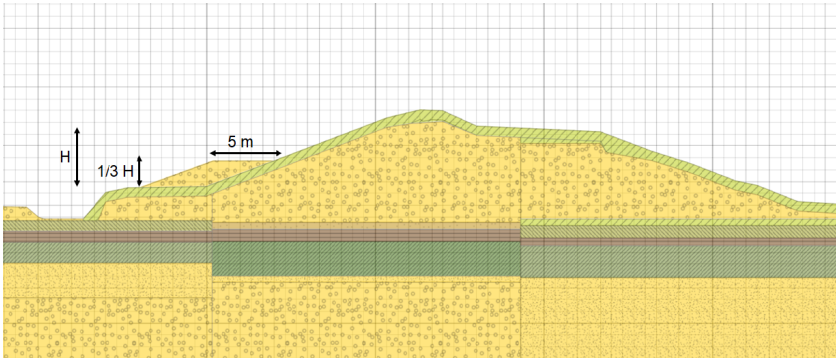


Figure 3.17: Example of the addition of a 5 meter berm in D-stability

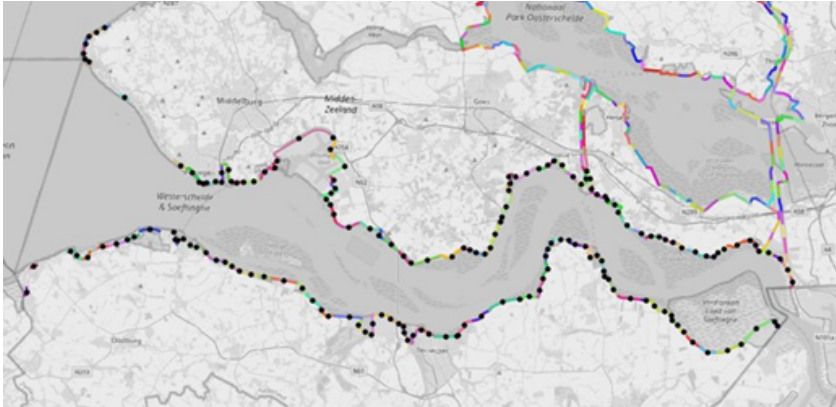


Figure 3.18: OKADER sections in the western Scheldt

Fragility curves in the Western Scheldt

This chapter compares the results of the proposed method to construct new fragility curves, described in the previous chapter, with those of the typology-defined fragility curves. Site-specific fragility curves are computed for both macro-stability and piping. They will be referred to as typology-defined fragility curves and site-specific fragility curves, respectively. Results are obtained for three different dike sections in the Western Scheldt. The new calculated fragility curves for macro-stability and piping are presented and analyzed in the first sections of this chapter. In the last part, the implications of the reinforcement cost are presented.

4.1. Fragility curves for macro-stability

Applying the proposed methods results in the fragility curve depicted in Figure 4.1. The assigned typology for section DP745 and the water level probability density function (PDF) used for reference are shown alongside the site-specific curve. The low sea level rise scenario, with water level statistics for 2023, as calculated for Kennisprogramma Zeespiegelstijgin (KP-ZSS), is used to construct the water level PDF of each section. Each fragility curve has a secondary axis for the water level PDF.

Section DP745

The new fragility curve for section DP745 can be found in Figure 4.1. What can be seen is that the site-specific fragility curve is located more to the higher water levels compared to the typology-defined fragility curve. However, the slope of the site-specific curve is lower than that of the typology-based curve. As a result, the site-specific curve has more overlap with the water level PDF. Figure 4.2 provides a zoomed-in view of the lower tail of the curves.

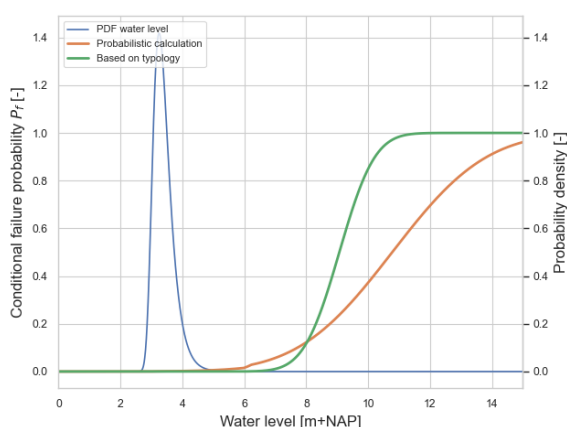


Figure 4.1: Fragility curve with site-specific calculation and typology for macro-stability (section DP745)

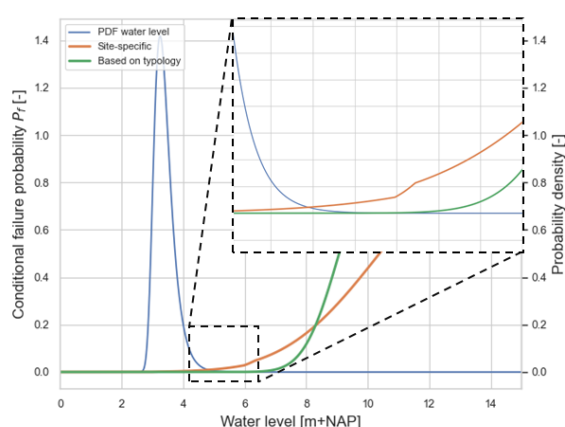


Figure 4.2: Zoomed-in view of the lower tail of the fragility curves for macro-stability (section DP745)

Section DP399

Figure 4.3 shows the newly constructed fragility curve for the failure mechanism macro-instability at section DP399. The result of the new analysis is compared with the typology-defined fragility curves. It can be observed that the new fragility curve developed for macro-stability demonstrates a significant difference compared to the assigned type of the section. First, and most importantly, the site-specific calculated curve is located far more to the right than the typology-defined curve, indicating that higher water levels are needed for the dike section to fail. Second, the slope of the curve is slightly greater than the type 4 curve, indicating a smaller degree of uncertainty.

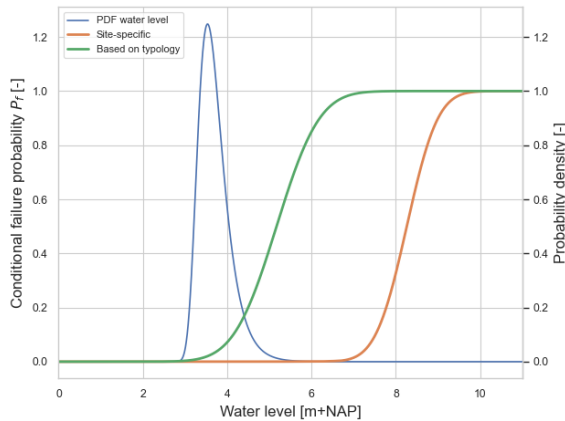


Figure 4.3: Fragility curve with site-specific calculation and typology for macro-stability (section DP399)

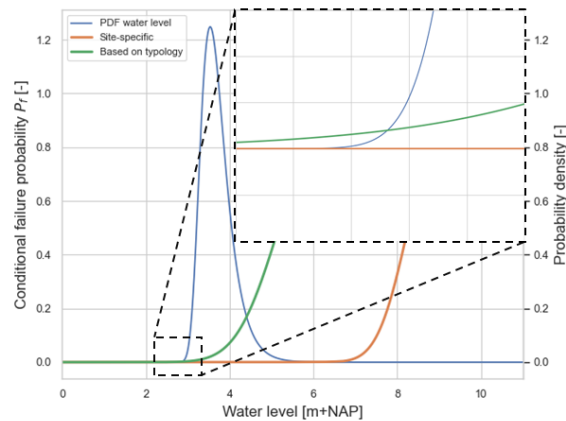


Figure 4.4: Zoomed-in view of the lower tail of the fragility curves for macro-stability (section DP399)

Section DP167

The corresponding fragility curve associated with macro-stability for section DP167 is depicted in Figure 4.5. The most notable thing is the large difference in the location of the curves. In this case, the site-specific curve is located more to the lower water levels, suggesting lower section reliability than when the typology curve is used. It can be observed that the slopes of both curves are comparable.

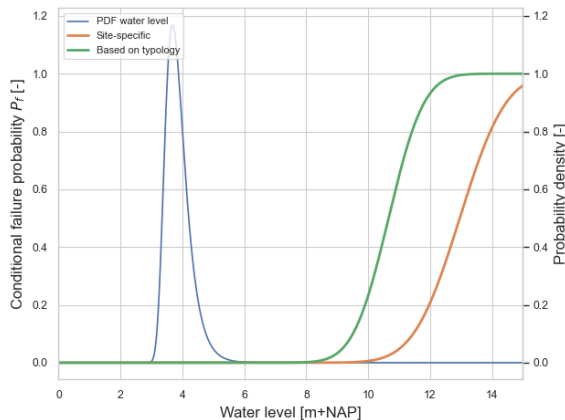


Figure 4.5: Fragility curve with site-specific calculation and typology for macro-stability (section DP167)

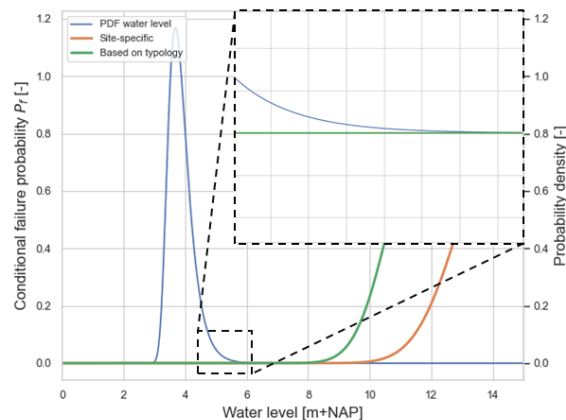


Figure 4.6: Zoomed-in view of the lower tail of the fragility curves for macro-stability (section DP167)

Failure probabilities

The failure probabilities are computed to compare the reliability between the site-specific calculated fragility curves and the typology-defined curves of each section better. Applying the integration method given by Equation 2.6, the yearly failure probability of each section is computed. The resulting failure probabilities are shown in Table 4.1. As expected from the curves displayed in Figure 4.3 and Figure 4.5, the new site-specific calculated fragility curves result in a reduction in failure probability, as opposed to

the typology fragility curves. It is worth highlighting that for section DP745, using site-specific calculation increases failure probability by a factor 10^5 . However, it should be noted that these differences are relative. Considering the probabilities, they are already small, so big differences at low probabilities have less significance compared to the same difference between larger probabilities (e.g., the difference between 10^{-1} and 10^{-2} has more impact than the difference between 10^{-3} and 10^{-4}).

Table 4.1: Failure probabilities for the site-specific calculated fragility curves and typology-defined fragility curves for the failure mechanism macro-stability

Section	Failure probability with site-specific calculation	Failure probability with typology
DP745	$1.89 \cdot 10^{-3}$ per year	$7.31 \cdot 10^{-8}$ per year
DP399	$7.88 \cdot 10^{-6}$ per year	$5.07 \cdot 10^{-2}$ per year
DP167	$1.63 \cdot 10^{-10}$ per year	$1.41 \cdot 10^{-8}$ per year

4.2. Factors of influence macro-stability

This section aims to investigate and analyze the factors that influence the outcome of the reliability analysis, thus the fragility curve. Identifying and evaluating these factors contribute to understanding the reliability of the investigated dike sections and gaining insight into the differences between the site-specific fragility curves and the typology-defined ones.

4.2.1. Influence coefficients

In the results of D-Stability, α -values (influence coefficients) are provided for several stochastic variables. The α -value indicates the degree of influence of the stochastic parameter on the calculated failure probability. The α -value ranges between -1 and 1, where negative values correspond to loads and positive values correspond to strengths. The closer the α -value is to -1 or 1, the greater the influence of the respective parameter on the failure probability. In Figure 4.7, the contribution of each stochastic solicitation variable with at least 5% contribution is given for all three dike sections. The chart represents the alpha values squared and multiplied with 100%. The calculations show that the failure probability is, in all cases, very sensitive to the pre-overburden pressure (POP), the model factor and to a lesser extent, the shear strength ratio S of the blanket layer.

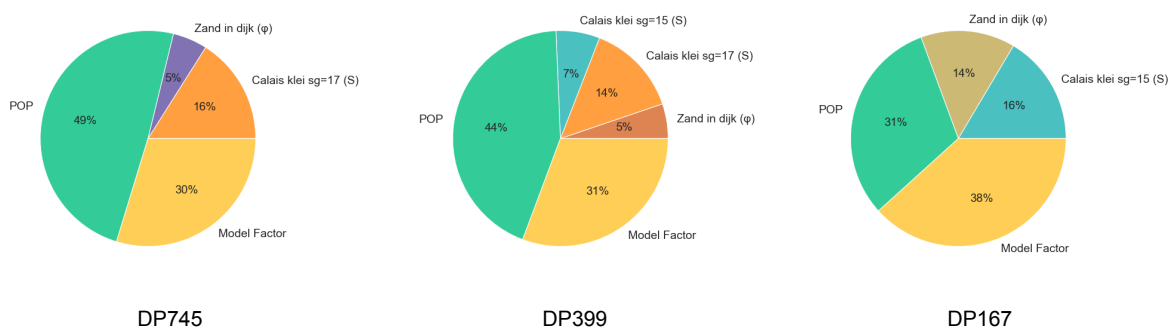


Figure 4.7: Influence of the stochastic variables of macro-stability for water level at the lower part of the berm

The magnitude of the α -value somewhat reflects the contribution of a soil type to the portion of the slip circle. When a significant portion of the slip circle passes through a particular soil type, this is reflected in a higher α -value. This is visible in the calculation with the extreme water levels 0.3 m below the crests (Figure 4.8), where a relatively large shift of the slip circle occurs and the contribution of certain layers disappears. In the case of DP167, the circle moves to a deeper layer and a different soil layer becomes important.

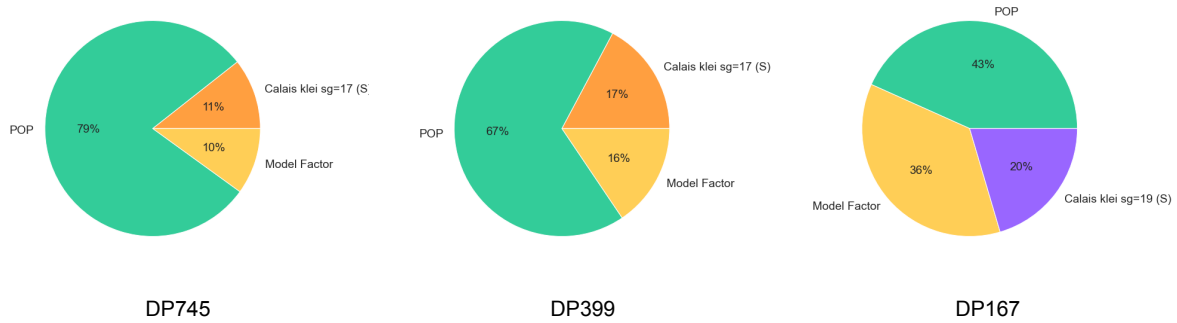


Figure 4.8: Influence of the stochastic variables for macro-stability for a water level 0.3 m under crest height

4.2.2. Comparison river dike sections

To better understand how typology-defined fragility curves can be applied, it's important to distinguish between the parameters used to create these curves in river areas and those used to develop the new site-specific curves. This clarification will provide valuable insight into the applicability of these curves.

Examining the pre-overburden pressure (POP) in Figure 4.9, it can be observed that the lower values along the coast are larger than the POP values used for the typologies. Another noticeable aspect is that the standard deviation for the site-specific fragility curve is larger. Considering these deviations, this explains why the POP value is important.

Looking at the friction angle of the core material depicted in Figure 4.10, an important factor in determining the resistance of sliding for macro-stability, it is evident that the mean values and standard deviations used for the site-specific calculated curves and the typologies are very similar.

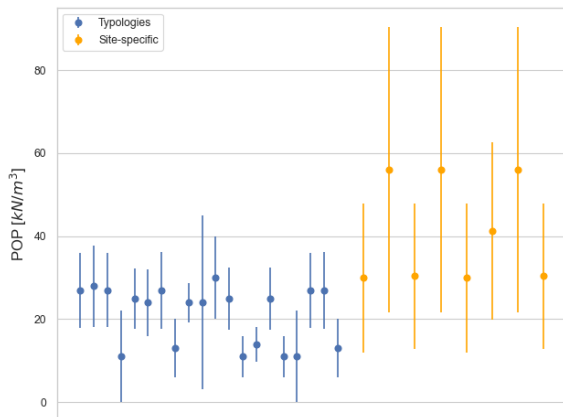


Figure 4.9: Pre-overburden pressures (POP) typology-defined fragility curves and site-specific fragility curves with one standard deviation error bar

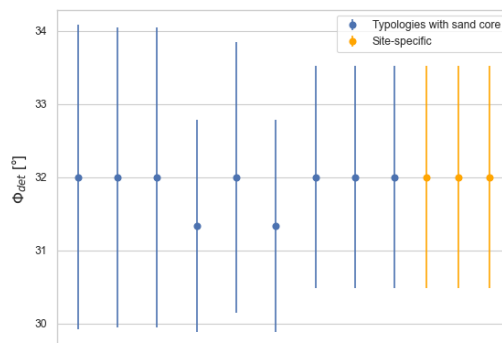


Figure 4.10: Friction angle core material typology-defined fragility curves and for the site-specific fragility curves with one standard deviation error bar

In Figure 4.11, it can be observed that when the dimensions of the dikes are taken into account, it is as expected that the cross-sections of the sea dikes are significantly higher. There is approximately a 2 meter difference between the tallest dike in the river area and the lowest river dike considered in the new site-specific fragility curves.

It can be seen that two out of three cross-sections of the dike are 5 metres wider than the longest distance in the river area when comparing the width of the dike sections from the centre of the crest to the inner toe (Figure 4.12). However, it is interesting to note that the ratios for the cross-sections under consideration, depicted in Figure 4.13, are comparable in size to those of the cross-sections in the river area when comparing the height to the specified width.

The last parameters to compare are regarding the blanket layer in the stability analysis since this layer acts as a counterforce. In Figure 4.14 and Figure 4.15, the thickness and weight per square meter of

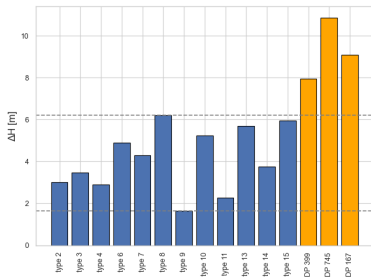


Figure 4.11: Height difference crest and hinterland

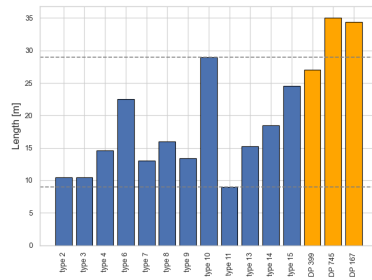


Figure 4.12: Length from the middle of the crest to the inner toe

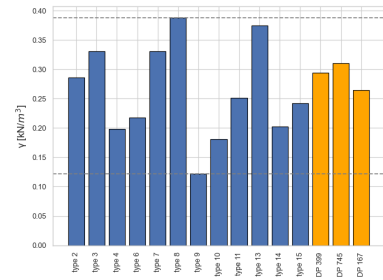


Figure 4.13: Ratio height difference and crest to toe length

the blanket are given. Figure 4.16 presents the shear strength ratio of the most contributing soil in the blanket. What can be noted is that there is a big variation in blanket thickness and weight, but no clear distinction between the typologies and site-specific calculations is found. The same holds for the shear strength ratio.

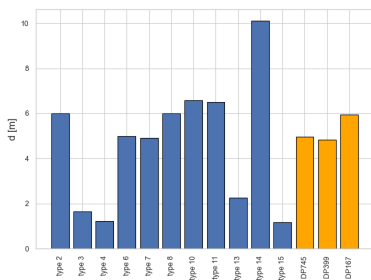


Figure 4.14: Thickness of the blanket layer

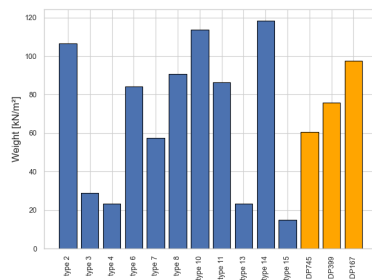


Figure 4.15: Weight of the blanket layer (thickness times volumetric weight)

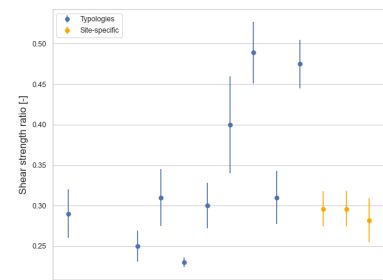


Figure 4.16: Shear strength ratio of the most contributing undrained soil layer in the blanket

4.3. Fragility curves for piping

The newly computed piping fragility curves are compared to the assigned typology fragility curve for the associated section and are presented in this section. As for the graphs regarding macro-stability, the fragility curves and the water level PDF for piping are presented similarly.

Section DP745

The result for section DP745 is given Figure 4.17. The figure shows that the fragility curve based on typology and the site-specific look similar. The slope of the site-specific curve is less steep and the site-specific fragility curve is located more to the right. Zooming in on the tail of the curve (Figure 4.18), it is observed that the new fragility curve has more overlap with the water level PDF, indicating lower reliability.

Section DP399

Figure 4.19 illustrates the fragility curve for section DP399, derived using site-specific calculations. Once again, the new curve is shifted to the right compared to the typology-based curve. The big difference in fragility curves suggests a great difference in failure probability. Zooming in on the tails of the curves as in Figure 4.20, it can be seen that both curves have limited overlap with the water level PDF. However, the typology curve still displays greater overlap, resulting in a higher probability of failure relative to the site-specific curve.

Section DP167

Figure 4.21 presents the fragility curves for section DP167, illustrating that the site-specific curve is located at the lower water levels in comparison to the typology-based fragility curve. Again a zoomed-in view of the lower tails is displayed in Figure 4.22 for indicative purposes. It is clear that the site-specific curve has lower reliability as opposed to the typology fragility curve.

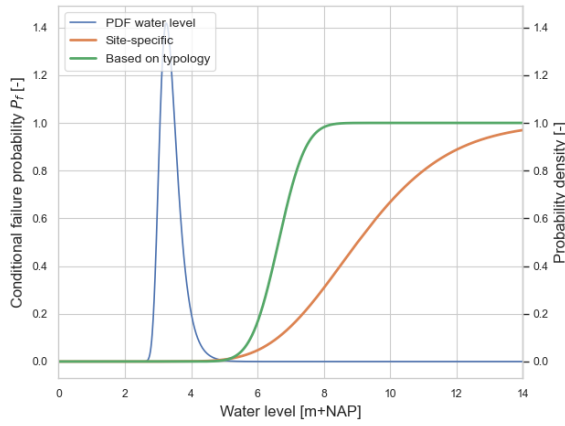


Figure 4.17: Fragility curve with site-specific calculation and typology for piping (section DP745)

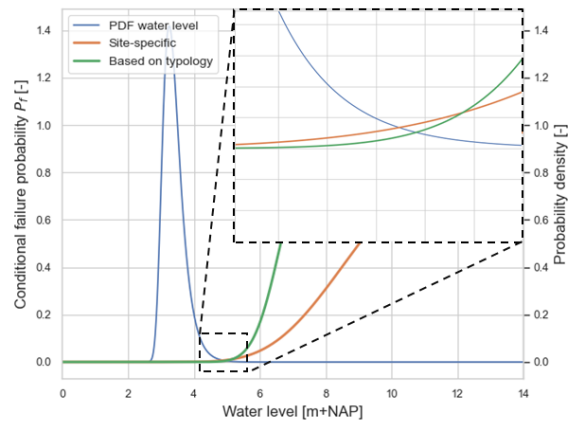


Figure 4.18: Zoomed-in view of the lower tail of the fragility curves for piping (section DP745)

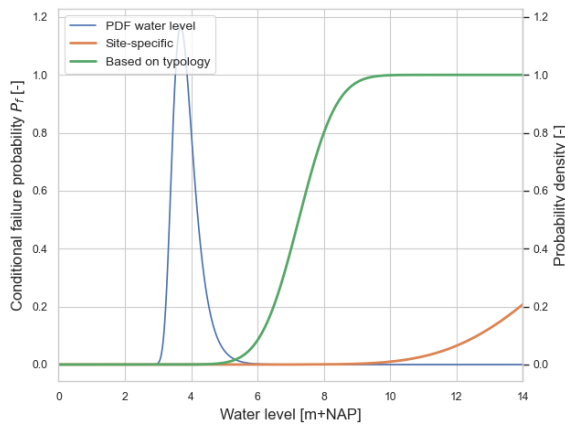


Figure 4.19: Fragility curve with probabilistic calculation and typology for piping (section DP399)

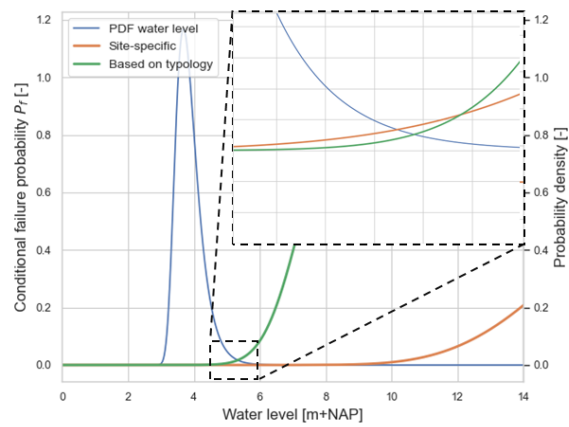


Figure 4.20: Zoomed-in view of the lower tail of the fragility curves for piping (section DP399)

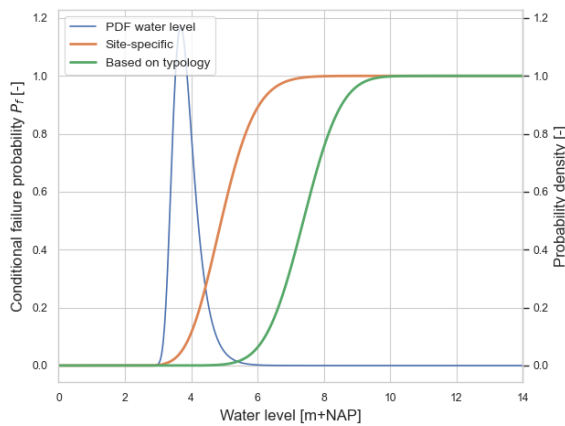


Figure 4.21: Fragility curve with site-specific calculation and typology for piping (section DP167)

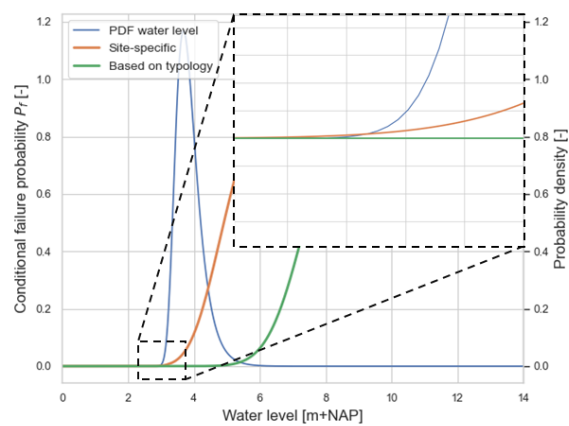


Figure 4.22: Zoomed-in view of the lower tail of the fragility curves for piping (section DP167)

Failure probabilities

Like in Section 4.1, the failure probabilities for each section and fragility curve are calculated. When analyzing Table 4.2, notably, the failure probability increases when the site-specific fragility curve is used instead of the typology for two of the three sections. For section DP745, the failure probability increases with a factor 10^3 and a factor 10^4 for section DP167. Implying the typology-defined curves overestimate the resistance of these sections. While for section DP399 the curves may suggest otherwise, the difference in failure probability (a factor 10^3) is less than expected. This can be explained, as described previously when examining the overlap of the tails with the water level PDF. The overlap of both curves is relatively small.

Table 4.2: Failure probabilities for the site-specific fragility curves and typology-defined fragility curves for the failure mechanism piping

Section	Failure probability with site-specific calculation	Failure probability with typology
DP745	$3.05 \cdot 10^{-2}$ per year	$4.97 \cdot 10^{-5}$ per year
DP399	$1.53 \cdot 10^{-7}$ per year	$6.32 \cdot 10^{-4}$ per year
DP167	$1.13 \cdot 10^{-2}$ per year	$4.18 \cdot 10^{-4}$ per year

4.4. Factors of influence piping

4.4.1. Influence coefficients

Looking at the fragility curves for the three sub-mechanisms of piping (Figure 4.23), it can be observed that the fragility curve for Sellmeijer at section DP745 and DP399 has the lowest failure probability for each water level. This sub-mechanism dominates the fragility curve since the probability of failure for a dependent and parallel system is determined by the lowest probability for each water level, as explained in Figure 3.9.

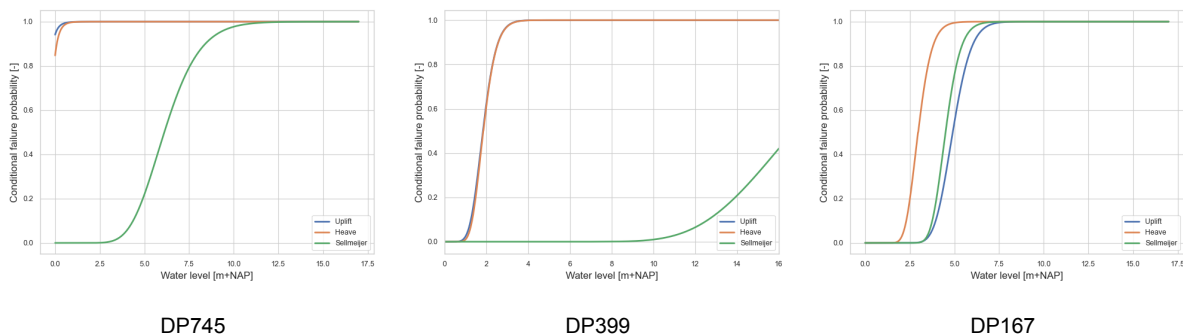


Figure 4.23: Fragility curves of for the failure mechanism piping

The importance factors from the First Order Reliability Method (FORM) analysis for the sub-mechanism Sellmeijer are presented in Figure 4.24. Note that the importance factor of the water level is excluded from the results since the water level is taken as a deterministic value.

Based on the analysis, it can be concluded that for the failure mechanism piping, the influence of the hydraulic conductivity (k), model factor (m_p) and the seepage length (L) are dominant. The 70%-quantile of the grain size distribution (d_{70}) has to a lesser extent, influence on the failure probability for the sub-mechanism of Sellmeijer. For all three sections, the hydraulic conductivity has the same magnitude of influence, as well as for the seepage length and model factor.

The obtained results are not surprising, considering the selected coefficient of variance based on the provided data by the water board Scheldestromen and *Schematiseringshandleiding piping* Table 2.2. With the selected uncertainty with a coefficient of variance of 0.5, it is understandable that this hydraulic conductivity has such an influence. The coefficient of variance expresses the relationship between a stochastic variable's mean and standard deviation. It permits comparison of variates since it is free from

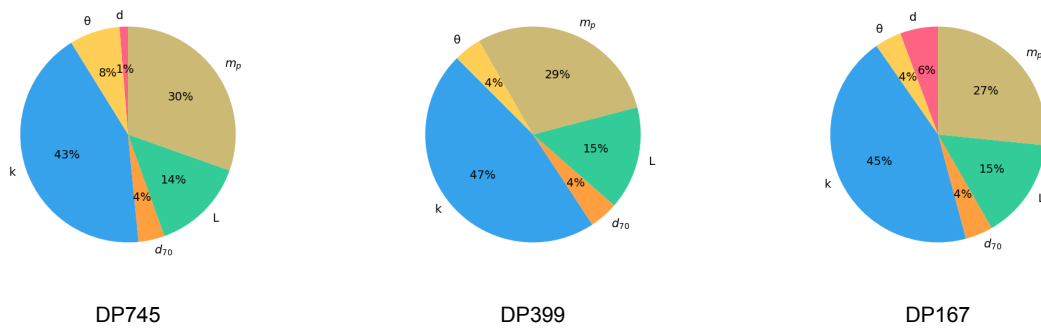


Figure 4.24: Influence of the stochastic variables for piping

scale effects; it is dimensionless (Brown, 1998). The same coefficient of variance for the aforementioned parameters is chosen for each reliability analysis, explaining the similarity in the charts displayed in Figure 4.24.

4.4.2. Comparison river dike sections

It was shown in the previous part that hydraulic conductivity (k) has a big impact on piping reliability analysis outcomes. Figure 4.25 presents the average value of the hydraulic conductivity used for the typologies and the site-specific curves, along with one standard deviation. It is clear that the Western Scheldt cross-sections display a lower k -value. Specifically, for cross-sections DP745 and DP399, this value is ten times smaller than the lowest value found in typologies based on the river area. Section DP167 demonstrates a comparable hydraulic conductivity, corresponding to the lowest value observed within the typologies.

The soil grain size distribution is an important physical property, having a great influence on the erosion and movement of water through the soil (Dong et al., 2022). Taking into account the 70%-fractile of the grain size distribution (d_{70}) and the hydraulic conductivity (k), the permeability of the soil can become apparent. Figure 4.26 shows the k -value plotted versus the d_{70} . The graph illustrates a consistent trend: higher values of hydraulic conductivity generally correspond to higher values of d_{70} , as expected. As can be seen, all three cross-sections in the Western Scheldt are located in the lower-left corner of the graph, indicating a low permeable soil compared to the typologies.

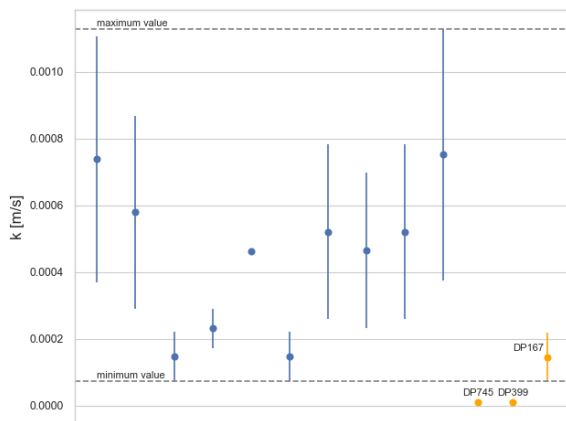


Figure 4.25: Hydraulic conductivity (k) with one standard deviation for the site-specific fragility curves (orange dots) and the typologies (blue dots)

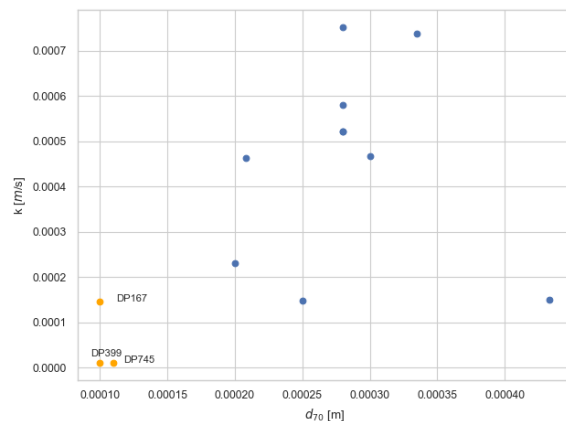


Figure 4.26: Hydraulic conductivity (k) vs d_{70} for the site-specific fragility curves (orange dots) and the typologies (blue dots)

While hydraulic conductivity provides information about the soil's permeability, the thickness of the permeable layer is also crucial in understanding the volume of water that can flow through the soil, which is important for piping. Transmissivity (kD), which is the multiplication of the hydraulic conductivity and the thickness of the soil layer, is therefore considered in the division into typologies.

Figure 4.27 shows the kD -values for the typologies and the site-specific computations with the border-lines for the typologies. When considering transmissivity, the difference between the cross-sections and the lowest value in the typologies becomes smaller compared to hydraulic conductivity. However, the smallest value in the typologies still exhibits a transmissivity three times greater (117 [m/d]) than section DP745 (29 [m/d]). The kD -value of section DP167 lies interestingly in between the two boundaries, indicating a more or less suitable typology-defined fragility curve could be assigned to this section.

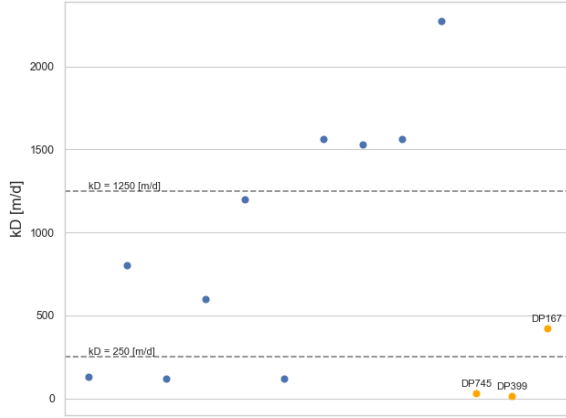


Figure 4.27: Transmissivity (kD) for the site-specific fragility curves (orange dots) and the typologies (blue dots)

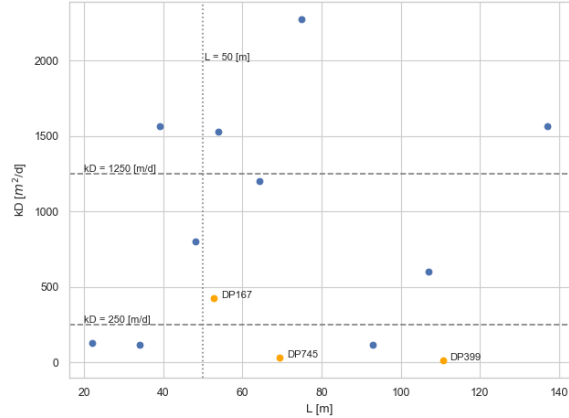


Figure 4.28: Transmissivity (kD) vs seepage length (L) for the site-specific fragility curves (orange dots) and the typologies (blue dots)

The other two characteristic properties of the typologies of piping are the blanket layer thickness and the seepage length. Figure 4.29 shows the seepage length of the typologies and site-specific calculations and Figure 4.30 the blanket layer thickness. Both figures show little distinction between the typologies and the examined cross-sections.

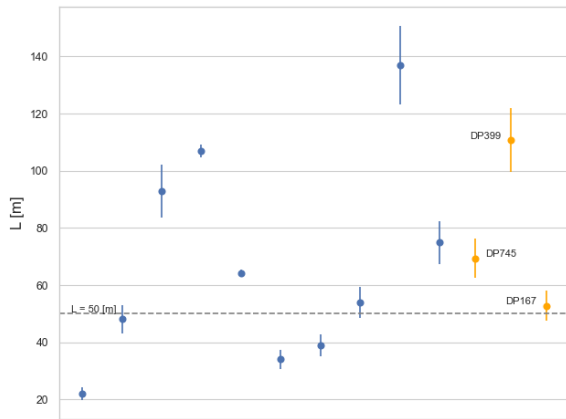


Figure 4.29: Seepage length (L) with one standard deviation for the site-specific fragility curves (orange dots) and the typologies (blue dots)

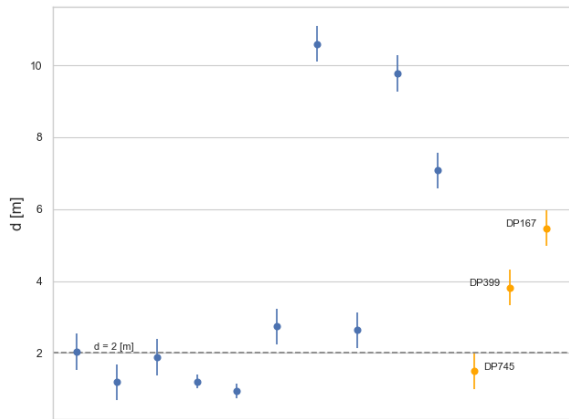


Figure 4.30: Blanket layer thickness (d) with one standard deviation for the site-specific fragility curves (orange dots) and the typologies (blue dots)

Results cost calculation

This chapter presents the results obtained from the analysis of the cost of reinforcement for the dike sections. The cost of reinforcement is a significant aspect to consider in comparing the two fragility curve methods. The first part of the section ignores the height requirement, while the second part includes it. The reinforcement scheme of *Hoogwaterbeschermingsprogramma* (2023) is neglected in the cost calculation.

5.1. Cost of reinforcement

This first section presents the results of the reinforcement calculation only for a situation considering the failure mechanisms macro-stability and piping. To gain a better understanding of the impact of the chosen fragility curve method, this paragraph delves deeper into one specific dike section and one scenario of sea level rise (SLR).

Figure 5.1 presents the failure probability progress and reinforcement cost for section DP745 in the low SLR scenario. The left graph depicts the reinforcement cost in time, the y-axis represents the reinforcement cost, and the x-axis indicates the time. The other two graphs display the failure probability progress in time for both fragility curve approaches, where a saw-tooth pattern emerges because the failure probabilities increase over time due to SLR and reinforcements are needed to comply with the standards. In all three graphs, the stars on top represent a reinforcement step.

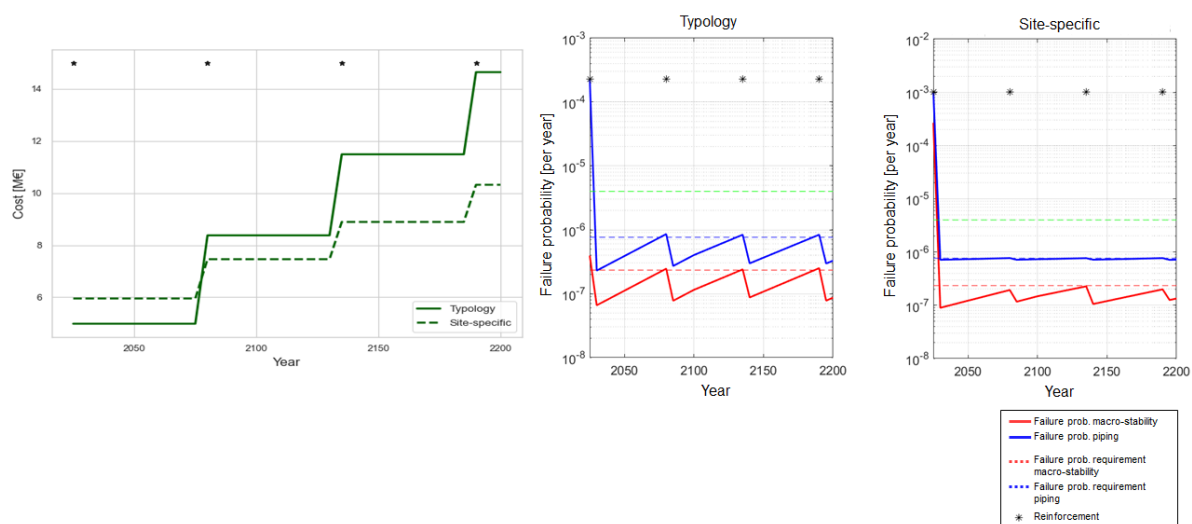


Figure 5.1: Cost of reinforcement in time and the failure probability progress for typology and site-specific fragility curve approach for SLR scenario low at section DP745

The figure demonstrates two things. First, the initial failure probability for the site-specific fragility curves, for both piping and macro-stability, resulted in higher initial investments for the site-specific fragility curve approach (dashed line). Second, each reinforcement step after the first reinforcement

round has a lower investment cost for the site-specific approach compared to the typology approach. The explanation for this difference has to do with the strength increase due to reinforcements; detailed information about this is given in Section 5.3.1. Looking at the reinforcement costs, it is clear that the site-specific fragility curve in the initial reinforcement round, on top of the innovative piping measure, also requires a measure to meet the requirements for macro-stability. This is done via a stability wall. In the case of the typology fragility curves, a small ground measure suffice to meet the requirements for the failure mechanism macro-stability. Piping also needs measures to comply with the standards, as can be seen from the failure probability progress graph for the typology approach.

5.1.1. Cost comparison

To better understand the dike reinforcement costs, the previous part of this paragraph only examined one dike section for one SLR scenario. However, this report considers multiple dike sections and scenarios. Figure 5.2 shows three plots for the reinforcement cost in time for the three sections. Each plot shows the cost of reinforcement under the four SLR scenarios. The solid lines represent the reinforcement cost if the typology-defined fragility curves are used, while the dashed lines represent the site-specific fragility curves.

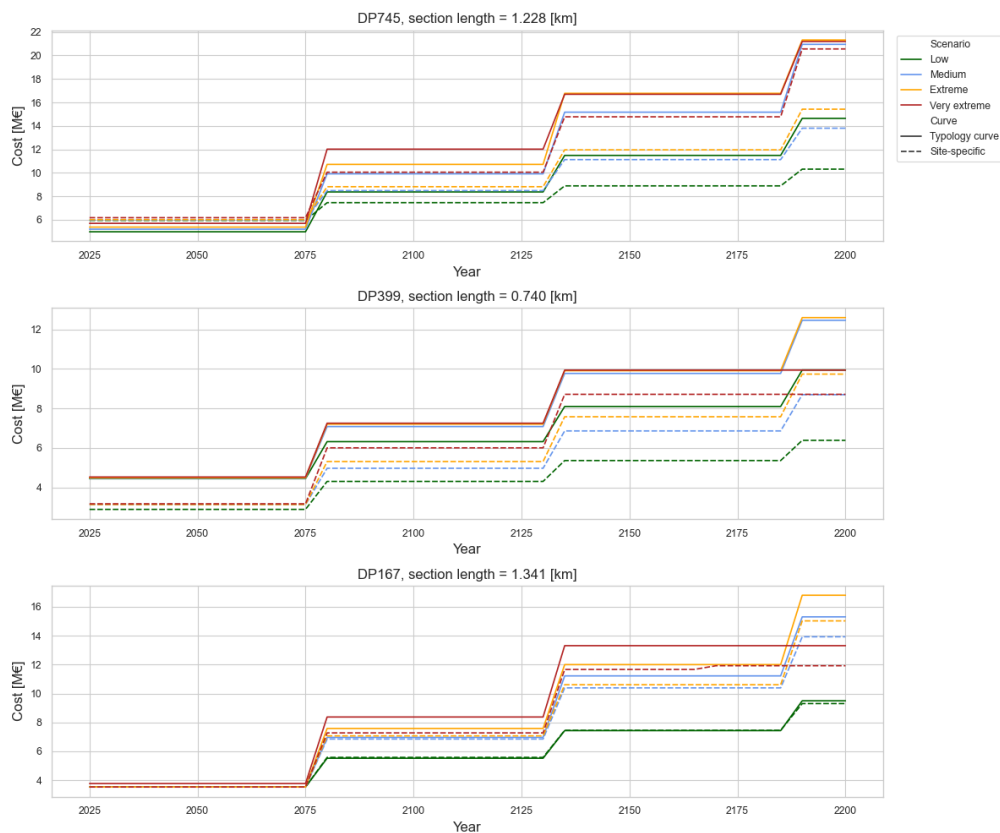


Figure 5.2: Reinforcement cost probabilistic calculated fragility curves and typology-defined fragility curves for each dike section under different sea level rise scenarios

What stands out is that in 2200, the costs for a heavier scenario do not necessarily result in the highest reinforcement costs. This can be observed with DP399 and DP167, where the medium and extreme scenarios appear to have higher reinforcement costs than the very extreme scenario. This seems counterintuitive, but these costs have not been adjusted to account for the residual value. For example, in the case of DP167, reinforcement has just been carried out when considering the medium and extreme scenarios (blue and yellow lines), while in the case of the very extreme (red line) scenario, this reinforcement is yet to take place. The next paragraph explains how the costs are adjusted to enable a fairer comparison of reinforcement costs.

5.1.2. Present value

When making an economic assessment, costs are often converted to present value. This conversion accounts for the time value of money. By considering the present value, the future cash flows associated with reinforcement costs are discounted, using a discount rate, to reflect their present-day value. The further an investment lies in the future, the less it contributes to the total present value. For converting the costs to present value, a discount rate of 1.6% per year is applied as used in KP-ZSS. Investments that are projected 50 years ahead now only contribute 45% to the present value if this discount rate is applied ($1 / 1.016^{50} = 0.45$) (Ministerie van Financiën, 2020).

The total reinforcement cost in 2200 is converted to present value with 2025 as the base year to compare the difference between the two fragility curve approaches. The residual value of the reinforcement, which represents the remaining worth of the reinforcement at the end of the duration of the analysis, is subtracted from the overall costs. The residual lifespan is determined as a percentage of the total lifespan of the reinforcement. The resulting present value using the site-specific approach is subtracted from the present value of the typology approach and divided by the typology-based present value.

To illustrate the impact of time on the reinforcement costs, Figure 5.3 (future value) and 5.4 (present value) depict the percentual differences between the two fragility curve approaches. In these figures, a positive difference indicates that the site-specific fragility curve approach results in fewer reinforcement investments compared to the typology-based approach. Looking at section DP745, the difference in reinforcement cost decreases when converted to present value. Where for scenario extreme, it was almost 30% in normal value, it decreases to just over 10% when considering present value. The differences for section DP399 stay approximately the same when converted to present value; only in the case of the SLR scenario very extreme does the percentual difference is almost twice as high.

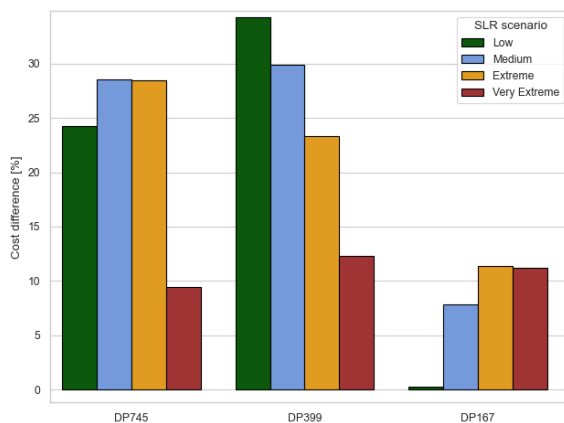


Figure 5.3: Percentual cost difference for reinforcement between probabilistic calculated and typology-defined fragility curves for the year 2200

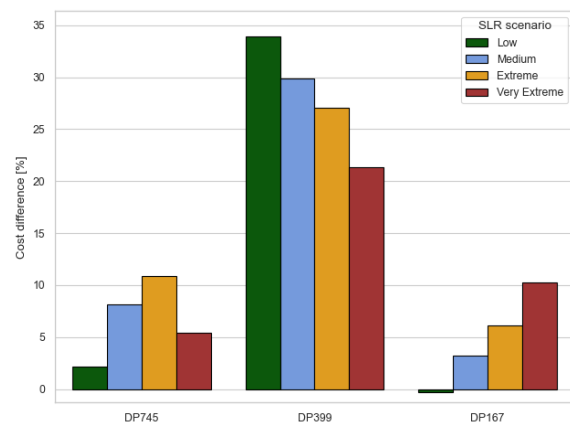


Figure 5.4: Percentual cost difference for reinforcement between probabilistic calculated and typology-defined fragility curves in present value with a discount rate of 1.6% for the year 2200

Table 5.1 provides the percentage differences for each section and sea level rise scenario. It presents the normal cost in the first column and the corresponding present value (PV) in the second column. What can be noted from this table is the small difference in present value for sections DP745 and DP167, with a maximum difference of approximately 10%. The biggest occurring difference is found for SLR scenario low at section DP399, displaying a difference of 34%. A more in-depth analysis on the driving factors of these differences is given in Section 5.3.

5.2. Inclusion height requirement

This section delves into the cost of reinforcing, incorporating height requirements into the cost calculation. Evaluating various factors such as dike dimensions and reinforcement types, gain insight into dominant factors determining dike reinforcement under sea different amounts of sea level rise. First, a comparison between the fragility curve approaches is made, and the cost analysis is presented in the second part.

Table 5.1: Percentual cost difference for reinforcement between probabilistic calculated and typology-defined fragility curves for the year 2200

	Low		Medium		Extreme		Very extreme	
		PV		PV		PV		PV
DP745	24 %	2 %	29 %	8 %	28 %	11 %	10 %	5 %
DP399	34 %	34 %	30 %	30 %	23 %	27 %	12 %	21 %
DP167	0 %	0 %	8 %	3 %	12 %	6 %	11 %	10 %

5.2.1. Cost comparison

Figure 5.5 shows three plots, each representing a different section. Again, the y-axis represents the reinforcement cost, while the x-axis indicates the time. Each plot displays the reinforcement cost under the four timelines of sea level rise. The probabilistic calculated fragility curves and typology-defined fragility curves are used to assess the cost variations of both approaches. It can be observed that for sections DP745 and DP399, the difference between the approaches is very limited and the moments of reinforcing run synchronously every 50 years. Section DP167 requires immediate reinforcements to meet the safety standards when using the probabilistic calculated fragility curves (dashed lines). In contrast, the typology-defined curves (solid lines) allow for a delay in the initial reinforcements. Also, section DP167 has a higher reinforcement cost for the probabilistic approach compared to the typology approach. It is important to note that the costs presented in these graphs are presented in normal costs and have not yet been converted into present value.

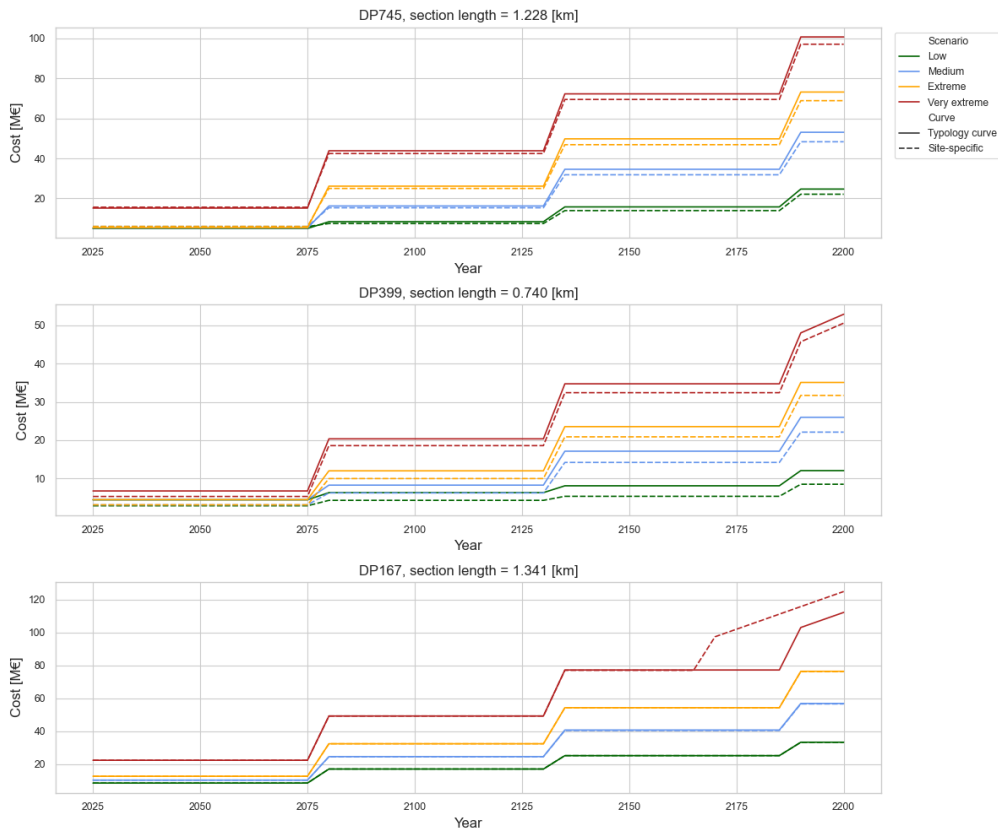


Figure 5.5: Reinforcement cost probabilistic calculated fragility curves and typology-defined fragility curves for each dike section under different sea level rise scenarios including height requirement

5.2.2. Present value

As described in Section 5.1.2, the cost is converted to present value. The percentual difference in present value is depicted in Figure 5.7, where a negative value means that the typology-based approach has a lower present value compared to the probabilistic approach (i.e. less expensive). To portray the influence of the timing of reinforcing, the percentual difference for normal (or future) values are presented in Figure 5.6 side by side with the percentual difference for the present value in 2200.

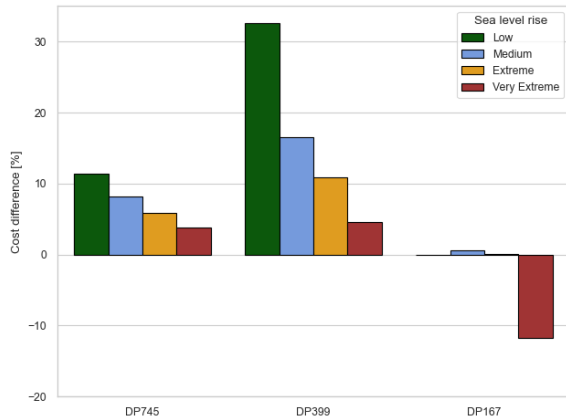


Figure 5.6: Percentual cost difference for reinforcement between probabilistic calculated and typology-defined fragility curves for the year 2200 including height requirement

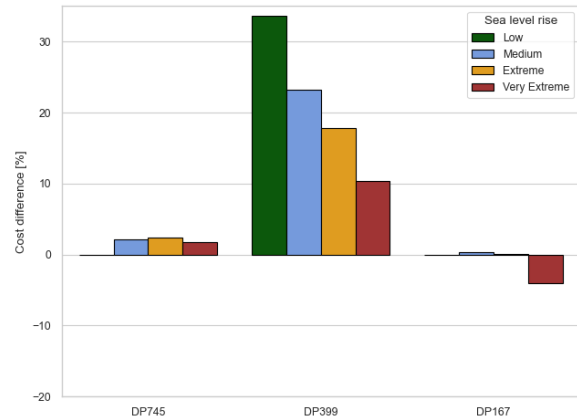


Figure 5.7: Percentual cost difference for reinforcement between probabilistic calculated and typology-defined fragility curves in present value with a discount rate of 1.6% for the year 2200 including height requirement

The percentual differences for each section and sea level rise scenario are presented in Table 5.2. The table includes the normal cost in the first column and the corresponding present value (PV) in the second column. For section DP745, the difference in cost between the approaches is already small. It decreases to a neglectable value for all four scenarios of sea level rise when looking at the present value. Looking at section DP167, the differences between the approaches are also negligibly small and remain approximately the same when converted to present value. Section DP399 has a greater difference in present value, indicating the typology-defined curves have a larger reinforcement nearer to the present, with the 30% difference for the sea level rise scenario low. This indicates that in this scenario, the use of the probabilistic fragility curves leads to a reduction in cost compared to the typology approach.

What is interesting is that for sections DP745 and DP399, the difference decreases with the increasing sea level rise scenario. This indicates that sea level rise is becoming more dominant. This does not hold for DP167, where in the very extreme scenario, the difference in cost between the approaches increases to 11%. Overall, if the mean is taken from all dike sections and SLR scenarios, a 7% decrease in cost is observed if the probabilistic calculated curves are used. If converted to present value, also a difference of 7% is found. Considering the most probable scenario, the difference in present value is 12%.

Table 5.2: Percentual cost difference for reinforcement between probabilistic calculated and typology-defined fragility curves for the year 2200 including height requirement

	Low		Medium		Extreme		Very extreme	
		PV		PV		PV		PV
DP745	11 %	0 %	8 %	2 %	6 %	3 %	4 %	2 %
DP399	33 %	34 %	17 %	23 %	11 %	18 %	5 %	11 %
DP167	0 %	0 %	1%	0 %	0 %	0 %	-12 %	-4 %

5.3. Cost analysis

In this section, a cost analysis is performed. The cost is then broken down into different components to gain insight into the key factors that influence the reinforcement costs. Furthermore, the cost is compared between the two fragility curve approaches to assess any differences or variations.

5.3.1. Strength increase in OKADER

To better understand the impact of the chosen fragility curve approach, it is important to relate the initial failure probabilities of the dike sections back to the reinforcement cost. Differences in the failure probabilities are shown in Table 5.3. What stands out, when combined with the difference in reinforcement cost in 2200 (see Figure 5.7), is the larger failure probability for the site-specific approach with a lower cost of reinforcing for section DP745. As for the other two sections, the fragility curve providing the lowest failure probability also initiates a lower cost in reinforcement. Interestingly, for section DP745, the failure probabilities for both macro-stability and piping are higher using the site-specific fragility curves compared to the typology-defined fragility curves.

Table 5.3: Comparison failure probabilities between the site-specific and typology-defined fragility curve approach

Section	Macro-stability		Piping	
	Site-specific	Typology	Site-specific	Typology
DP745	$1.89 \cdot 10^{-3}$ per year	$7.31 \cdot 10^{-8}$ per year	$3.05 \cdot 10^{-2}$ per year	$4.97 \cdot 10^{-5}$ per year
DP399	$7.88 \cdot 10^{-6}$ per year	$5.07 \cdot 10^{-2}$ per year	$1.53 \cdot 10^{-7}$ per year	$6.32 \cdot 10^{-4}$ per year
DP167	$1.63 \cdot 10^{-10}$ per year	$1.41 \cdot 10^{-8}$ per year	$1.13 \cdot 10^{-2}$ per year	$4.18 \cdot 10^{-4}$ per year

At first glance, the difference may seem odd. However, this can be explained by the way OKADER calculates reinforcements. OKADER needs additional fragility curves for different berm lengths to calculate how much berm length is required to comply with the standards. This allows OKADER to estimate the amount of reinforcement needed to meet the dike's requirements at a specific amount of sea level rise. In OKADER, the fragility curve is defined using a mean and standard deviation of the cumulative distribution function (CDF) of the standard normal distribution. The mean of the fragility curve corresponds to the water level at which the failure probability equals 0.5, hereafter mentioned as h^* . The typology fragility curve approach shifts h^* with predefined steps for different berm lengths, while for the site-specific approach, new fragility curves are computed with thus a new shift in h^* . Figure 5.8 displays for section DP745 this shift of h^* in the case of the failure mechanism piping, with a red arrow. In the figure, the intersection of the dashed line with the fragility curves is the water level h^* . In Figure 5.9, the shift for the piping fragility curves used in the typology approach is shown.

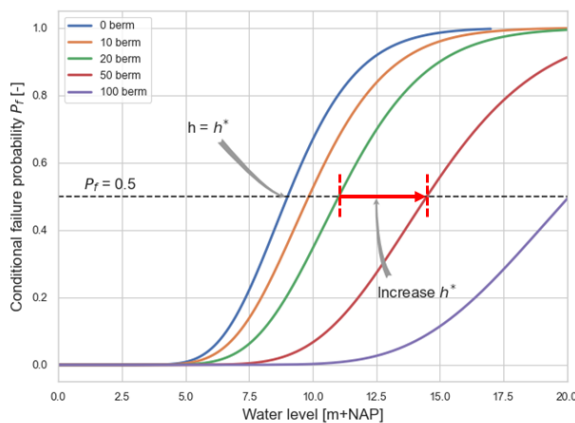


Figure 5.8: Increase in h^* with the addition of a piping berm for section DP745

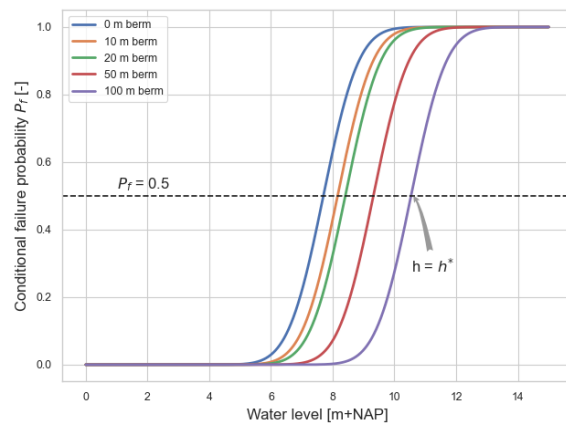


Figure 5.9: Predefined increase in h^* typology-defined approach

As mentioned before, when using the site-specific curve, the effect of these reinforcements is recalculated and incorporated into the fragility curves. The site-specific fragility curves have a notable greater increase in h^* for the same amount of reinforcement compared to the typology approach. In other words, the site-specific fragility curve requires less reinforcement than the typology curve to meet the same requirements, leading to lower reinforcement costs. The calculated increase of h^* under the influence of different berm lengths (illustrated by the red arrow in Figure 5.8) for all three sections and the typology approach is visually depicted in Figure 5.10 for macro-stability and in Figure 5.11 for piping.

In both figures, the blue line represents the increase of h^* under the addition of a certain berm length, as modelled by the typology-defined approach. The other three lines are for the considered sections. While for piping, more calculations with different berm lengths can be performed rather quickly, thus creating a more smooth line, macro-stability has computationally more expensive calculations. Thus, only new calculations for macro-stability are done using a 5 m berm and a 10 m berm, hence the kink in the graphs in Figure 5.8.

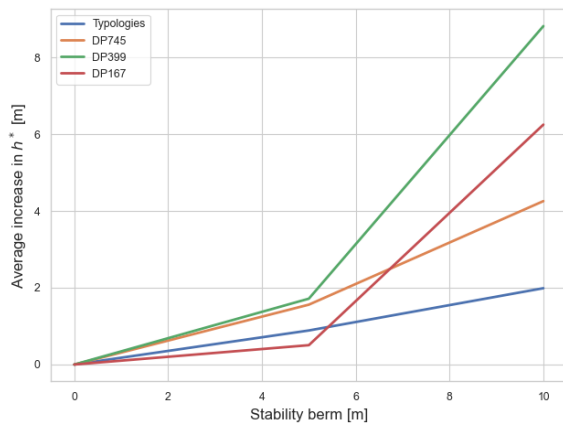


Figure 5.10: Increase in h^* as a function of a stability berm

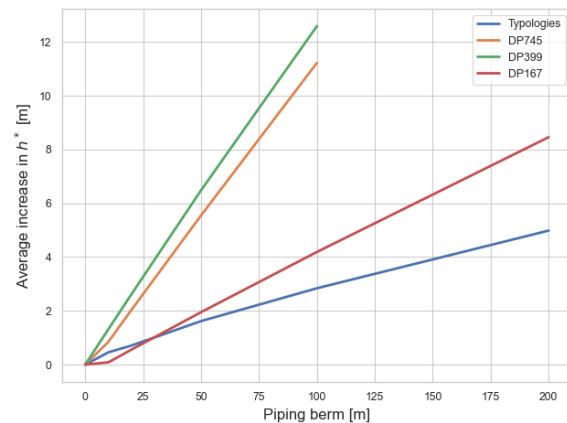


Figure 5.11: Increase in h^* as a function of a piping berm

To illustrate the impact of the strength increase due to a berm, new calculations are performed using the increase of h^* as modelled by the typology approach (the blue line in Figure 5.10 and Figure 5.11). The percentual difference between the typology-defined fragility curve approach and the site-specific fragility curves with the strength increase is shown in Figure 5.13. A significant increase in difference can be noted for section DP745. In the case of a low SLR scenario, the difference with the typology approach increases from 0% to -47%, meaning the site-specific approach is more expensive in this case. This difference arises from the fact that for macro-stability and piping, section DP745 has a much higher probability of failure compared to the typology-defined curves. For the other two sections, the change in difference is not that significant. However, if the average over all scenarios and OKADER sections is taken, a difference of -5% is observed, which is still negligibly small.

5.3.2. Factors determining reinforcement cost

The final cost of reinforcing a dike is affected by several factors. In Figure 5.14, you can see a breakdown of the factors that determine the total in the case of the low SLR scenario. The calculated cost of reinforcing in these graphs is for the case when only macro-stability and piping are considered.

The "Ground measures" refer to the expenses needed for earthen reinforcements, like heightening and widening the dike body. "Infrastructure" refers to the existing road infrastructure, including all connections, entrances, and exits. The consequence of the presence of road infrastructure on or in the expansion zone of the dike is that the existing infrastructure must be replaced, relocated, or repaired when modifying or expanding the dike.

Where a regular piping measure is constructed using an earthen embankment, the "Innovative piping measure" addresses the piping problem in the vertical direction in the form of vertical impermeable geotextile or a coarse sand barrier. In this case, only limited space is required at the inner toe of the dike. The other three measures are structural ones and are more self-explanatory in their meaning.

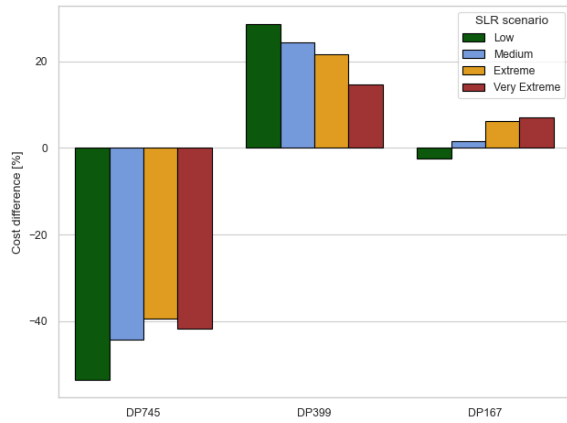


Figure 5.12: Percentual cost difference present value for reinforcement between site-specific and typology-defined fragility curves using typology strength increase excluding height requirement using the increase in h^* from the typologies

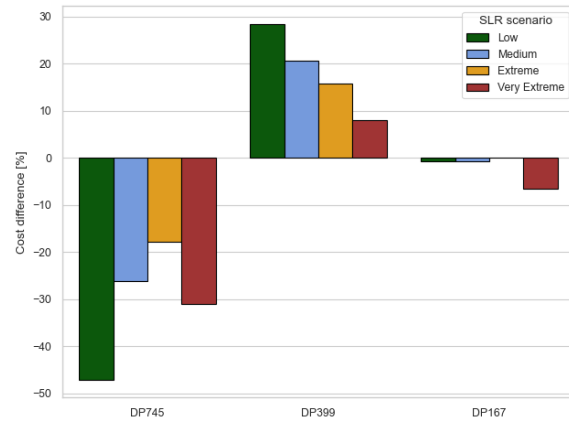


Figure 5.13: Percentual cost difference present value for reinforcement between site-specific and typology-defined fragility curves using typology strength increase including height requirement using the increase in h^* from the typologies

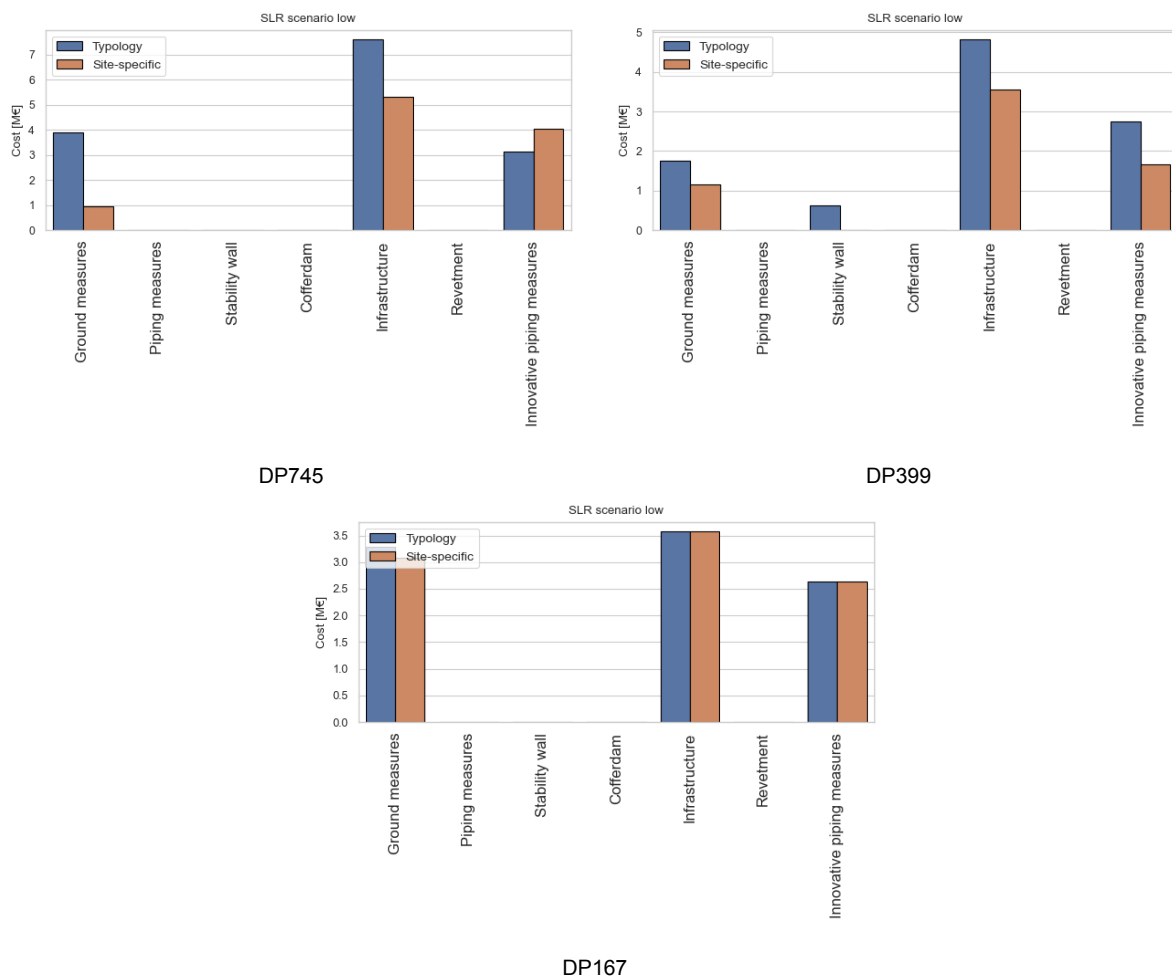


Figure 5.14: Cost of the elements determining the total reinforcement cost in 2200 under the SLR scenario low

Infrastructure

From the graphs in Figure 5.14, it can be seen that for all three sections, the infrastructure contributes the most to the reinforcement cost in the case of low SLR scenario. It can be noted that for both DP745 and DP399, the extra cost of infrastructure for the typology approach comes from the fact that more ground measures are taken to reinforce the sections. For DP167, both these factors have the same amount of cost regardless of the fragility curve approach.

The cost of the infrastructure is, in the case of low SLR, relatively high compared to the other measures because the other interventions required to meet the dike's standards are still relatively small in this scenario. Other differences in the cost can be observed for sections DP745 and DP399; for example, the higher investment cost for innovative piping measures at section DP745 for the site-specific fragility curves or the greater cost for ground measures at section DP399 for the typology approach.

When the height requirement is also included in the cost calculation (see Figure 5.16), it can be seen that here too, the infrastructure is a significant factor determining the cost, resulting in relatively small differences in reinforcement cost. For sections DP745 and DP399, there is a notable difference between the typology approach and the site-specific one. However, when the cost is converted to present value, the differences decrease significantly. Depicted in Figure 5.15, at each dike section, the first moment of reinforcing is for both fragility curve approaches the same, which contributes the most to the present value.

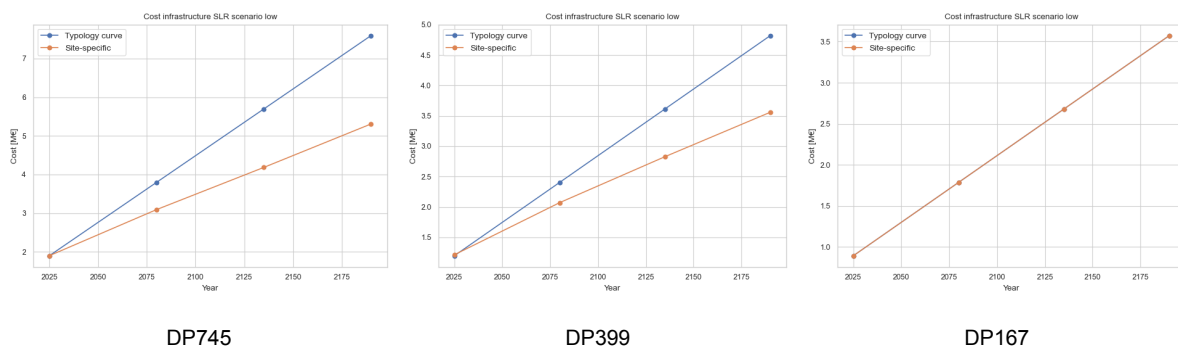


Figure 5.15: Cost of infrastructure over time for SLR scenario low for the case without the height requirement

Revetment

When considering all three failure mechanisms (height, stability and piping), the four factors that contribute to the costs are ground measures, infrastructure, revetment and innovative piping measures. The ratio of these factors is fairly comparable for all three sections. As stated before, looking at Figure 5.16, it can be observed that besides the infrastructure being an important aspect, the revetment becomes an important part of the total reinforcement cost when the height requirement is included in the cost calculation.

What can be observed from these graphs is the cost for the revetment is that for section DP399, the cost of the revetment has a smaller share of the total cost compared to the other two sections. This can be explained by looking at the crest elevation increase. In Figure 5.17, it can be seen that larger crest elevations are required for sections DP745 and DP167, which consequently leads to higher investment costs for the revetment.

In the case of a very extreme SLR, it becomes clear that the revetment plays a dominant role in all three sections. The bar graphs shown in Figure 5.18 explain the observed trend in Table 5.2 in the decrease in difference in the total reinforcement cost between the two fragility curve approaches when considering the increasing scenario of SLR. In each section, the cost of the revetment has a substantial contribution to the total reinforcement cost.

Currently, it is not possible to directly derive fragility curves and failure probabilities for revetments to use in OKADER to dimension the necessary measures for the outer slope separately. In the cost calculation, it is assumed that the revetment and outer slope are linked to the height requirements of the dike section (de Grave, 2022).

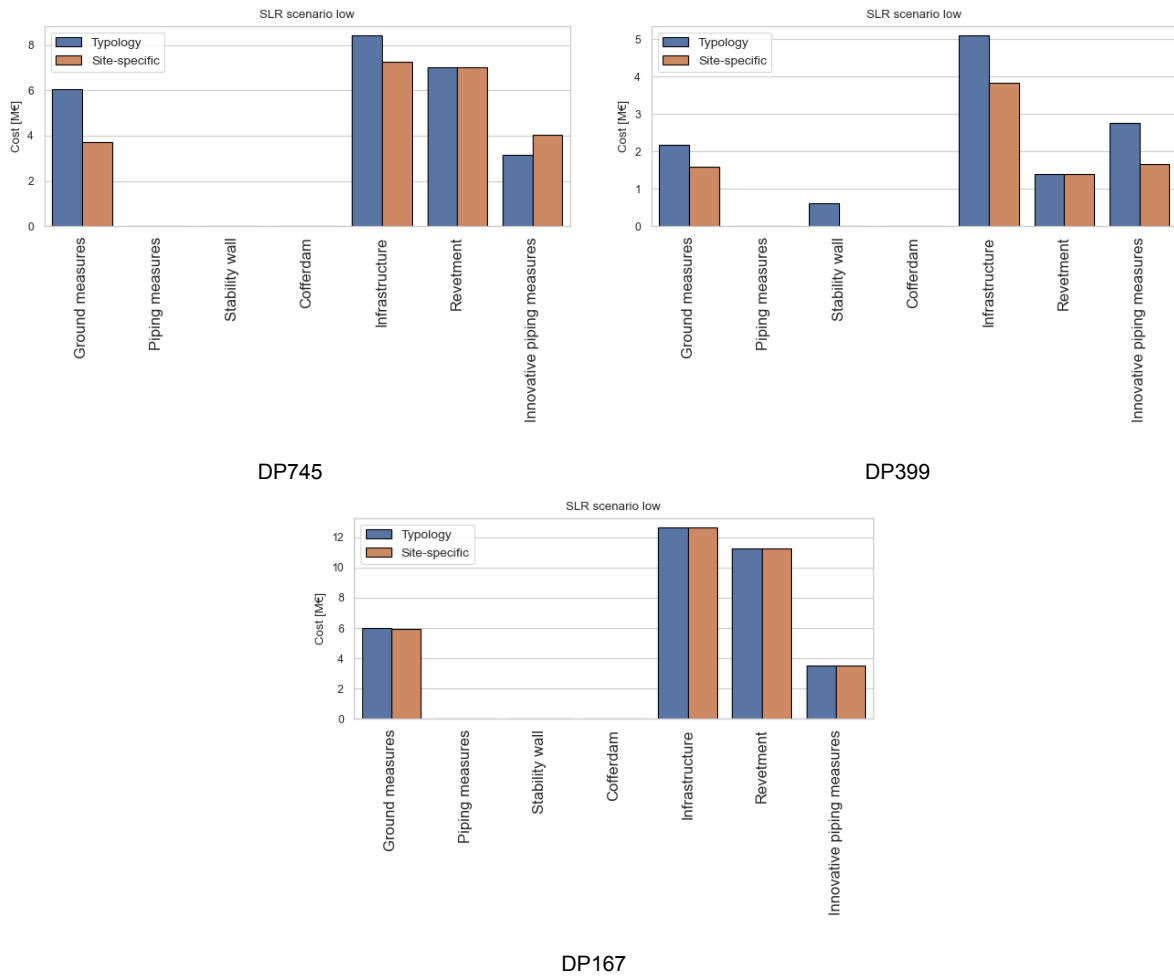


Figure 5.16: Cost of the elements determining the total reinforcement cost in 2200 under the SLR scenario low including height requirement

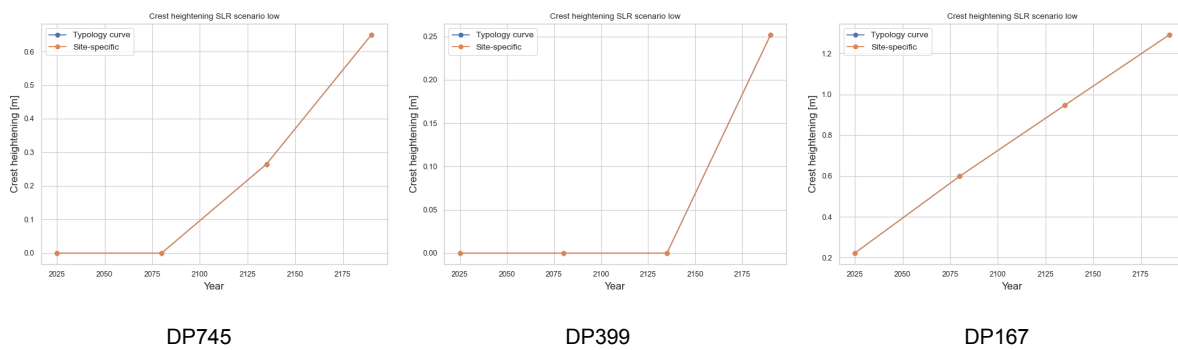


Figure 5.17: Required increase in crest height over time for all three sections

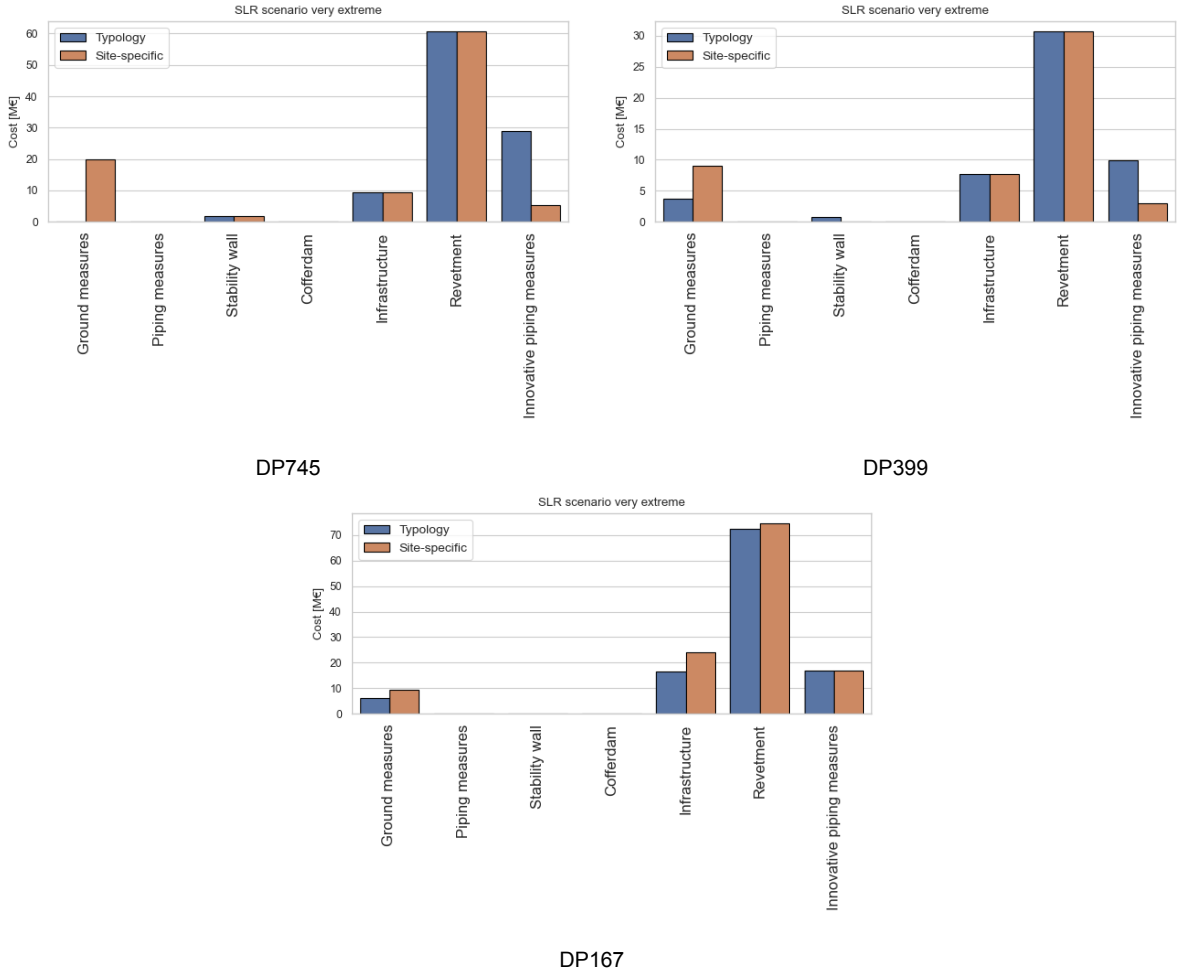


Figure 5.18: Cost of the elements determining the total reinforcement cost in 2200 under the SLR scenario very extreme including height requirement

As described above, as the sea level rises more quickly, the revetment predominantly determines the costs for reinforcing. Because these costs are associated with the increase in crest height, they are directly linked to sea level rise. The significant impact of the revetment (and consequently, the crest height) can be observed when comparing the calculated increase in required crest height, as determined by OKADER, with the corresponding computed cost of reinforcement.

Figure 5.19 illustrates the calculated reinforcements needed in time and the associated costs for sections DP167 under the scenario very extreme. The two graphs on the left represent the reinforcement calculations of OKADER, with the green line representing the reinforcements needed to comply with the standards regarding the crest height. On the right, the graphs for the total reinforcement cost are shown. For the other two regarded sections, the comparison can be found in Appendix H

What can be observed in Figure 5.19 is that the reinforcements for piping (blue line), stability (red line), and height (green line) are synchronized. The set design lifetime of 50 years, as explained in Section 3.6, can nicely be seen in the graph. When looking at the total costs for these reinforcements (Figure 5.20), it can be noticed that the shape of the line is predominantly dominated by the reinforcements needed for the height. This confirms the notion that the costs are dominated by the height factor as the sea level rises more rapidly. From Figure 5.21, it can be concluded that crest height increases the same for both approaches as expected since the water level statistic and hydraulic load level are the same for both calculations.

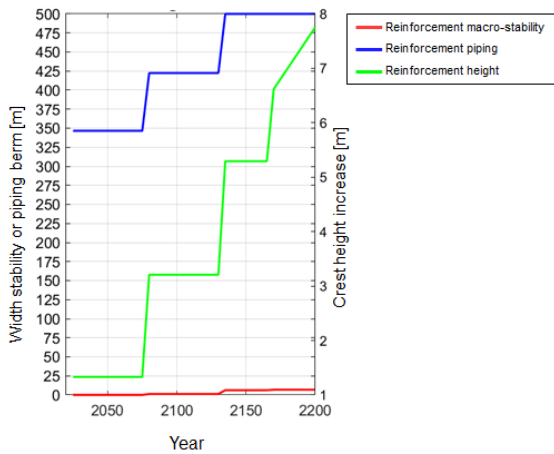


Figure 5.19: DP167: OKADER reinforcement requirements

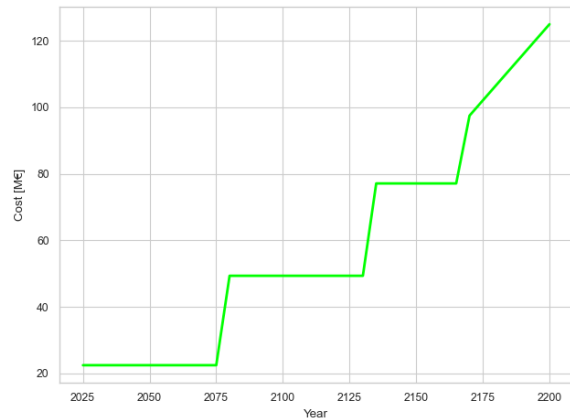
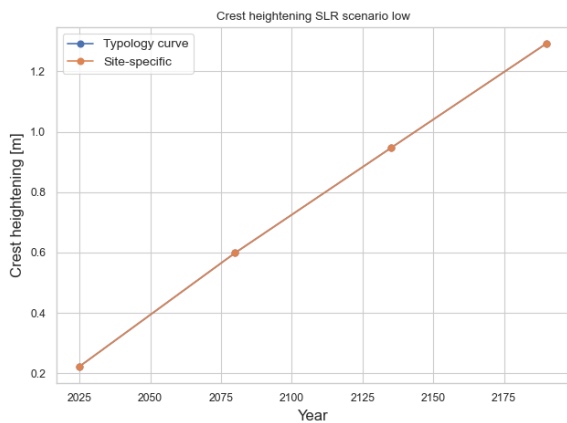
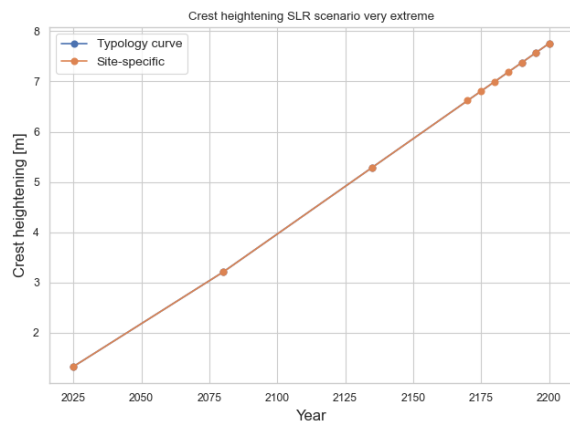


Figure 5.20: DP167: cost of reinforcement



SLR scenario low



SLR scenario very extreme

Figure 5.21: Crest height evolution for DP167 for SLR scenario low and very extreme

6

Discussion

The outcomes of this research have provided insight into the factors that influence the fragility curve, the difference in parameters used for the river-based typologies and the new reliability analysis for dikes in the Western Scheldt, and the difference in reinforcement cost for the two fragility curve approaches. The reliability analysis produces importance factors that explain how the parameters have an impact on the reliability. From the cost calculation, it becomes evident what are driving factors in determining the reinforcement cost under sea level rise.

A first notion is made regarding the computed failure probabilities for the site-specific fragility curve approach. Especially for the case of the failure mechanism piping at sections DP745 and DP167, it is noted that the computed failure probabilities are relatively large, contrary to what is expected in tidal areas. This study makes several critical assumptions which influence the results. The reliability analysis applies a steady-state assumption regarding the duration of the load. The loading duration around coastal dikes is lower, resulting in a different phreatic line than river dikes. Pol (2022) proposed including the time effect in the reliability analysis for piping. In the case of the piping failure mechanism, considering time-dependent effects can reduce the failure probability by a factor of 3 - 10⁴ for coastal dikes. While for macro-stability, van Leeuwen (2019) stated in her research: "It is, therefore, useful to take time dependency into account when determining the correct safety factor for impermeable dikes, but it is not useful in determining the correct safety factor for permeable dikes because a stationary calculation is sufficient". Because the cores of the dikes in the Western Scheldt primarily consist of sand, this study omits this aspect.

The reliability analysis produces importance factors explaining how the parameters impact the reliability. In the case of the failure mechanism piping, the parameter with the most significant influence was the hydraulic conductivity (*k*-value). The influence of this parameter originates from the uncertainty around the chosen parameter distribution, which is, in the case of the *k*-value, relatively high compared to the other parameters. As expected, the soil encountered in the tidal areas consists of finer sands with a smaller hydraulic conductivity and grain size than sands in the riverine areas. Tidal areas are influenced by the ebb and flow of tides, which create dynamic environments where finer sediment particles tend to accumulate. The continuous action of tidal currents effectively sorts the sediments, causing finer sands to dominate the soil composition in these regions. It was observed that the sections DP745 and DP399 had significantly smaller *k*-values compared to the typologies. Section DP167 had a *k*-value which was more comparable to the lower bounds of the *k*-values encountered in the typologies. Overall, none of the typologies has a suitable combination of *k*-value and seepage length for the considered sections.

The Sellmeijer calculation method used for the assessment is fitted based on tests conducted with homogeneous river sand. The research project conducted in the Hedwigepolder revealed that tidal sand is at least 40% stronger than the current calculation models indicated. It can be stated that tidal sand is demonstrably stronger than what can be expected based on the current Sellmeijer model. In the Western Scheldt, tidal sand has a significant presence, which means that the dikes in areas with tidal sand have, in reality, a lower probability of failure due to piping ("Dijken op getijdenzand: veel sterker dan gedacht", 2023; Hijma & Oost, 2019). This effect is not incorporated in this study and therefore, the failure probabilities do not truly represent reality.

Next to the hydraulic conductivity, the model factor for piping greatly impacts the reliability. The model factor concerns the modelling uncertainty of the dikes' ability to resist internal erosion. The Sellmeijer equation's theoretical assumptions about constant parameters for constant drag factor and internal friction angle, which are in actuality unknown and accounted for by the model factor, give rise to the model factor's significance. Including time dependency, tidal sands and other effects not discussed, like residual strength, will lead to more realistic results for the reliability analysis of piping.

In this research, the pre-overburden pressure (POP) is the most influential parameter on the failure probability for the site-specific fragility curves regarding macro-stability. The regarded POP values are, on average, higher for the sea dikes in the Western Scheldt than those in the typologies. As a result of temporarily changing water pressures and loads, the thin, soft soil layers can consolidate relatively well, leading to an expected higher limit stress. Additionally, the tidal influence and sea level rise positively affect the POP value, causing the characteristic values used in the typologies, which are based on a national database used for the typologies, to be comparably low.

Another critical factor to mention is that the influence of overtopping has also been neglected. This was initially reasoned from the perspective of Kennisprogramma Zeespiegelstijging (KP-ZSS) that it is not applicable. However, the phreatic line does impact the probability of failure, and infiltration through overtopping causes an elevated phreatic line, thereby increasing the probability of failure. Although not taken into account in the reliability analysis, a brief investigation was conducted for section DP399 to examine the effect of a change in the phreatic line on the failure probability, which can be found in Appendix G.

Despite significant differences in the calculated failure probabilities between the two fragility curve methods, the cost analysis reveals that using site-specific fragility curves only reduces costs by 19% in future value and 13% in present value averaged over all sections and SLR scenarios. Removing and replacing the existing infrastructure on and immediately behind the dike is the most significant cost component for reinforcing the dike sections. This results in relatively small differences between the two methods. Including the height requirement, the differences between the two approaches decrease to 7% in future value and 7% in present value averaged over all sections and SLR scenarios. The revetment, coupled with the height requirement, plays a significant role in the costs when adding the height requirement. Since this research used the same height requirement for both approaches, the percentual cost difference decreases. If the SLR scenario is very extreme, the cost for the revetment completely dominates the total reinforcement costs, leading to a negligible difference of 1% in future value and 3% in present value, averaged over the three sections.

In the case of the site-specific approach, new fragility curves with added reinforcement were calculated because OKADER needs different fragility curves to calculate the required reinforcement to comply with the standards. In contrast, the typology approach uses standardized shifts of the fragility curve. The shift of the site-specific fragility curve is, in two out of the three cases, larger compared to the standardized shift. Meaning that for the same increase in berm length, the site-specific fragility curve is more strongly reinforced. As a result, the site-specific fragility curve requires fewer reinforcements than the typology-defined curve to meet the same requirement, resulting in lower reinforcement costs. In the case of DP167, this compensates for the fact that the site-specific approach has lower reinforcement costs, even though the failure probabilities for macro-stability and piping are initially higher.

For the ultimate goal of Kennisprogramma Zeespiegelstijging, which includes assessing the total reinforcement needs of the Netherlands, the methodology using typology-defined fragility curves seems to be sufficient for dikes in the Western Scheldt since other factors, like existing roads, are more important. Almost all dike sections are accompanied by a road, which means that infrastructure costs will play a dominant role in all cases. Furthermore, the assessed dike sections primarily protect rural areas, thereby limiting the impact of space constraints in this study. However, the majority of areas around the Western Scheldt are also rural, indicating that this effect will likely play a smaller role in the total reinforcement costs of the Western Scheldt. It needs to be examined how the various cost components relate to each other when considering a coastal dike with limited available space, like urban areas.

Conclusion and recommendations

7.1. Conclusion

The main objective of this research was to compare the assessment of future reinforcement cost for sea dikes in the Western Scheldt using site-specific fragility curves versus typology-defined fragility curves. By constructing fragility curves for macro-stability and piping in three different dike sections across the Western Scheldt, this research aimed to assess the potential differences in cost predictions between the two approaches.

This research has shown that the typology-defined fragility curves underestimate the strength for macro-stability in two out of three cases with a factor 10^4 and factor 10^6 , while it overestimates it for the piping failure mechanism in two out of the three cases with a factor 10^3 and factor 10^2 . The pre-overburden pressure appeared as the most important factor influencing the failure probability of the macro-stability failure mechanism and was, on average, larger for the site-specific fragility curves. The failure mechanism of piping was most influenced by the hydraulic conductivity, where, as expected, much finer soils were encountered in the Western Scheldt with smaller values for the hydraulic conductivity.

From the results, it can be concluded that the use of site-specific fragility curves resulted in a decrease of 13% in present cost of reinforcement, averaging over all sea level rise scenarios until the year 2200. If the height requirement is included in the cost calculation, the difference decreases to 7%, averaging over all sea level rise scenarios. In Kennisprogramma Zeespiegelstijging, it is important to obtain information on the final dike dimensions and the associated reinforcement costs. Although the difference in the computed failure probabilities shows otherwise, the results indicate that the use of the typology-defined fragility curves does not lead to significantly different predictions in reinforcement costs for dikes in the Western Scheldt compared to the use of site-specific fragility curves.

The reinforcement cost depends on various factors. Looking purely at the reinforcements regarding macro-stability and piping, 'the infrastructure' has the largest contribution in terms of costs. 'Infrastructure' refers to the cost associated with replacing, relocating, or repairing the road infrastructure on or within the expansion zone of the dike when modifying or expanding it. If the same height requirement is included for the typology-defined approach and the site-specific approach, the cost for the revetment also becomes important. As the sea level rise scenario becomes more severe, the cost of revetment becomes dominant. This becomes apparent when considering the reinforcement costs in the very extreme scenario; the revetment dominates the costs for all three sections. The fixed costs mainly determine the costs of a dike reinforcement: the fact that you are going to reinforce a dike.

7.2. Recommendations

Based on the findings and conclusions presented in this thesis, further recommendations can be proposed to enhance and expand the current research, addressing potential areas for future exploration and improvement.

- The dominance in reinforcement cost is attributed to the revetment. It is recommended to adjust OKADER to calculate the revetment separately.
- Including time dependency, tidal sands and residual strength will improve the accuracy of the fragility curves.
- If more accurate results regarding the costs are needed, it is advised to construct 1 or 2 separate typologies for piping and include the reinforcements needed in the calculation since most dike sections in the Western Scheldt are similar in dimension and subsoil.
- This research is focused on the Western Scheldt with many rural parts. It is recommended to check the different cost components for dikes in urban areas.
- It is recommended to validate the models for Uplift-Van and Sellmeijer further in order to reduce the model factor.
- We can never get rid of uncertainty in the sea level rise predictions, but it can be minimised by updating the sea level rise predictions with measurements and implementing adaptive planning.

References

- Brown, C. E. (1998). Coefficient of variation. In *Applied multivariate statistics in geohydrology and related sciences* (pp. 155–157). Springer.
- Brus, D. J., Lamé, F. P. J., & Nieuwenhuis, R. H. (2009). *National baseline survey of soil quality in the Netherlands*.
- Casciati, F., & Faravelli, L. (1991). A knowledge-based system for seismic vulnerability assessment of masonry buildings. *Computer-Aided Civil and Infrastructure Engineering*, 6(4), 291–301.
- CETMEF, CIRIA, & USACE. (2007). *The international levee handbook*. CIRIA C 731.
- de Grave, P. (2021). *Gebruikershandleiding okader*. HKV + Deltares.
- de Grave, P. (2022). *Toepassingsleidraad okader voor KP-ZSS spoor ii*. Rijkswaterstaat.
- Deltares. (20014). *KOSTen voor versterken WATERkeringen*.
- Diermanse, F. (2016). *WBI - Onzekerheden, overzicht van belasting- en sterkteonzekerheden in het wettelijk beoordelingsinstrumentarium* (tech. rep.). Deltares.
- Dijken op getijdenzand: veel sterker dan gedacht*. (2023). <https://www.deltares.nl/nieuws/dijken-op-getijdenzand-veel-sterker-dan-gedacht>
- Discontovoet*. (2023). <https://www.rwseconomie.nl/discontovoet>
- Dong, Z., Mao, D., Ye, M., Li, S., Ma, X., & Liu, S. (2022). Fractal features of soil grain-size distribution in a typical tamarix cones in the taklimakan desert, china. *Scientific Reports*, 12.
- Duits, M. (2021). *Hydra-NL voor het Kennisprogramma Zeespiegelstijging*. HKV.
- Duits, M. (2022). *Hydra-NL op de Hollandsche IJssel*. HKV.
- Fiolet, D., Knops, D., Gensen, M., Dupuits, G., & Kindermann, P. (2022). *Landelijke set fragility curven t.b.v KP-ZSS*. Witteveen+Bos and HKV.
- Grave, P. d., & Baarse, G. (2011). *Kosten van maatregelen - Informatie ten behoeve van het project Waterveiligheid 21e eeuw*. Deltares.
- Helpdesk Water. (2017). *Hydraulische belastingen wettelijk beoordelingsinstrumentarium 2017*.
- Hijma, M., & Oost, A. (2019). *Getijdenafzettingen en piping: een quickscan*. Deltares.
- Hu, C., Youn, B., & Wang, P. (2019). *Engineering design under uncertainty and health prognostics*. Springer.
- HWBP*. (2023). <https://www.hwbp.nl/over-hwbp>
- Importance factors from FORM method*. (2022). http://openturns.github.io/openturns/master/theory/reliability_sensitivity/importance_form.html
- Informatiehuis Water. (2022). *Waterveiligheidsportaal*. Retrieved November 9, 2022, from <https://waterveiligheidsportaal.nl/#/nss/nss/current>
- IPCC. (2021). Summary for policymakers. *Climate Change 2021: The Physical Science Basis. Contribution of Working Group I to the Sixth Assessment Report of the Intergovernmental Panel on Climate Change*.
- Jongejan, R. (2017). *Wbi2017 code calibration* (tech. rep.). Rijkswaterstaat.
- Jonkman, S., Jorissen, R., Schweckendiek, T., & van den Bos, J. (2021). *Flood defences, lecture notes CIE5314*. TU Delft.
- Jonkman, S., Steenbergen, R., Morales-Nápoles, O., Vrouwenvelder, A., & Vrijling, J. (2018). *Probabilistic design: Risk and reliability analysis in civil engineering, lecture notes CIE4130*. TU Delft.
- Kanning, W., Teixeira, A., van der Krogt, M., & Rippi, K. (2016). *Derivation of the semi-probabilistic safety assessment rule for inner slope stability* (tech. rep.). Deltares.
- KNMI. (2021a). *Klimaat signaal '21: Hoe het klimaat in nederland snel verandert*.
- KNMI. (2021b). *Zeespiegel stijgt door na 2100*. <https://www.knmi.nl/over-het-knmi/nieuws/zeespiegel-stijgt-door-na-2100>
- Knoeff, H. (2016). *MEMO Faalkansbegroting*. Kennisplatform Risicobenadering.
- Kok, M., Jongejan, R., Nieuwjaar, M., & Tanczos, I. (2017). *Fundamentals of Flood Protection*. Ministry of Infrastructure; the Environment; the Expertise Network for Flood Protection.

- Kolen, B., Caspers, J., & Pol, J. (2021). *Actualisatie okader voor toepassing bij de IRM-MER*. HKV.
- Lebrun, R., & Dufloy, A. (2009). Do rosenblatt and nataf isoprobabilistic transformations really differ? *Probabilistic Engineering Mechanics*, 24, 577–584.
- Mahmood, Z., Qureshi, M. U., Memon, Z. A., & Imran Latif, Q. B. a. (2022). Ultimate limit state reliability-based optimization of mse wall considering external stability. *Sustainability*, 14(9).
- Map of the Netherlands with Provinces*. (2023). <https://freevectormaps.com/netherlands/NL-EPS-01-0002?ref=atr>
- Melnikov, R., Zazulya, J., Stepanov, M., Ashikhmin, O., & Maltseva, T. (2016). Ocr and pop parameters in plaxis-based numerical analysis of loaded over consolidated soils. *Procedia Engineering*, 165, 845–852.
- Ministerie van Financiën. (2020). *Rapport Werkgroep discontovoet 2020*. Rijksoverheid.
- Ministerie van Infrastructuur en Waterstaat. (2021). Kennisprogramma zeespiegelstijging.
- Oerlemans, C., Botterhuis, T., & Thonus, B. (2022). *Pilotfase RMM*. HKV.
- PBL. (2023). *Low probabilities - large consequences Reducing the vulnerability of the Dutch population to floods*. <https://themasites.pbl.nl/o/flood-risks/>
- Pol, J. (2022). *Time-dependent development of backward erosion piping* (Doctoral dissertation). <https://doi.org/10.4233/uuid:eb5ed3b2-4210-489e-b329-59722a0c50a0>
- Programma Integraal Riviermanagement*. (2021). https://www.platformparticipatie.nl/irm/irm_/default.aspx
- R. van der Meij. (2020). D-Stability installation manual, tutorial and scientific manual.
- Rijkswaterstaat. (2016). *Achtergrondrapport ontwerpinstrumentarium 2014* (tech. rep.). Rijkswaterstaat Water, Verkeer en Leefomgeving.
- Rijkswaterstaat. (2021a). *Schematiseringshandleiding macrostabiliteit* (tech. rep.). WBI 2017. Ministerie van Infrastructuur en Milieu.
- Rijkswaterstaat. (2021b). *Schematiseringshandleiding piping* (tech. rep.). WBI 2017. Ministerie van Infrastructuur en Milieu.
- Rijkswaterstaat. (2021c). *Tijdlijnen voor spoor 2 kennisprogramma zeespiegelstijging*.
- Rijkswaterstaat. (2022). Kennisprogramma zeespiegelstijging. <https://www.rijkswaterstaat.nl/water/waterbeheer/bescherming-tegen-het-water/maatregelen-om-overstromingen-te-voorkomen/kennisprogramma-zeespiegelstijging>
- Rijkswaterstaat. (2023). Waterkeringen. <https://www.rijkswaterstaat.nl/water/waterbeheer/bescherming-tegen-het-water/waterkeringen>
- Schweckendiek, T., & Kanning, W. (2017). *Reliability updating for slope stability of dikes, approach with fragility curves (background report)* (tech. rep.). Deltares.
- Schweckendiek, T., van der Krogt, M., Rijneveld, B., & Teixeira, A. M. (2017). *Handreiking faalkans-analyse macrostabiliteit* (tech. rep.). Deltares.
- Sellmeijer, H., Cruz, J., van Beek, V., & Knoeff, H. (2011). Fine-tuning of the backward erosion piping model through small-scale, medium-scale and ijdijk experiments. *European Journal of Environmental and Civil Engineering*, 15, 1139–1154.
- Simanjuntak, Y., Goeman, D., Koning, M., & Haasnoot, J. (2018). Shansep approach for slope stability assessments of river dikes in the netherlands.
- Spoorenberg, C. (2019). *Rapportage Waterbouw Proevenverzameling waterschap Scheldestromen 1.0*. Fugro.
- 't Hart, R. (2018). *Fenomenologische beschrijving faalmechanisme WBI* (tech. rep.). Deltares.
- TAW. (1999). *Technische rapport: Zandmeevoerende wellen* (tech. rep.). Technisch Adviescommissie voor de Waterkeringen.
- TAW. (2004). *Technisch rapport waterspanningen bij dijken* (tech. rep.). Rijkswaterstaat.
- Teixeira, A. (2021). *Aan de slag met d-stability en fragility curves* (tech. rep.). Deltares.
- Terzaghi, K. (1942). *Theoretical soil mechanics*. JOHN WILEY; SONS, INC.
- Van, M., Koelewijn, A., & Barends, F. (2005). Uplift phenomenon: Model, validation, and design. *International Journal of Geomechanics*, 5. [https://doi.org/10.1061/\(ASCE\)1532-3641\(2005\)5:2\(98\)](https://doi.org/10.1061/(ASCE)1532-3641(2005)5:2(98))
- van der Meer, J., Horst, W., & Velzen, E. (2008). Calculation of fragility curves for flood defence assets.
- van Leeuwen, P. (2019). *An analysis of the influence of the flood duration on slope stability*. TU Delft.
- van Montfoort, M., Dupuits, G., & Zethof, M. (2020). *Memo fragility curves* (tech. rep.). HKV.
- van Sabben, A., Beulink, L., van Schaick, S., Pieterse, J., Derksen, R., & Jongerius, Y. (2022). *Wbi2017 basisrapport* (tech. rep.). Waterschap Scheldestromen.

- van Schaick, S. (2021). *Hoofdrapport Veiligheidsoordeel WBI2017 Normtraject 29-3*. Waterschap Scheldestromen.
- van Schaick, S. (2022). *Hoofdrapport Veiligheidsoordeel WBI2017 Normtraject 32-4*. Waterschap Scheldestromen.
- van Schaick, S., & van Sabben, A. (2021). *Hoofdrapport Veiligheidsoordeel WBI2017 Normtraject 30-3*. Waterschap Scheldestromen.
- Vergouwe, R. (2014). *The national flood risk analysis for the netherlands*. Rijkswaterstaat.
- Verruijt, A. (2001). *Grondmechanica*. TU Delft.
- Zethof, M., Kuijper, B., Oerlemans, C., Jansen, M., van Engelen, T., Knops, D., & van den Berg, B. (2022). *Systeemanalyse zuidwestelijke delta*. Rijkswaterstaat.



Importance factors FORM method

The importance factors following from the First Order Reliability Method (FORM) are evaluated as follows: \mathbf{X} denotes a random vector which represents the uncertainties, $f_{\mathbf{X}}(x)$ the joint probability density, d a deterministic vector which represents the fixed variables, $g(\mathbf{X}, d)$ the limit state function of the model. The event described is written as $\mathcal{D}_f = \{\mathbf{X} \in \mathbb{R}^n / g(\mathbf{X}, d) \leq 0\}$, with $g(\mathbf{X}, d) = 0$ the so-called limit state surface. The probability of the event \mathcal{D}_f is P_f :

$$P_f = \int_{g(\mathbf{X}, d) \leq 0} f_{\mathbf{X}}(\mathbf{x}) d\mathbf{x}. \quad (\text{A.1})$$

The probability P_f can be estimated by the FORM (or SORM) approximation. The importance factors are a way to rank the importance of each input variable with respect to the realization of the event. The importance factors are not only evaluated for their direct significance but also for their interpretation as indicators of the impact when modelling the input components as random variables instead of fixed values ("Importance factors from FORM method", 2022). The importance factors can be defined as follows:

The iso-probabilistic transformation T is used to transform from physical space (\mathbf{X}) to standardized space (\mathbf{U}), such that the distribution of the random vector ($\mathbf{U}) = T \mathbf{X}$ has the following properties: \mathbf{U} and $\mathbf{R}\mathbf{U}$ have the same distribution for all rotations $\mathbf{R} \in \mathcal{SO}_n(\mathbb{R})$. In the standard space, the design point \mathbf{u}^* is the point on the limit state boundary nearest to the origin of the standard space. The design point \mathbf{x}^* in the physical space, where $\mathbf{x}^* = T^{-1}(\mathbf{u}^*)$. With β_{HL} being the reliability index, also known as the Hasofer-Lind reliability index, which denotes as $\beta_{HL} = \|\mathbf{u}^*\|$ (Lebrun & Dutfoy, 2009).

When the \mathbf{U} -space is normal, literature proposes to calculate the importance factor α_i^2 of the variable X_i as the square of the co-factors of the design point in the \mathbf{U} -space:

$$\alpha_i^2 = \frac{(u_i^*)^2}{\beta_{HL}^2} \quad (\text{A.2})$$

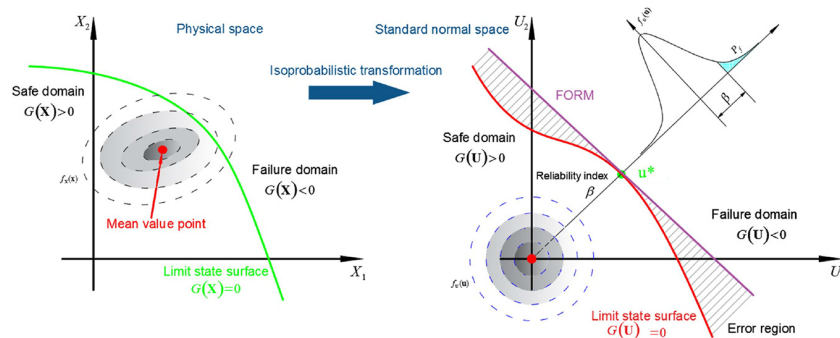


Figure A.1: Transformation from physical space to standard normal space (Hu et al., 2019)

B

Uplift and strength reduction

Uplift occurs if the water pressure in the aquifer at the inner side of the dike is larger than the weight of the ground layers on top. An increase in outside water level leads to higher pore water pressures in the aquifer, decreasing the effective stress of the interface to zero. The prevailing head in the pervious sand layer (the aquifer), is called the limit potential (ϕ_g). This potential is derived from the vertical soil stresses as follows:

$$\phi_g = \frac{\sigma'_{vs}}{\gamma_w} + \phi_p = \frac{\sum(\gamma_{ni} * d_i)}{\gamma_w} + \phi_p - d_z \quad [m] \quad (B.1)$$

where:

- σ'_{vs} = vertical effective stress interface [kN/m²]
- ϕ_p = polder level [m]
- γ_w = volumetric weight water [kN/m³]
- d_i = thickness layer i
- γ_{ni} = wet volumetric weight soil layer i [kN/m³]
- d_z = depth sand w.r.t. polder level [m]

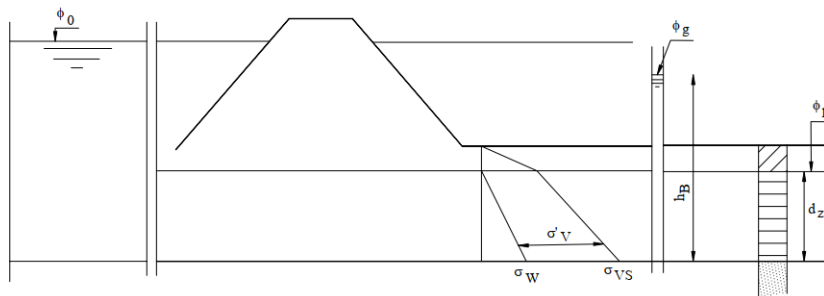


Figure B.1: Uplift ground level inner side dike (TAW, 2004).

Table B.1 is used to determine the head of the aquifer, in case of uplift conditions.

When uplift occurs, the pore pressure is reduced to the level of the prevailing phreatic pore pressure at a distance of about 3 m from the bursting point. This can be the polder level or the ground level. Also, when uplift occurs, the strength of the ruptured layer is reduced to zero over a zone of about 3 m, based on the estimation of the uplift zone according to *TR Waterspanningen bij dijken* (2004).

When there is a ditch present, it should be checked whether the effective blanket layer thickness is reduced. The procedure from the *TR Waterspanningen bij dijken* 2004 has been used and is depicted in Figure B.2.

Table B.1: Handling of uplift approach water board Scheldestromen

Safety factor	Blanket thickness	Head at uplift point	Strength at uplift location
< 0.9	< 4.0 m	Polder level	Reduce
< 0.9	≥ 4.0 m	Limit potential	Normal
$0.9 \leq \gamma \leq 1.0$	< 4.0 m	Polder level	Reduce
$0.9 \leq \gamma \leq 1.0$	≥ 4.0 m	Limit potential	Normal
> 1.0	n.v.t.	Calculate	Normal

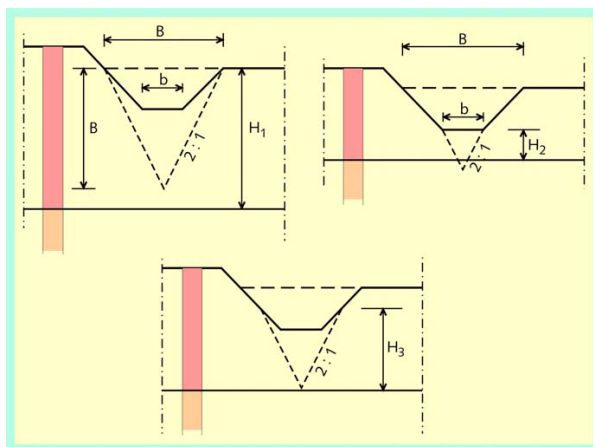
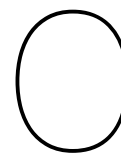


Figure B.2: Effective layer thickness for uplift conditions according to TR-26

Effective layer thickness

This appendix explains the adopted schematization of the groundwater level variation. The following situations are distinguished:

- **Safety factor < 0.9 & blanket < 4 m:** In this situation, uplifting occurs, and therefore, the strength reduction in the uplifting zone is also taken into account. The groundwater level gradually rises towards the polder level at a distance equal to 1 times the thickness of the cohesive layer from the inflection point of the ditch bottom on the dike side. The idea behind this is that there is also a potential loss over the thickness of the soft layer package, and therefore, the groundwater level directly below the toe ditch is higher than the polder level.
- **Safety factor between 0.9 and 1.1 & blanket < 4 m:** In this situation, both uplifting and buoyancy can occur. For this situation, calculations are performed according to both scenarios, uplifting and the limit potential. Based on the characteristics of the cross-section and the results, a decision is made on which scenario is relevant for this situation.
- **Safety factor > 1.1 :** No uplift. The groundwater level is not adjusted, and no strength reduction is applied.



Design cycle for calculating reinforcement cost

General approach

For determining the reinforcement cost, the following approach is used and also depicted in Figure C.1:

1. Determine hydraulic loads
2. Collect cost database
3. Input hydraulic boundary conditions with fragility curves
4. Chose calculation settings
5. Run OKADER
6. Reinforcement cost per section

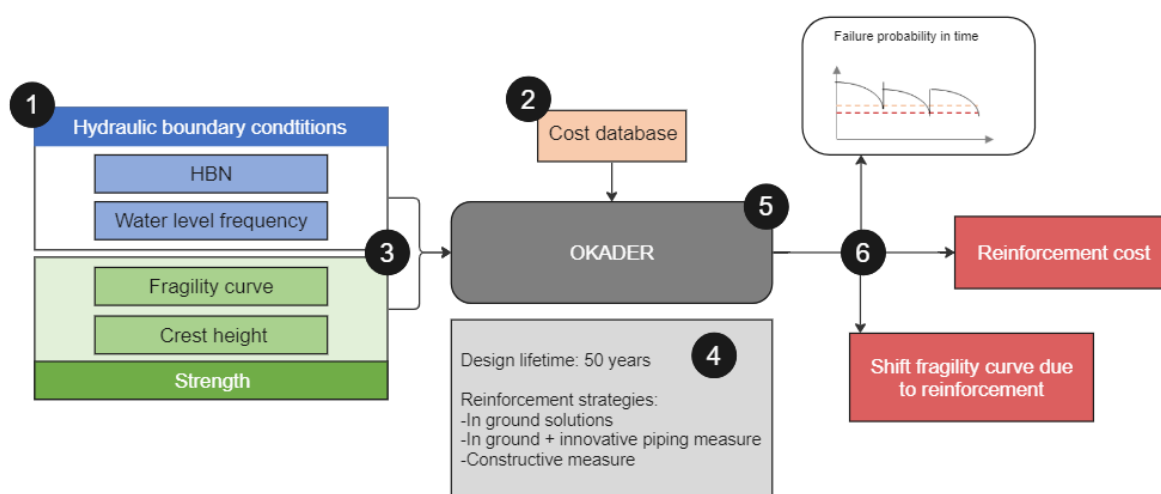


Figure C.1: General calculation method

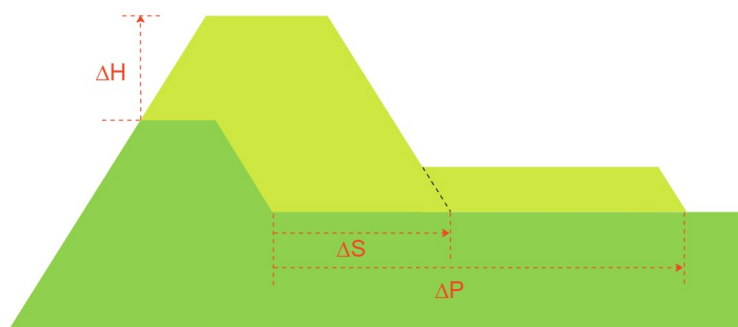
Cost database KOSWAT

The cost modelling of dikes happens with the model KOSWAT (KOSTen voor het versterken van WA-Terkeringen ¹). The computational model KOSWAT was created to quickly calculate the cost of a dike segment while a project is still in the exploratory stage. The following description in the appendix is given in Deltares, 20014. A cost estimate in KOSWAT is built entirely from a bottom-up approach. Firstly,

¹English: Reinforcement cost for flood defences.

a suitable design is created. Quantities are then determined by calculating the so-called Benoemde Directe Bouwkosten (BDBK) using unit prices. By multiplying these BDBK with Overhead Factors, the total investment costs are estimated according to the Standard Methodology for Cost Estimates in the Civil Engineering and Construction sector.

The new design needed is determined by following three parameters: heightening of the crest (ΔH), widening base for macro-stability (ΔS) and piping (ΔP), see Figure C.2. To find the new dimensions, firstly, the outer slope is extended till the new design height. The crest width stays the same, while the inner slope stays the same or decreases. Lastly, a berm of length $\Delta P - \Delta S$ is added if necessary (see Figure C.2).



miro

Figure C.2: Earthen dike reinforcement in KOSWAT

KOSWAT utilizes a database containing information about the surrounding area in the zone around the dike, including buildings, railways, and large water bodies. When there is limited space available for a fully ground-based dike reinforcement, KOSWAT offers several structural solutions. These solutions require less space but come at a higher cost. This is referred to as the displacement series in KOSWAT. As a result, a combination of measures is determined for a dike section (Figure C.3), resulting in a specific cost estimation (Grave & Baarse, 2011):

1. When there is not enough space for a fully green dike with a (long) piping berm, the first consideration is whether it is still possible to incorporate the measure regarding height and macro-stability (flattening of the inner slope) within the available space. The space required for a piping berm (ΔP minus ΔS) is saved by using a (light) seepage barrier or an innovative measure such as a Vertical Impermeable Geotextile or a Coarse Sand Barrier.
2. If it turns out that there is no available space to address the height and/or stability requirements in the ground, a stability wall will be implemented. In this case, the existing inner slope can be steepened to a default slope of 1:2. For the stability wall, KOSWAT utilizes an (anchored) sheet pile wall, and for a certain wall length (>20m), a diaphragm wall is used.
3. In areas where no space is available at all or where there is already existing construction within the current dike profile, KOSWAT opts for a cofferdam. In locations where there is already a pre-existing structural condition (such as a quay or city waterfront), KOSWAT uses a reference value based on the cost of a cofferdam.

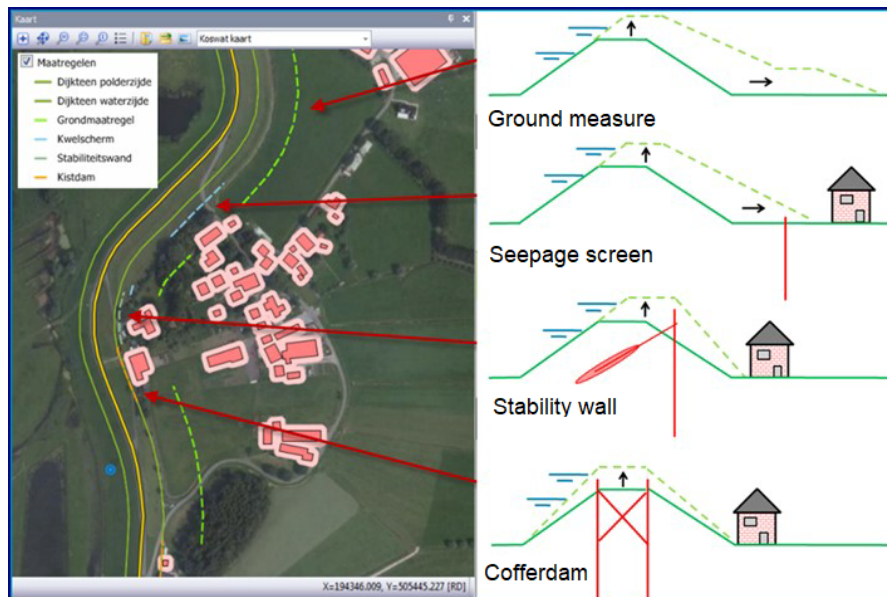


Figure C.3: KOSWAT mix of reinforcement measures (de Grave, 2022)

OKADER design cycle

As described in Section 3.6, OKADER is checking in cycles if the dike is meeting the legal requirements. Below the OKADER design cycle is described and visualized in Figure C.4:

1. Determining the failure probability per mechanism from local water level statistics and fragility curves.
2. Determine the maximum allowable probability of failure based on legal requirements.
3. Assessment: if a dike meets the requirements, go back to step 1 for a later time step. If it does not meet the requirements go to step 4.
4. Design: determine the new dike dimensions to comply with the requirements for the design life-time.
5. Determine reinforcement cost using the cost database KOSWAT.

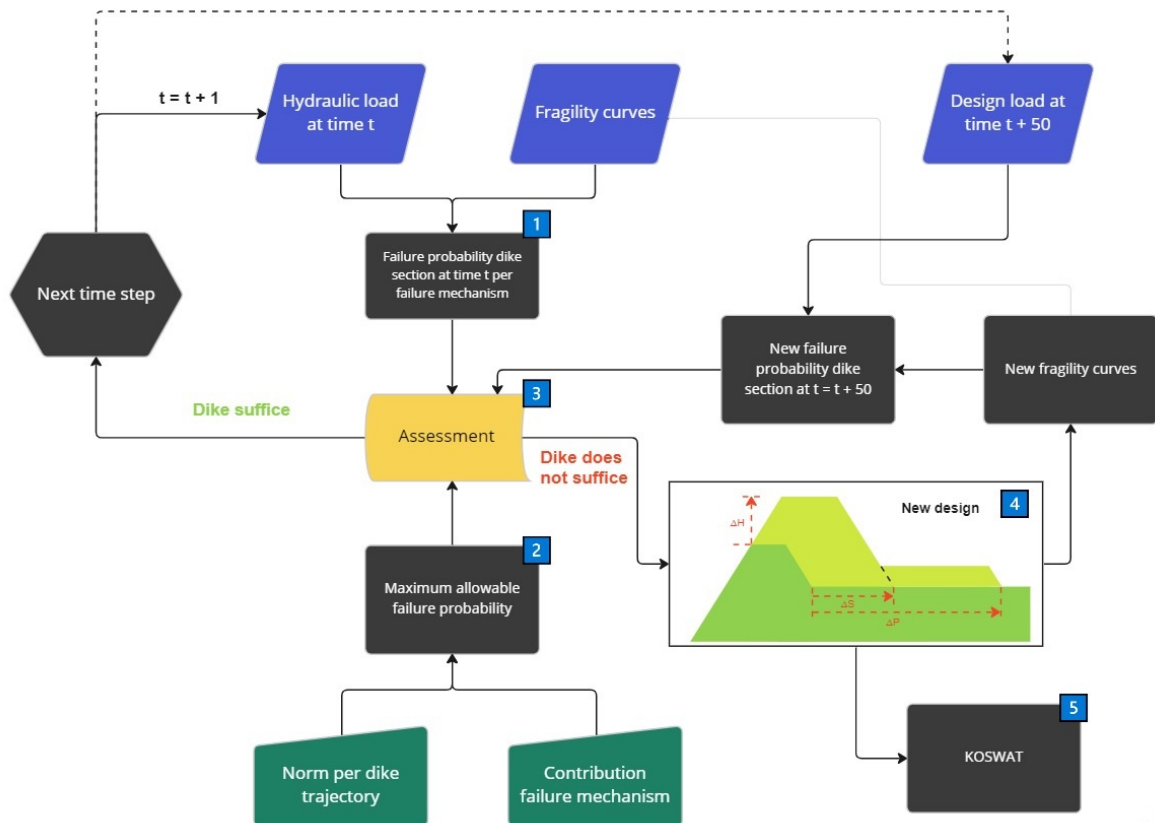
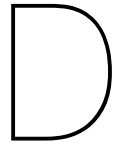


Figure C.4: Design cycle of OKADER



Water level frequency lines and HBN

In this appendix, the additional water level frequency line plots are presented that complement the analysis conducted in the main report. These plots are used as input for this study's other considered dike sections.

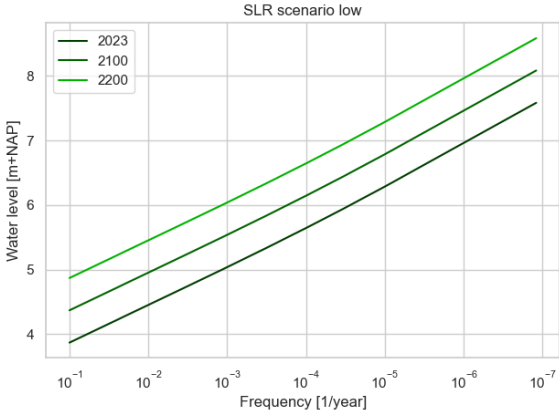


Figure D.1: Water level frequency lines section DP745 for scenario low

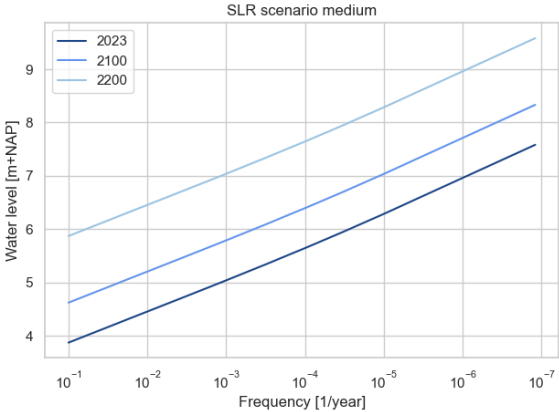


Figure D.2: Water level frequency lines section DP745 for scenario medium

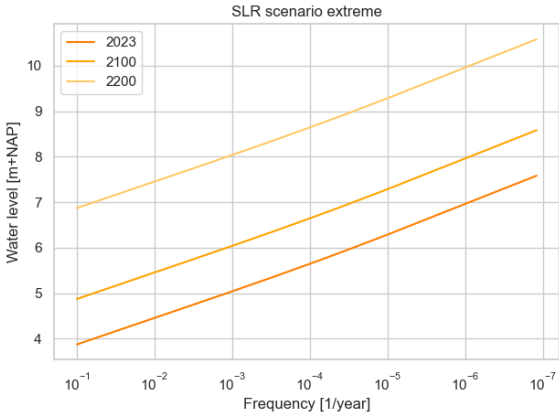


Figure D.3: Water level frequency lines section DP745 for scenario extreme

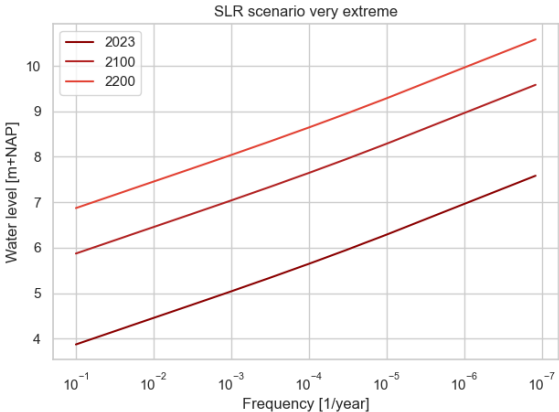


Figure D.4: Water level frequency lines section DP745 for scenario very extreme

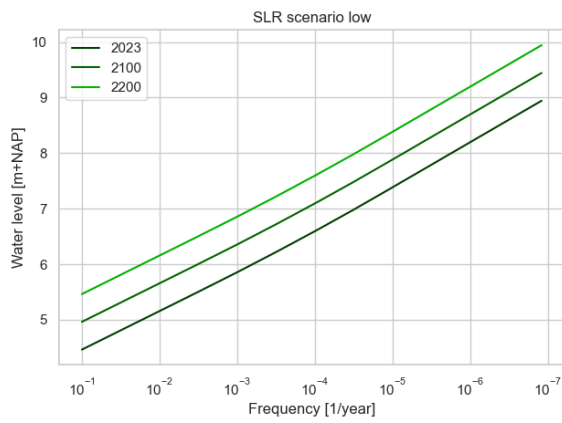


Figure D.5: Water level frequency lines section DP167 for scenario low

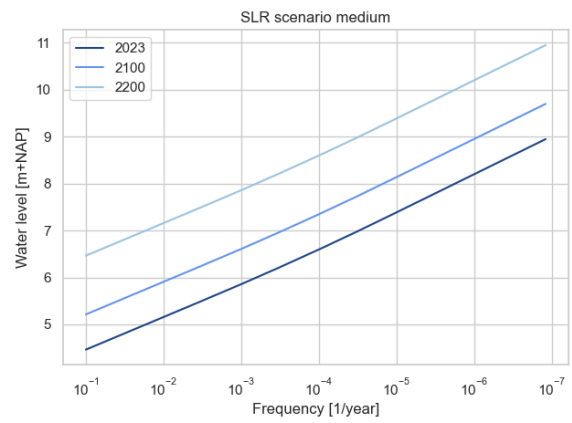


Figure D.6: Water level frequency lines section DP167 for scenario medium

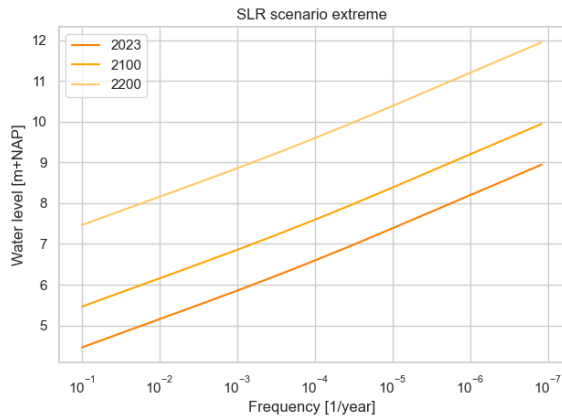


Figure D.7: Water level frequency lines section DP167 for scenario extreme

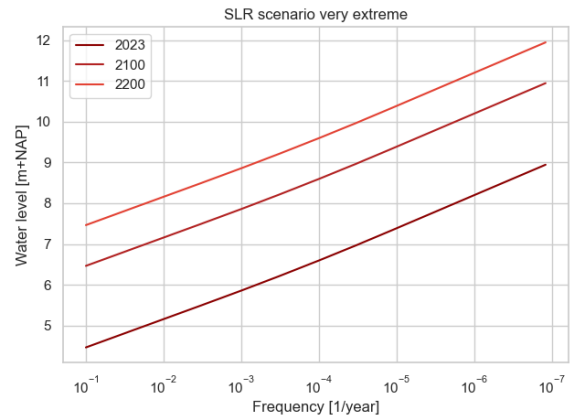


Figure D.8: Water level frequency lines section DP167 for scenario very extreme

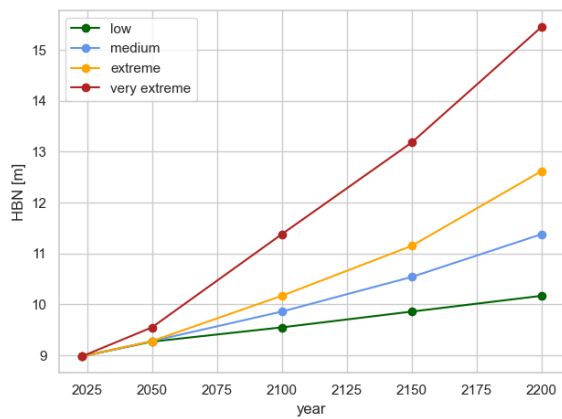


Figure D.9: HBN development lines for section DP745

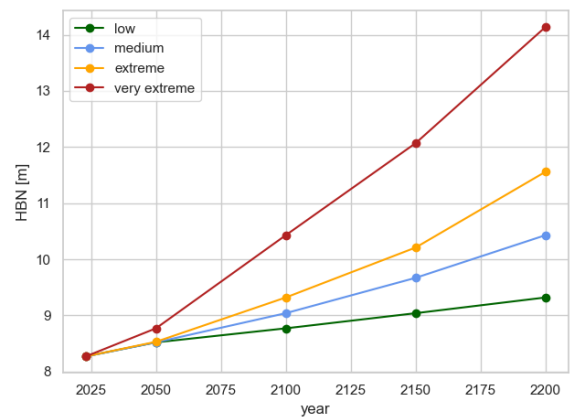
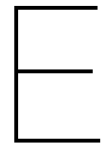


Figure D.10: HBN development lines for section DP167





Applied input variables

This appendix will provide an overview of the input variables used in the models. The characteristics and properties of each input variable, including its mean, distribution and, if applicable, the coefficient of variance, are given.

E.1. Macro-stability

The used strength parameters are based on a regional set of soil parameters provided by the water board and parameters provided in Schematiseringshandleiding Macro-stabiliteit (2021a). All distributions are lognormal since negative soil parameters do not exist. First, the cross-sections of the considered dike sections are given, and subsequently, the soil parameters of each section.

E.1.1. Schematization cross-sections

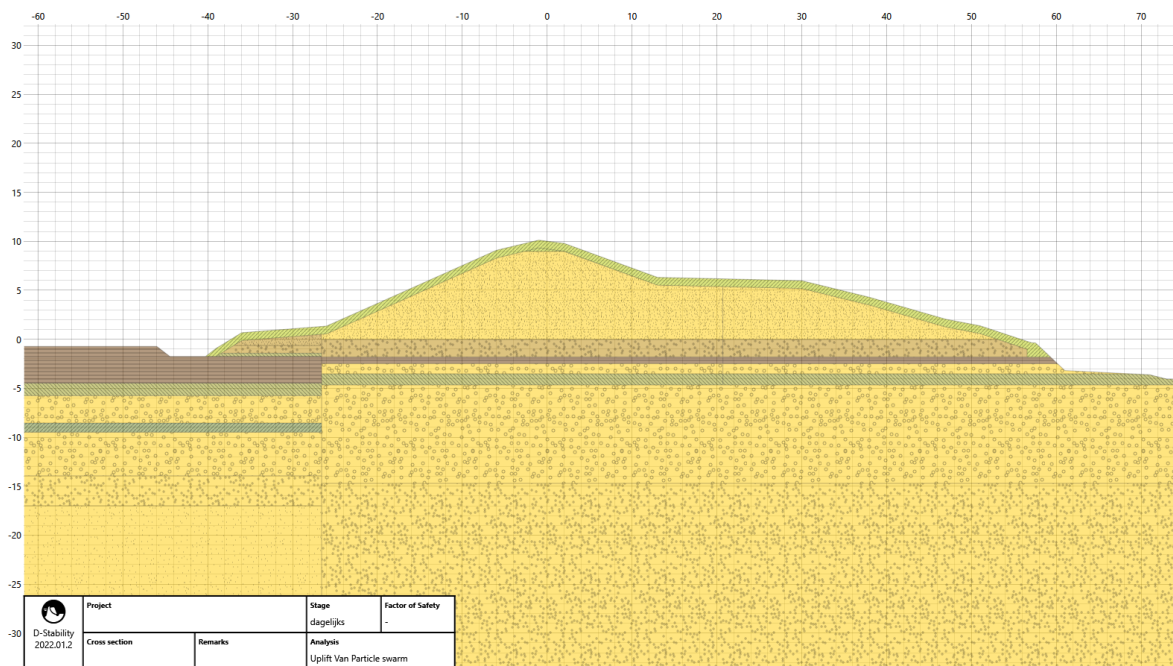


Figure E.1: Schematization cross-section for section DP745

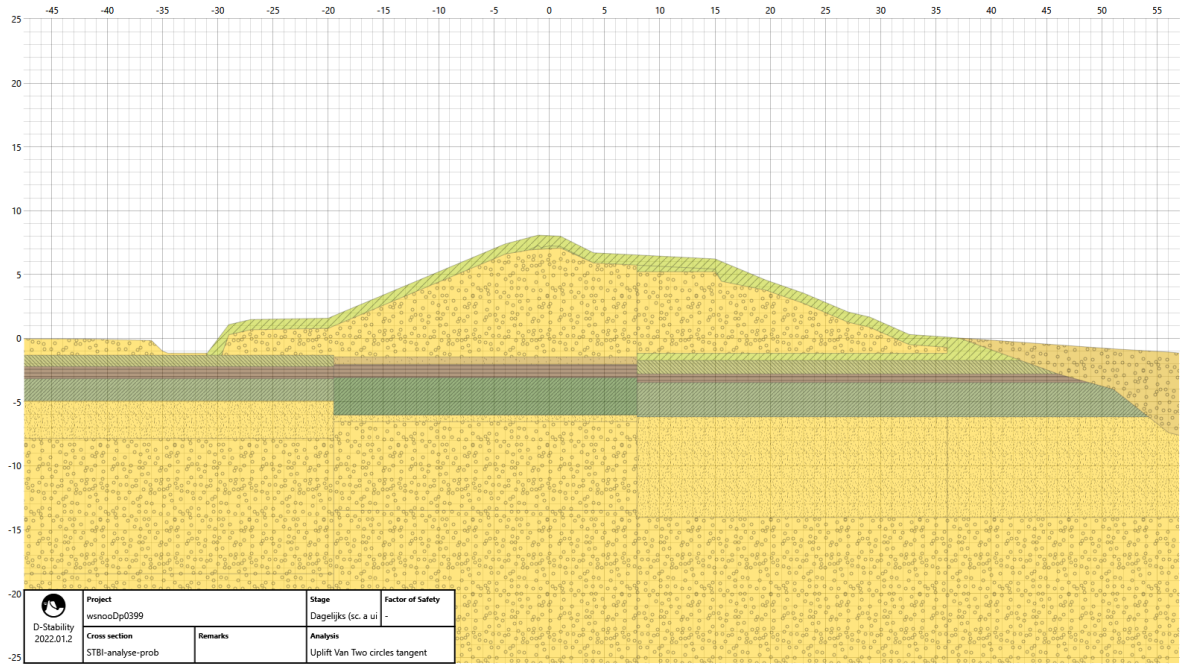


Figure E.2: Schematization cross-section for section DP399

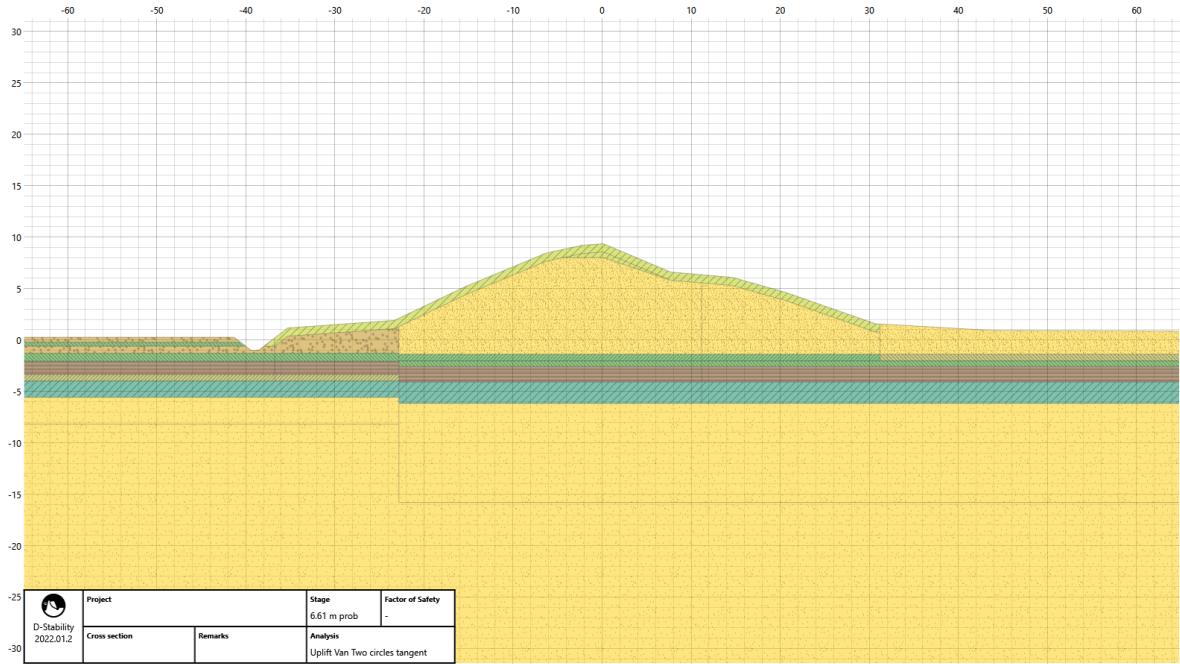


Figure E.3: Schematization cross-section for section DP167



E.1.2. Soil parameters for macro-stability

Table E.1: Strength parameters macro-stability DP745

Soil type	Parameter	Unit	μ	σ_{gem}	characteristic value
<i>Drained</i>					
Zand/Klei in dijk	phi	°	32	1.52	29.1
Duinkerke zand	phi	°	32	1.06	29.9
Calais zand	phi	°	32	1.06	29.9
Pleistoceen	phi	°	34	0.80	32.4
<i>Undrained</i>					
Hollandveen	S	-	0.42	0.022	0.39
	m	-	0.83	0.034	0.79
Calais klei sg=17	S	-	0.30	0.022	0.26
	m	-	0.89	0.021	0.88

Table E.2: Strength parameters macro-stability DP399

Soil type	Parameter	Unit	μ	σ_{gem}	characteristic value
<i>Drained</i>					
Zand/Klei in dijk	phi	°	32	1.52	29.1
Duinkerke zand	phi	°	32	1.06	29.9
Calais zand	phi	°	32	1.06	29.9
Pleistoceen	phi	°	34	0.80	32.4
<i>Undrained</i>					
Hollandveen	S	-	0.42	0.022	0.39
	m	-	0.83	0.034	0.79
Calais klei sg=17	S	-	0.30	0.022	0.26
	m	-	0.89	0.021	0.88
Duinkerke klei sg=17	S	-	0.30	0.022	0.26
	m	-	0.89	0.021	0.88
Calais klei sg=15	S	-	0.28	0.027	0.24
	m	-	0.88	0.021	0.87

Table E.3: Strength parameters macro-stability DP167

Soil type	Parameter	Unit	μ	σ_{gem}	characteristic value
<i>Drained</i>					
Zand/Klei in dijk	phi	°	32	1.52	29.1
Duinkerke zand	phi	°	32	1.06	29.9
Calais zand	phi	°	32	1.06	29.9
Pleistoceen	phi	°	34	0.80	32.4
<i>Undrained</i>					
Hollandveen	S	-	0.42	0.022	0.39
	m	-	0.83	0.034	0.79
Duinkerke klei sg=19	S	-	0.353	0.045	0.28
	m	-	0.91	0.021	0.90
Duinkerke klei sg=15	S	-	0.28	0.027	0.24
	m	-	0.88	0.021	0.87
Calais klei sg=15	S	-	0.28	0.027	0.24
	m	-	0.88	0.021	0.87

E.1.3. POP-value

For the limit stress the following POP-values are used under the daily conditions and are presented in Table E.4. The values are a result of the tests carried out by Fugro and are based on the SHANSEP model.

Table E.4: Stochastic input values for POP-value

Soil type	μ [kN/m ²]	σ_x [kN/m ²]	POP _{kar}
Hollandveen	56.03	34.45	15
Klei sg=19	41.16	21.39	10
Klei sg=17	29.87	18	10
Calais klei sg=15	30.40	17.50	10

E.2. Backward erosion piping

The variables in the tables below are a combination of standard values from Schematiseringshandleiding piping (2021b) and values used in the assessment of the water board Scheldestromen.

E.2.1. DP745

Table E.5: Input variables backward erosion piping DP745

Parameter	Unit	Symbol	Distribution	Mean	C.o.V.
70%-fractile of grain size distribution	m	d_{70}	Lognormal	0.00011	0.12
Thickness hinterland blanket	m	d	Lognormal	1.5	0.13
Seepage length	m	L	Lognormal	69.42	0.1
Volumetric weight sand submerged	kN/m^3	γ_{sub}	Deterministic	15.94	-
Saturated volumetric weight blanket	kN/m^3	γ_{sat}	Normal	11.78	0.080
Volumetric weight water	kN/m^3	γ_w	Deterministic	10.06	-
Drag factor coefficient	-	η	Lognormal	0.25	0.004
Bedding angle	deg	θ	Lognormal	37	0.035
Hydraulic conductivity aquifer	m/s	k	Lognormal	0.00001	0.5
Thickness aquifer	m	D	Lognormal	33	0.015
Damping factor	-	λ	Lognormal	0.898	0.0001
Critical heave gradient	-	i_{ch}	Lognormal	0.5	0.2
Hinterland phreatic level	m	h_p	Normal	-0.73	-0.00001
Model factor Sellmeijer	-	m_p	Normal	1	0.12
Model factor uplift	-	m_u	Normal	1	0.1
Kinematic viscosity	m^2/s	ν	Deterministic	1.33E-6	-
Reference value of 70%-fractile of grain size distribution	m	d_{70m}	Deterministic	0.000208	-
Reduction factor Sellmeijer	-	-	Deterministic	0.3	-

E.2.2. DP399

Table E.6: Input variables backward erosion piping DP399

Parameter	Unit	Symbol	Distribution	Mean	C.o.V.
70%-fractile of grain size distribution	m	d_{70}	Lognormal	0.0001	0.12
Thickness hinterland blanket	m	d	Lognormal	3.82	0.13
Seepage length	m	L	Lognormal	110.72	0.1
Volumetric weight sand submerged	kN/m^3	γ_{sub}	Deterministic	15.94	-
Saturated volumetric weight blanket	kN/m^3	γ_{sat}	Normal	14.97	0.063
Volumetric weight water	kN/m^3	γ_w	Deterministic	10.06	-
Drag factor coefficient	-	η	Lognormal	0.25	0.004
Bedding angle	deg	θ	Lognormal	37	0.035
Hydraulic conductivity aquifer	m/s	k	Lognormal	0.00001	0.5
Thickness aquifer	m	D	Lognormal	16.1	0.0295
Damping factor	-	λ	Lognormal	0.921	0.0001
Critical heave gradient	-	i_{ch}	Lognormal	0.5	0.2
Hinterland phreatic level	m	h_p	Normal	-0.17	-0.00001
Model factor Sellmeijer	-	m_p	Normal	1	0.12
Model factor uplift	-	m_u	Normal	1	0.1
Kinematic viscosity	m^2/s	ν	Deterministic	1.33E-6	-
Reference value of 70%-fractile of grain size distribution	m	d_{70m}	Deterministic	0.000208	-
Reduction factor Sellmeijer	-	-	Deterministic	0.3	-

E.2.3. DP167**Table E.7:** Input variables backward erosion piping DP167

Parameter	Unit	Symbol	Distribution	Mean	C.o.V.
70%-fractile of grain size distribution	m	d_{70}	Lognormal	0.0001	0.12
Thickness hinterland blanket	m	d	Lognormal	5.47	0.09
Seepage length	m	L	Lognormal	52.83	0.1
Volumetric weight sand submerged	kN/m^3	γ_{sub}	Deterministic	15.94	-
Saturated volumetric weight blanket	kN/m^3	γ_{sat}	Normal	18.56	0.080
Volumetric weight water	kN/m^3	γ_w	Deterministic	10.06	-
Drag factor coefficient	-	η	Lognormal	0.25	0.004
Bedding angle	deg	θ	Lognormal	37	0.035
Hydraulic conductivity aquifer	m/s	k	Lognormal	0.000145	0.5
Thickness aquifer	m	D	Lognormal	33.85	0.015
Damping factor	-	λ	Lognormal	0.99	0.0001
Critical heave gradient	-	i_{ch}	Lognormal	0.5	0.2
Hinterland phreatic level	m	h_p	Normal	0.27	-0.00001
Model factor Sellmeijer	-	m_p	Normal	1	0.12
Model factor uplift	-	m_u	Normal	1	0.1
Kinematic viscosity	m^2/s	ν	Deterministic	1.33E-6	-
Reference value of 70%-fractile of grain size distribution	m	d_{70m}	Deterministic	0.000208	-
Reduction factor Sellmeijer	-	-	Deterministic	0.3	-

Additional results reliability analysis

This appendix presents the resulting fragility curves for changing the most important parameter in the reliability analysis. The shifted fragility curves and changed failure probabilities are presented for macro-stability and piping.

F.1. Macro-stability

To visualize the influence of the POP value on the fragility curve, new calculations were performed without considering it. The results of the new fragility curves can be found in F.1. In each figure is the green line associated with the fragility in the situation excluding the POP value. For sections DP399 and DP167, the probabilistic calculation (orange line) shifts towards the left and is closer to the typology-defined curve. Section DP745 also shifts to the left. However, since the typology-defined curve and the probabilistic calculated curve were already close to each other, the fragility curve without POP also further deviates from the typology-defined curve. This behaviour of the curve is in line with the expectations since the POP value represents the maximum vertical pressure that the soil had in the past, making the soil layer more compact and, therefore, stronger (Melnikov et al., 2016).

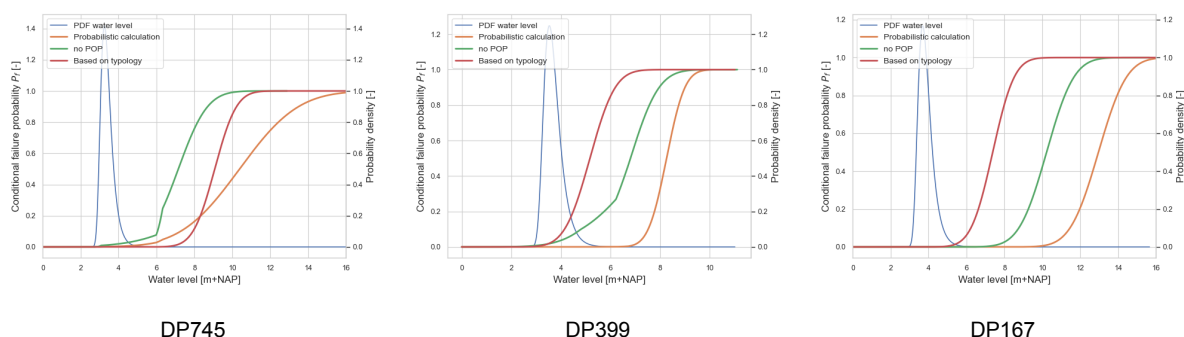


Figure F.1: Influence of the pre-overburden pressure on the fragility curve

Table F.1 displays the new failure probabilities when considering the fragility curves without using the POP value. What can be seen is that for sections DP399 and DP167, the failure probabilities decrease significantly with a factor 10^4 and 10^3 , respectively. The decrease in failure probability for section DP745 is minimal with a factor 10 since the failure probability was already somewhat high.

Table F.1: Failure probabilities for the fragility curves without the POP value

Section	Failure probability with probabilistic calculation	Failure probability with typology	Failure probability without POP value
DP745	$1.89 \cdot 10^{-3}$ per year	$7.31 \cdot 10^{-8}$ per year	$1.21 \cdot 10^{-2}$ per year
DP399	$7.88 \cdot 10^{-6}$ per year	$5.07 \cdot 10^{-2}$ per year	$2.75 \cdot 10^{-2}$ per year
DP167	$1.63 \cdot 10^{-10}$ per year	$4.18 \cdot 10^{-4}$ per year	$5.03 \cdot 10^{-7}$ per year

F.2. Backward erosion piping

To illustrate the influence of the hydraulic conductivity, new fragility curves are made with adjusted k -value. This new k -value is obtained by dividing the kD -value of the section assigned in KP-ZSS, by the aquifer thickness, after which new reliability computations have been carried out. The resulting graphs are presented in Figure F.2. For reference, the assigned typology curve and the probabilistic calculated curve are plotted to indicate the shift of the fragility curve due to the changed k -value.

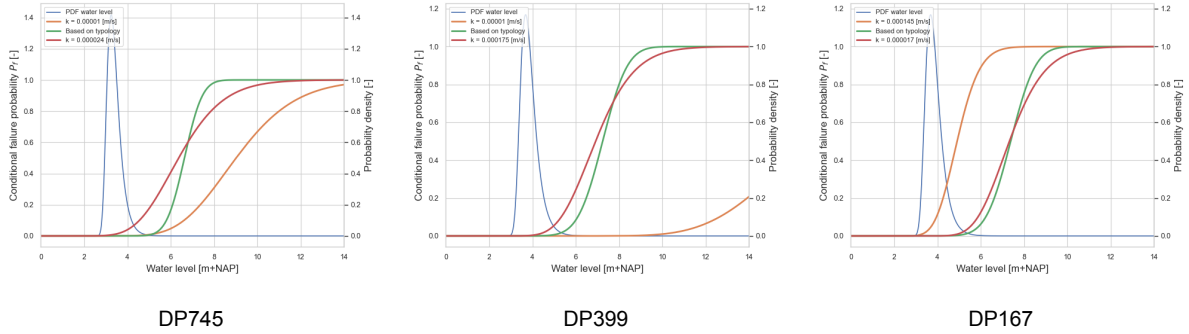


Figure F.2: Influence of the hydraulic conductivity on the fragility curve

The influence of the hydraulic conductivity can be better understood by considering the predicted failure probability. The failure probability was computed to show how the fragility curves differ from one another more clearly. The results of the new computations are shown in Table F.2. Looking at the failure probabilities, it can be noticed that when changing the k -value for sections DP399 and DP167, the failure probabilities become more similar to those computed with the typology-defined curves, only differentiating a factor 10. While it is remarkable that by changing the k -value the failure probability for section DP745 increases. This can be explained by the fact that the kD -value assigned in KP-ZSS is larger than the computed one.

Table F.2: Failure probabilities for fragility curves with adjusted k-value according to the kD -value of KP-ZSS

Section	Failure probability with probabilistic calculation	Failure probability with typology	Failure probability with adjusted k -value
DP745	$3.05 \cdot 10^{-2}$ per year	$4.97 \cdot 10^{-5}$ per year	$1.38 \cdot 10^{-2}$ per year
DP399	$1.53 \cdot 10^{-7}$ per year	$6.32 \cdot 10^{-4}$ per year	$7.19 \cdot 10^{-3}$ per year
DP167	$1.13 \cdot 10^{-2}$ per year	$4.18 \cdot 10^{-4}$ per year	$2.80 \cdot 10^{-3}$ per year





Phreatic line

One of the important parameters in dike stability analysis is the position of the phreatic line. In this appendix, a brief analysis has been conducted to visualize this influence. For this purpose, the decision has been made to choose a different schematization of the phreatic line, which is not representative of the considered dike sections. The choice has been made to linearly decrease the phreatic line from the entry point to the toe on the inner side. The test is conducted for section DP399 and can be found in Figure G.1.

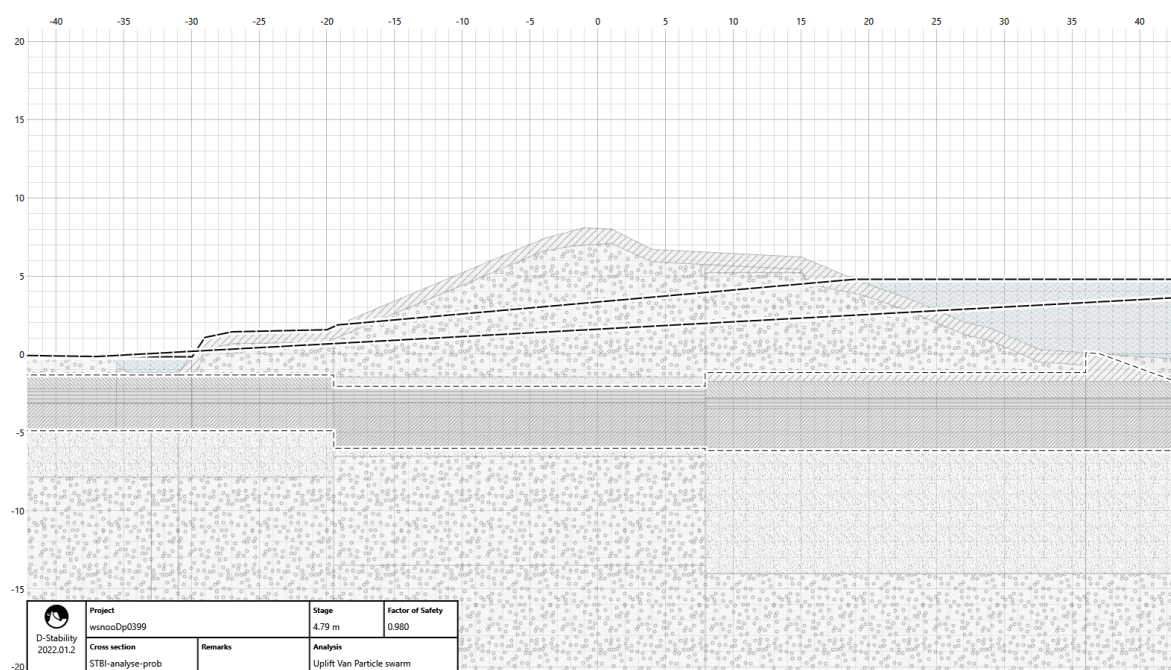


Figure G.1: Schematisation of the linear phreatic line for section DP399

The new fragility curve is computed following the proposed methods in this study. The resulting fragility curve is presented in Figure G.2. What can be observed is that the curve is less smooth (due to the linear interpolation) and shifted to the left. Also, the intersection with the water level PDF has increased, resulting in an increased failure probability. Comparing the probabilistic calculation (orange line) with the linear phreatic curve (green line), the failure probability increased from $7.88 \cdot 10^{-6}$ to $2.02 \cdot 10^{-4}$.

Also, a new fragility curve is computed where some degree of wave overtopping is taken into account. In this case, the phreatic line increases by 20 cm at the toe of the dike. This is done for water levels greater or equal to the height of the lower part of the outer berm, meaning the other 2 fragility points are unchanged. The resulting fragility curve is depicted in Figure G.3. The effect on the fragility curve is minimal since a small increase in the phreatic line is applied. The failure probability only increases from $7.88 \cdot 10^{-6}$ to $8.97 \cdot 10^{-6}$.

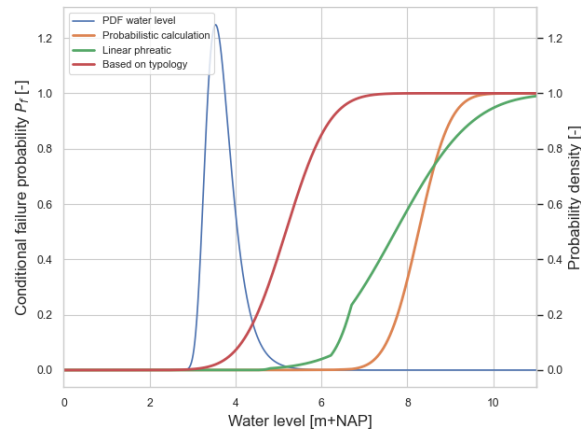


Figure G.2: Resulting fragility curve using typology, the proposed method and linear phreatic line for section DP399

The same methodology is applied to the section, but this time for an increase of 50 cm of the phreatic line at the toe. The resulting fragility curve is given in Figure G.4. What now can be noted is that although the curves are still quite similar, the failure probability increases from $7.88 \cdot 10^{-6}$ to $1.07 \cdot 10^{-5}$.

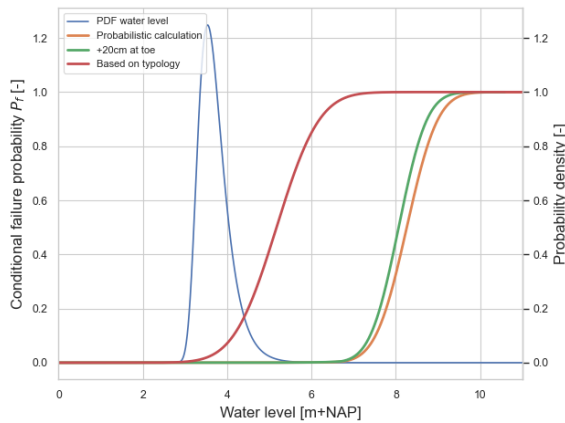


Figure G.3: Addition of 20 cm to the phreatic line at the toe of the dike for section DP399

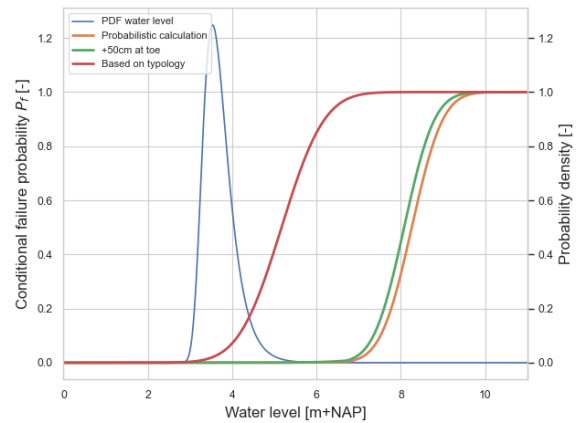
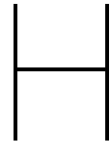


Figure G.4: Addition of 50 cm to the phreatic line at the toe of the dike for section DP399



Additional OKADER results

This appendix includes additional results and analysis from the OKADER calculations. For each OKADER section, the evolution of the cost for both fragility curve approaches per sea level rise (SLR) scenario can be found here. Also, additional analysis on certain parameters is presented here.

H.1. Reinforcements

Height requirements and total reinforcement cost

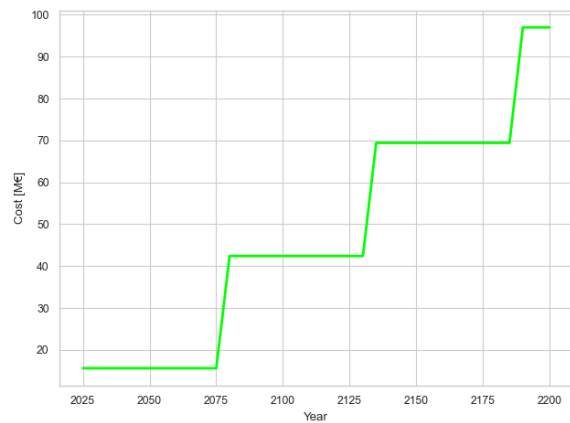
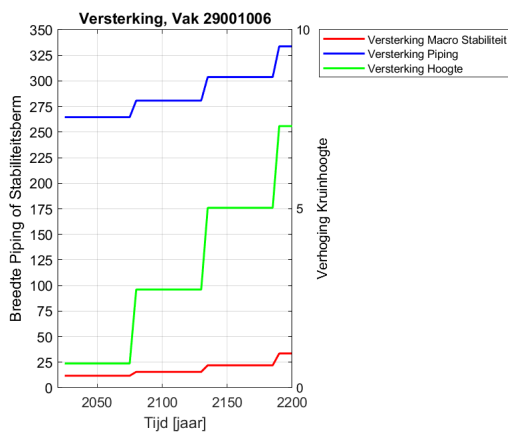


Figure H.1: DP745: OKADER reinforcement requirements

Figure H.2: DP745: cost of reinforcement

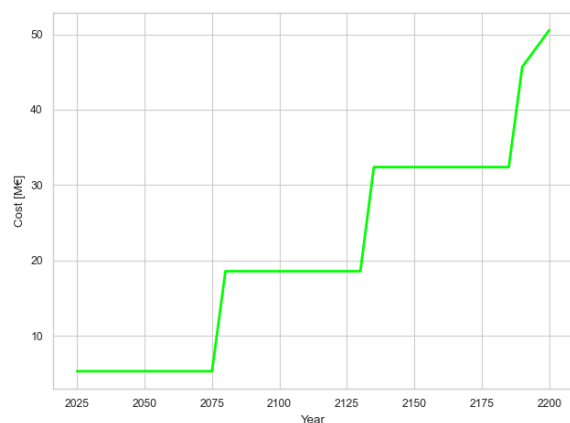
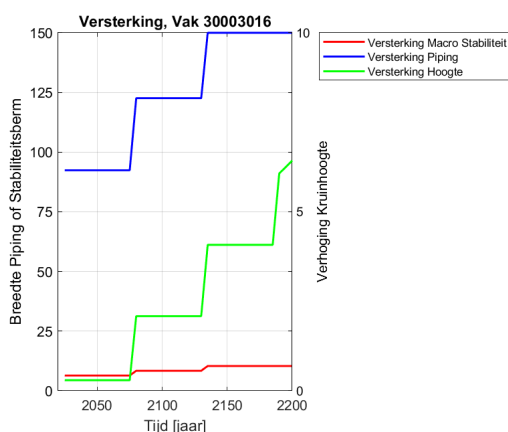


Figure H.3: DP399: OKADER reinforcement requirements

Figure H.4: DP399: cost of reinforcement

Figure H.5: Comparison reinforcements as calculated by OKADER and the reinforcement cost over time for SLR very extreme

Shift of the fragility curves

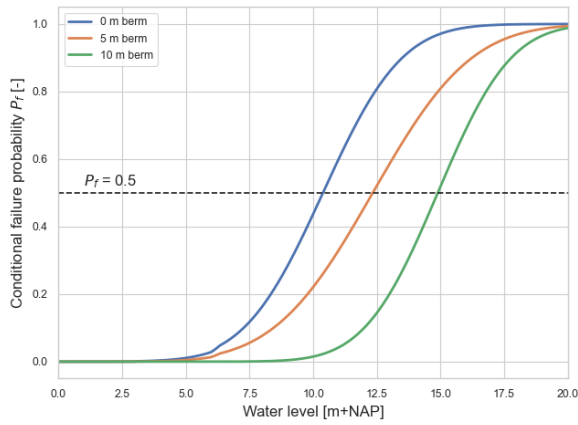


Figure H.6: Shift of the fragility curve with the addition of a stability berm for section DP745

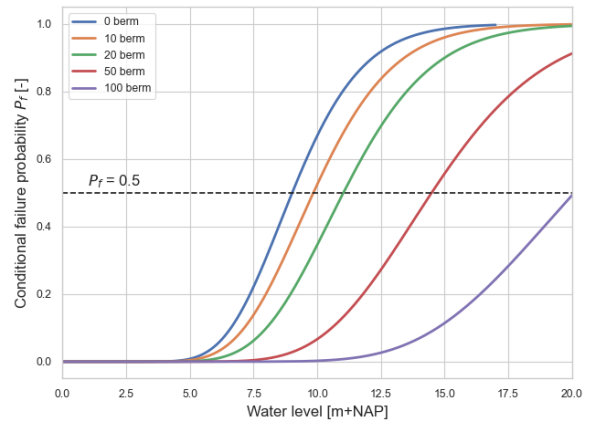


Figure H.7: Shift of the fragility curve with the addition of a piping berm for section DP745

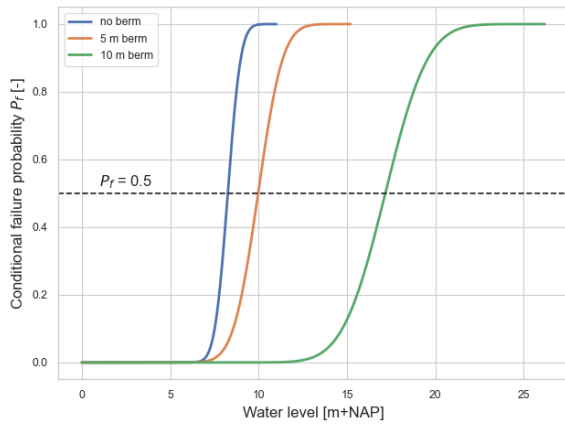


Figure H.8: Shift of the fragility curve with the addition of a stability berm for section DP399

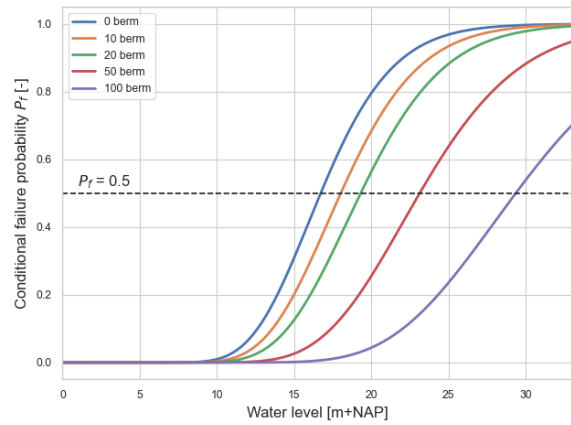


Figure H.9: Shift of the fragility curve with the addition of a piping berm for section DP399

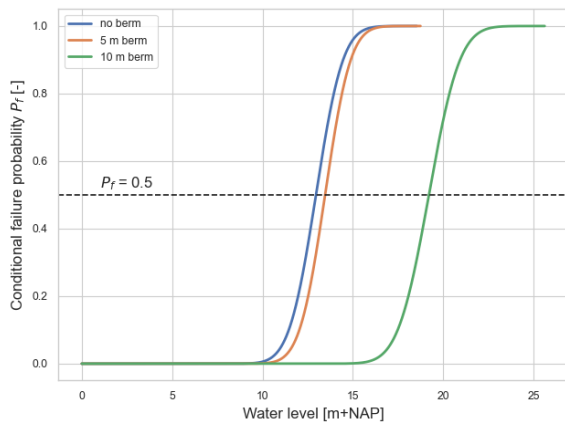


Figure H.10: Shift of the fragility curve with the addition of a stability berm for section DP167

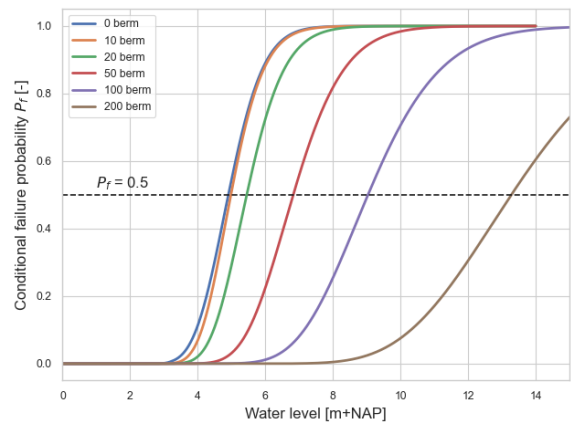
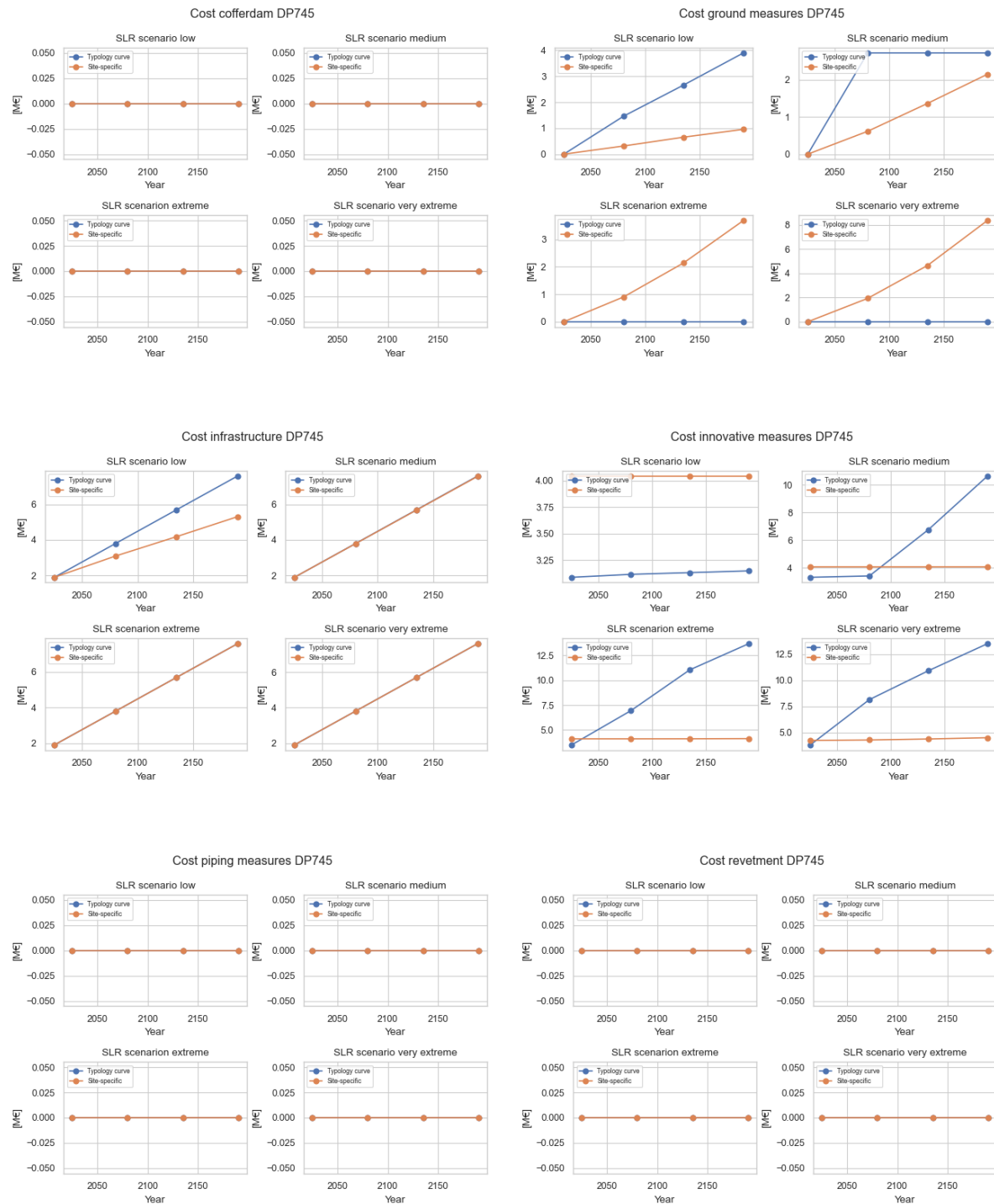


Figure H.11: Shift of the fragility curve with the addition of a piping berm for section DP167

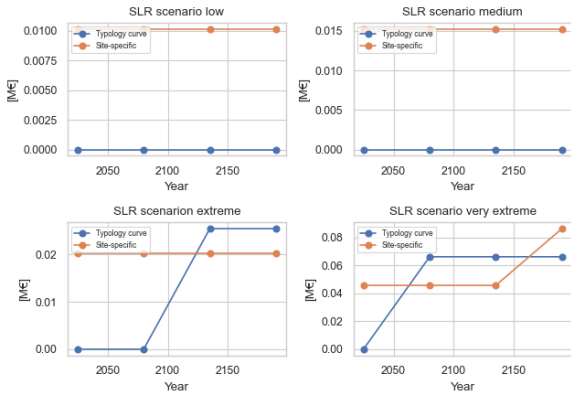


Factors determining cost

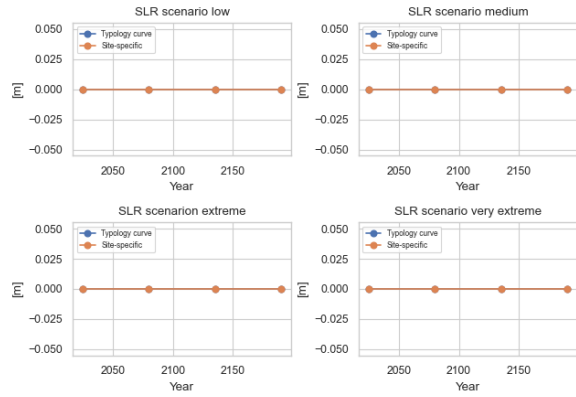
The following figures present the reinforcement cost under the four different sea level rise scenario. For each scenario, the cost is presented for both fragility curve approaches. All factors determining the cost are presented.



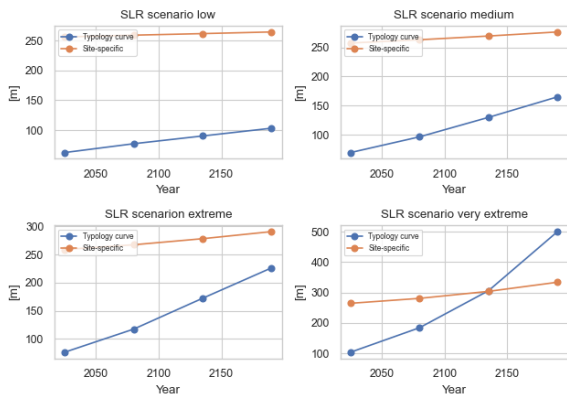
Cost stability wall DP745



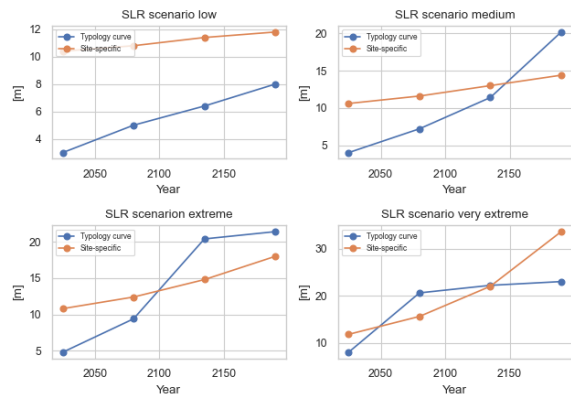
Crest heightening DP745



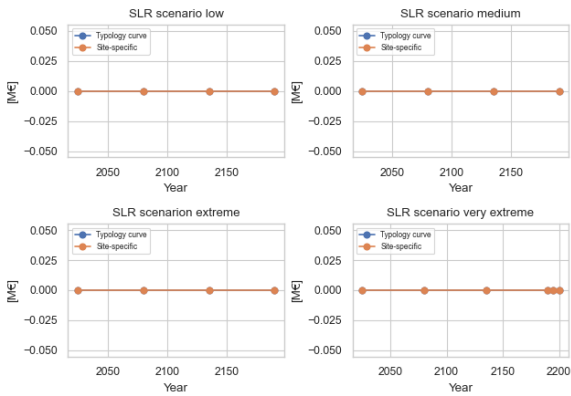
Dike base increase piping DP745



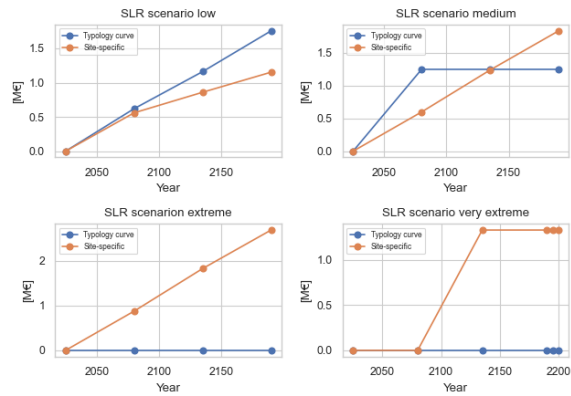
Dike base increase stability DP745



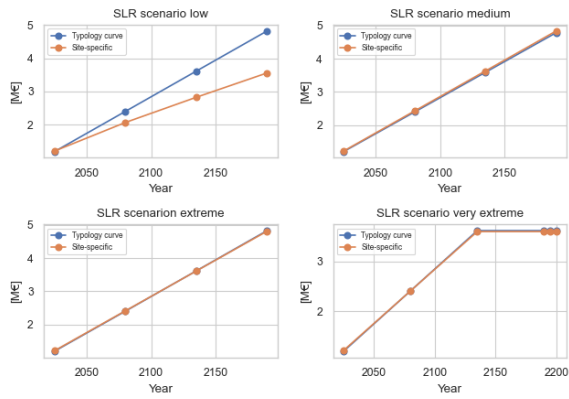
Cost cofferdam DP399



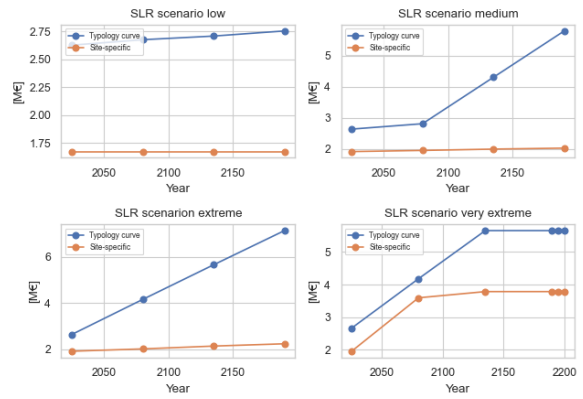
Cost ground measures DP399



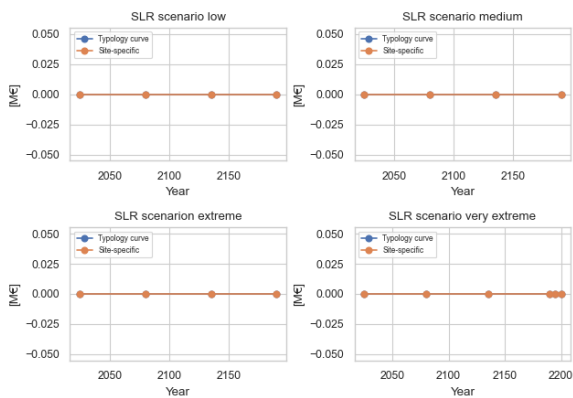
Cost infrastructure DP399



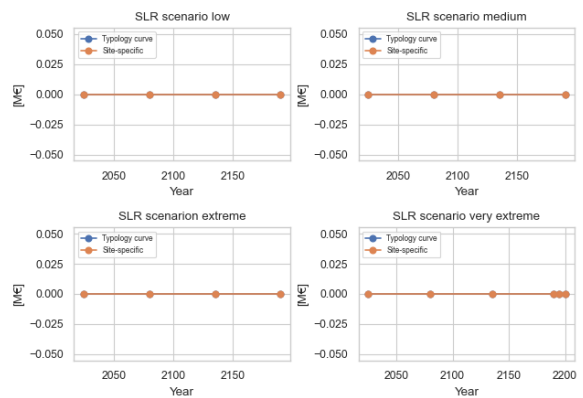
Cost innovative measures DP399



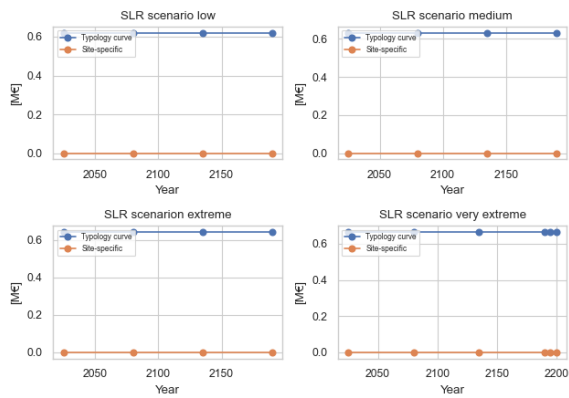
Cost piping measures DP399



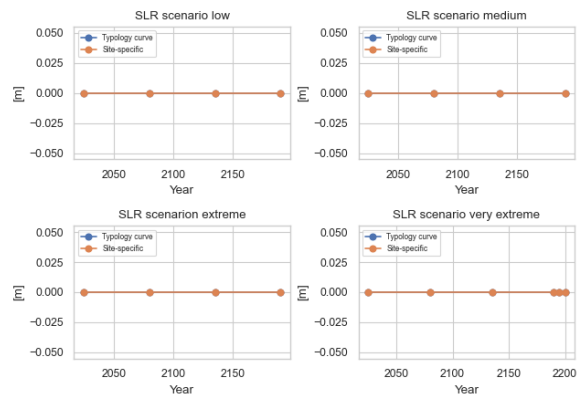
Cost revetment DP399



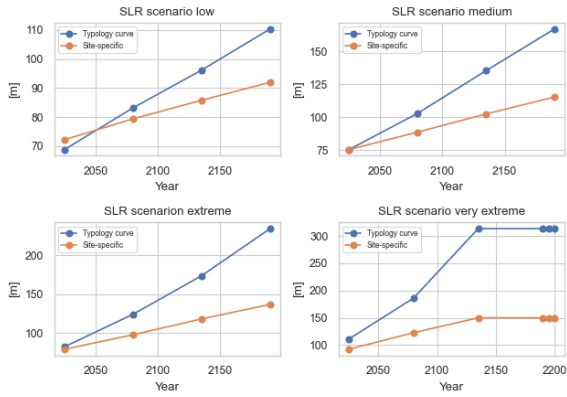
Cost stability wall DP399



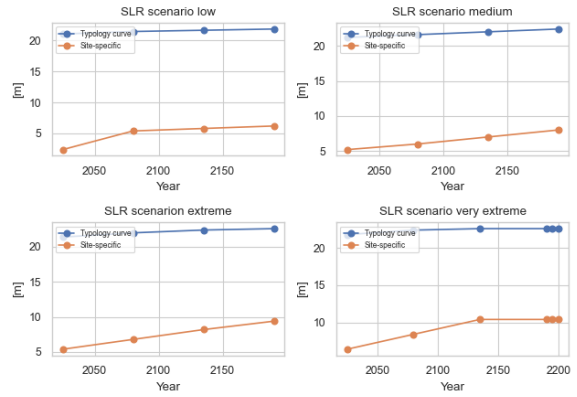
Crest heightening DP399



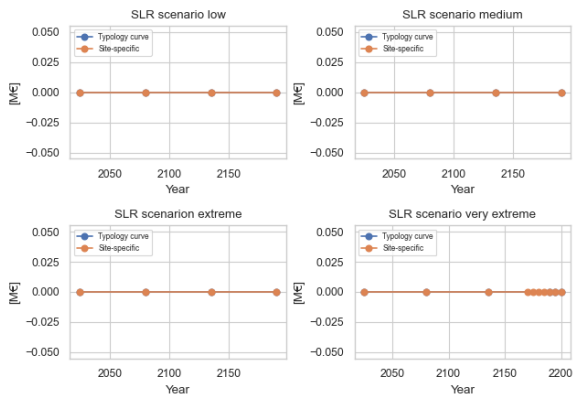
Dike base increase piping DP399



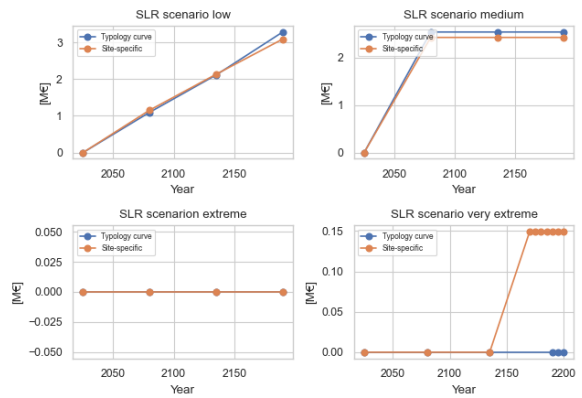
Dike base increase stability DP399



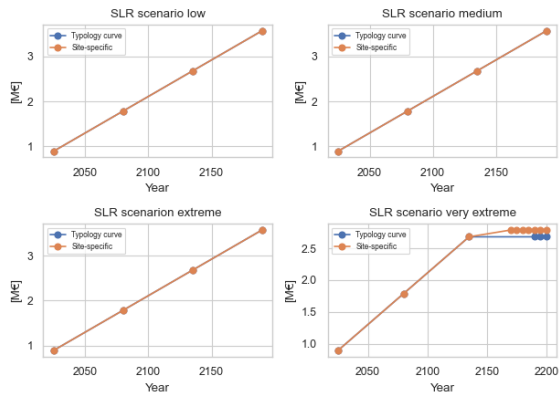
Cost cofferdam DP167



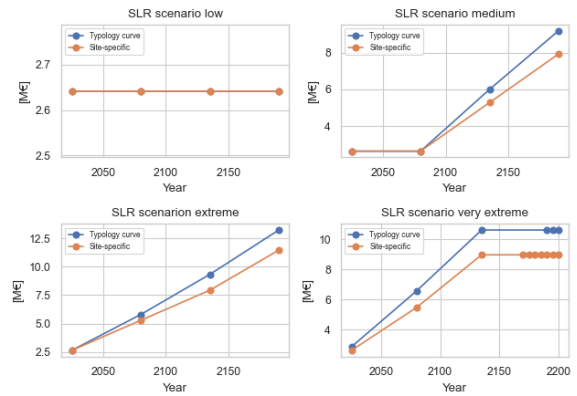
Cost ground measures DP167

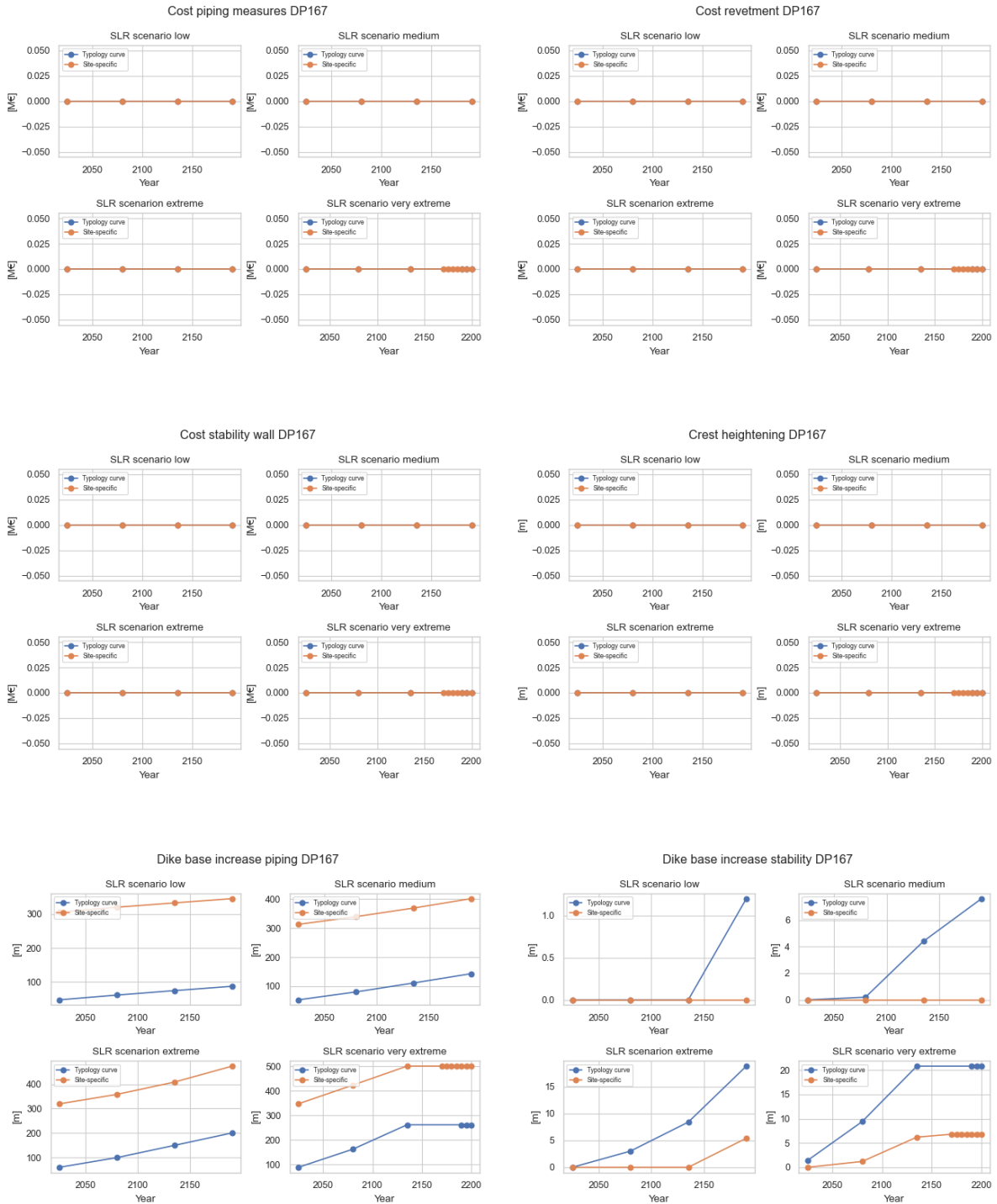


Cost infrastructure DP167



Cost innovative measures DP167

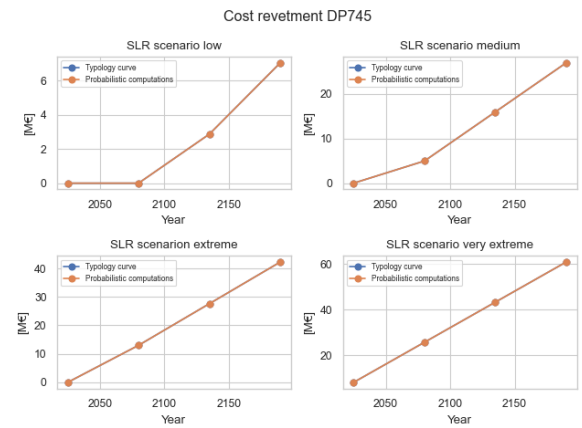
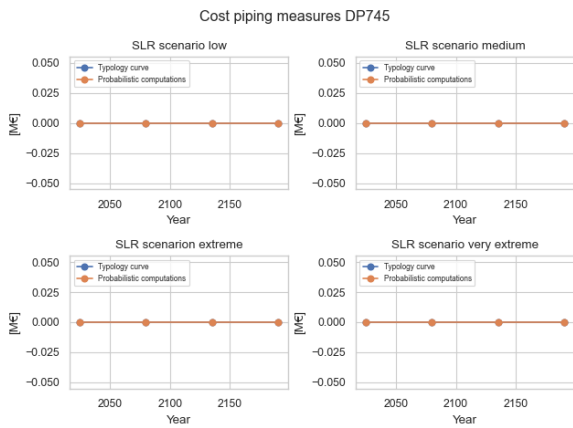
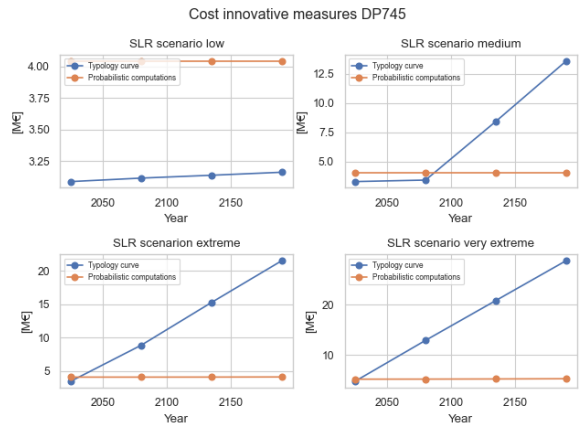
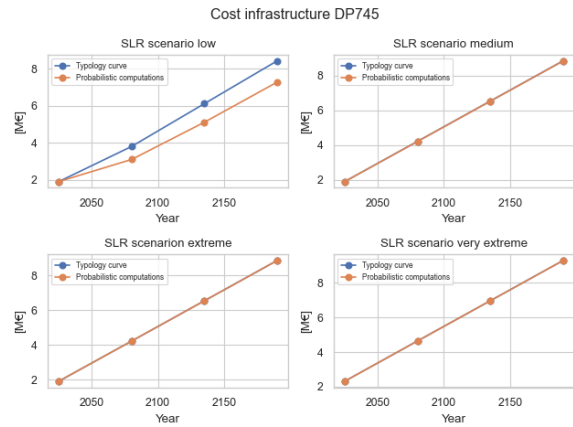
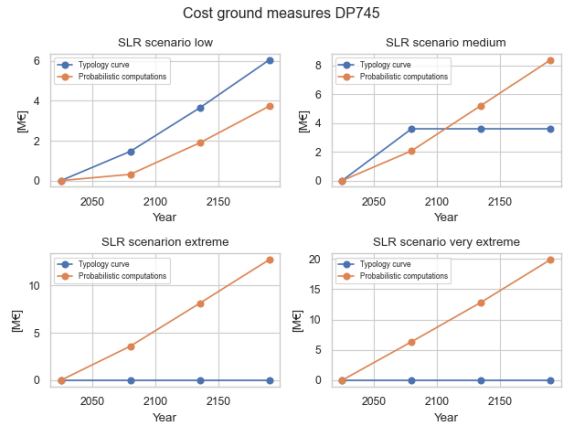
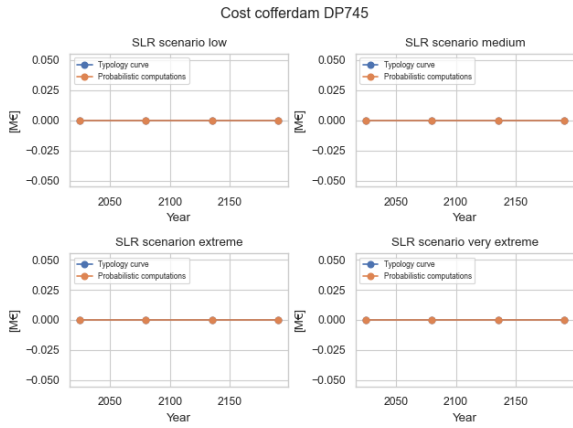


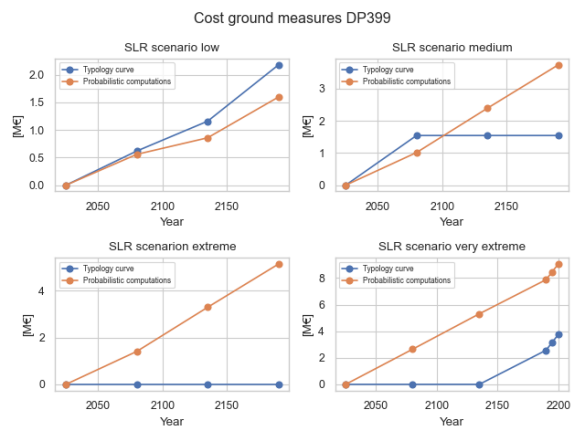
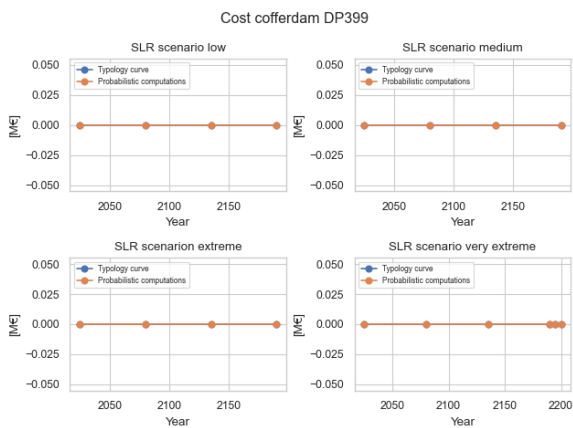
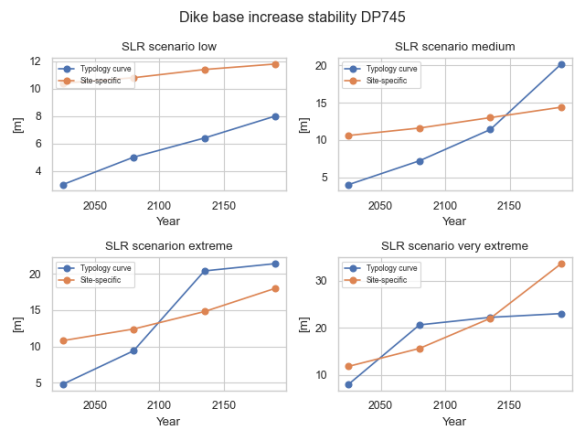
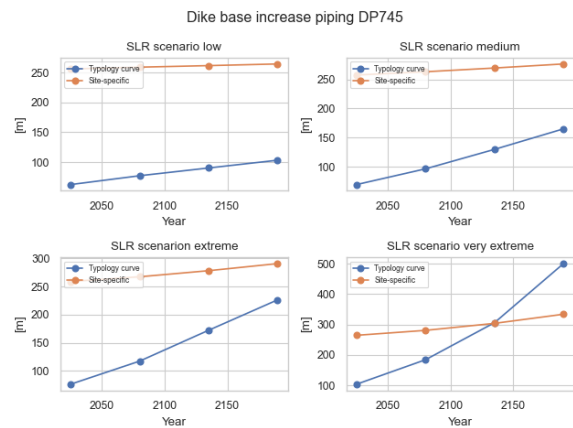
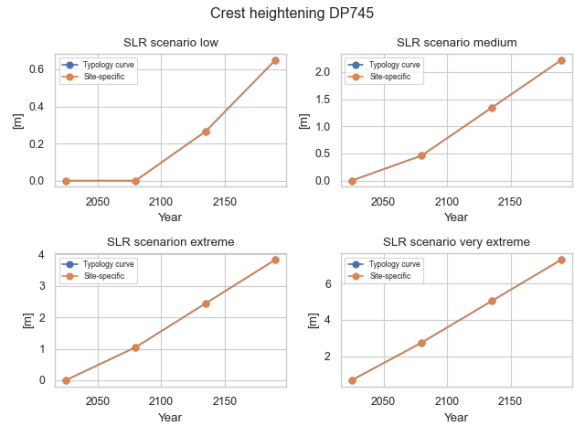
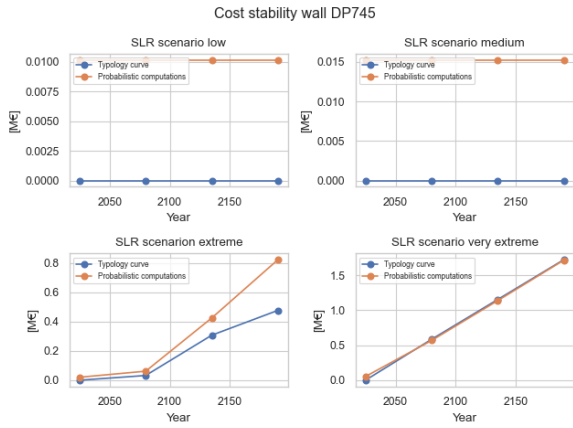


Factors determining cost with height requirement

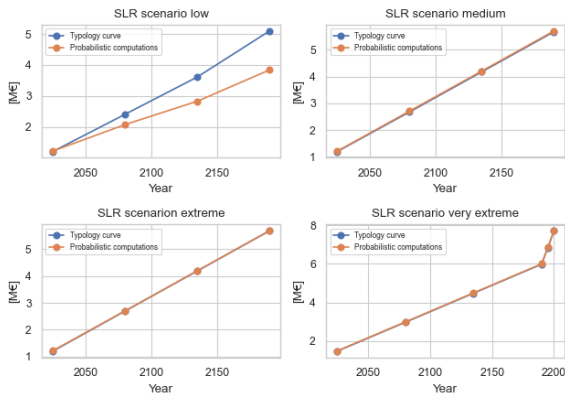
The following figures present the reinforcement cost under the four different sea level rise scenario and include the height requirement. For each scenario, the cost is presented for both fragility curve approaches.



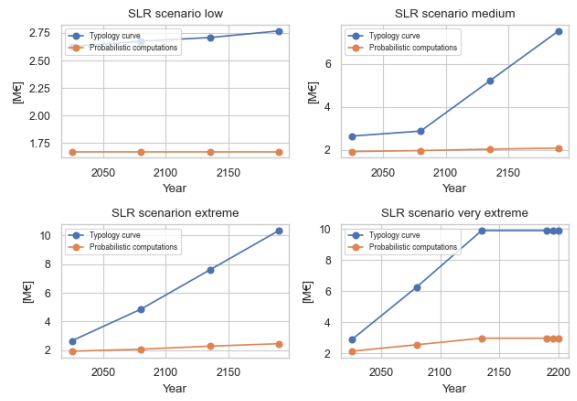




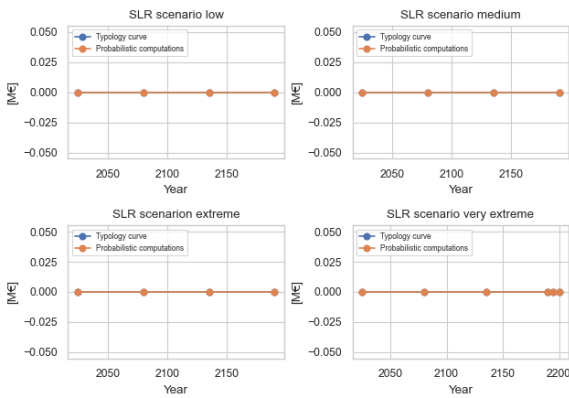
Cost infrastructure DP399



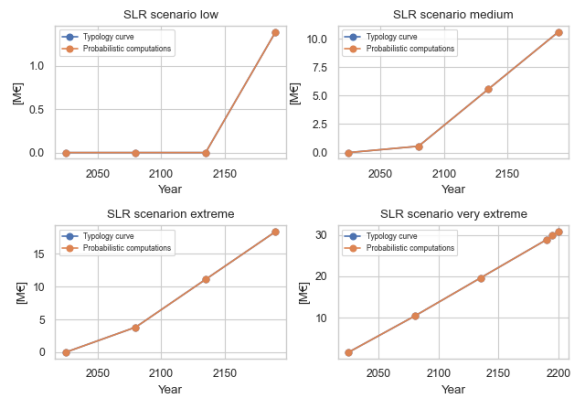
Cost innovative measures DP399



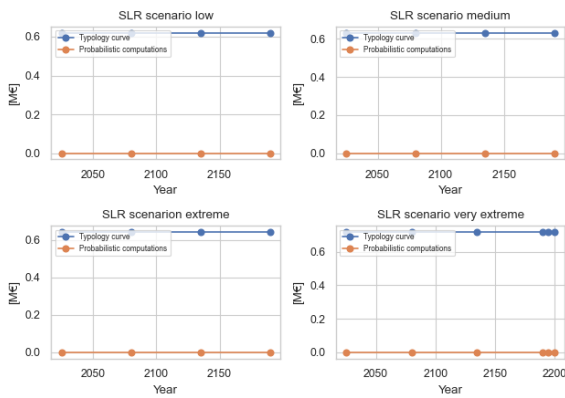
Cost piping measures DP399



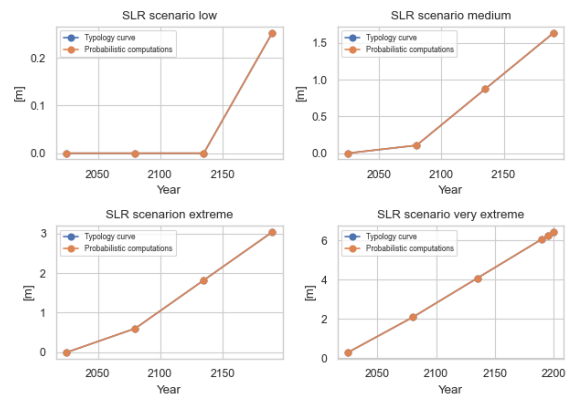
Cost revetment DP399



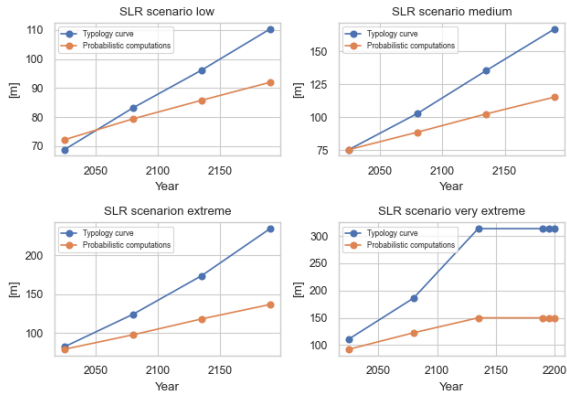
Cost stability wall DP399



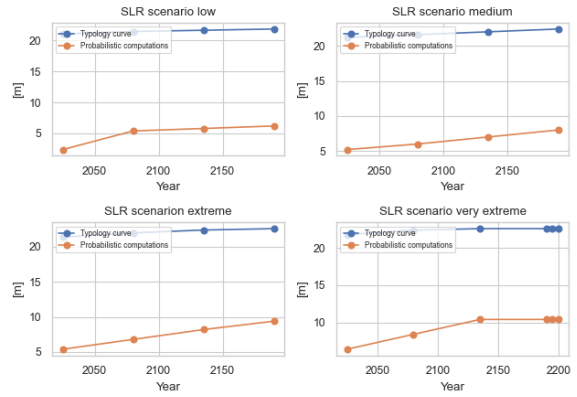
Crest heightening DP399



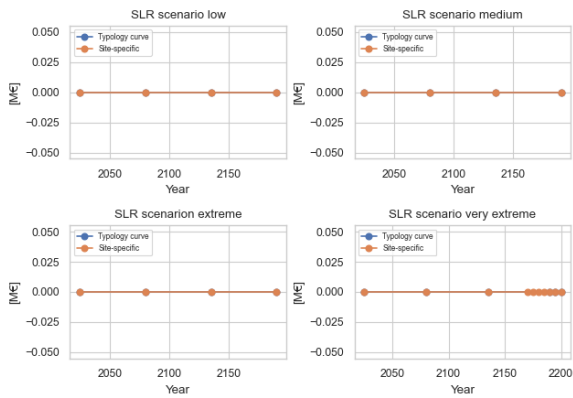
Dike base increase piping DP399



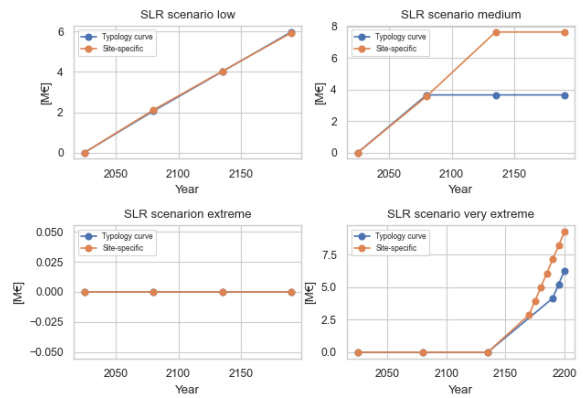
Dike base increase stability DP399



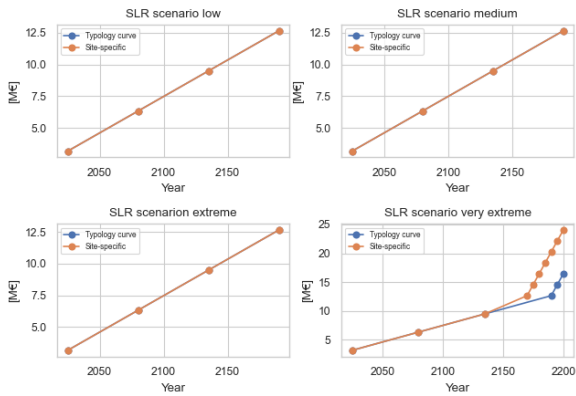
Cost cofferdam DP167



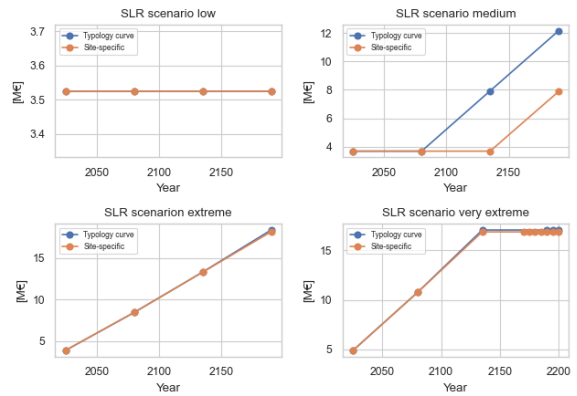
Cost ground measures DP167

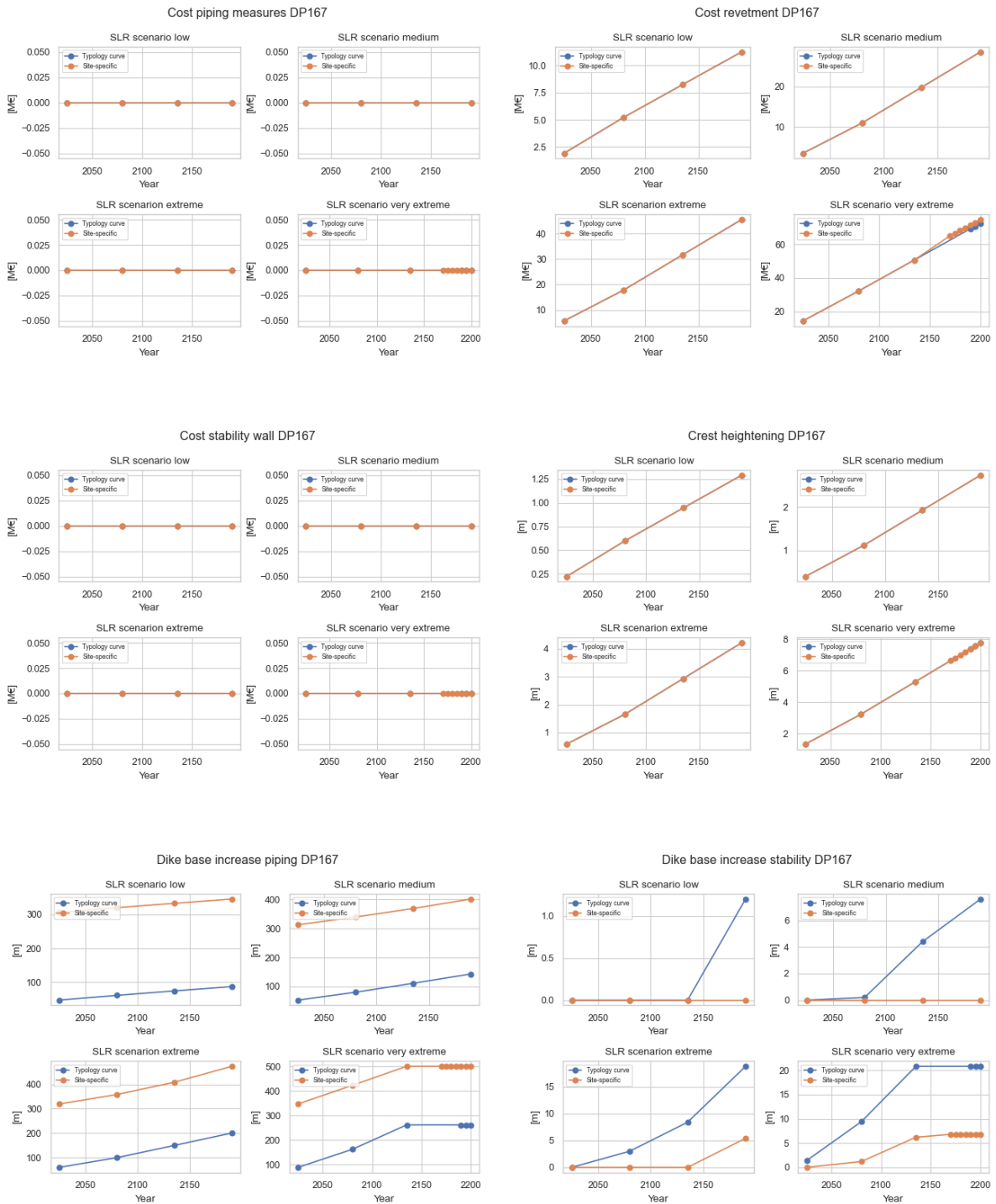


Cost infrastructure DP167



Cost innovative measures DP167

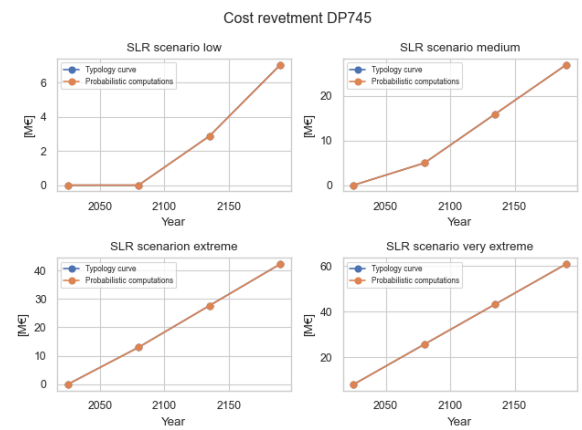
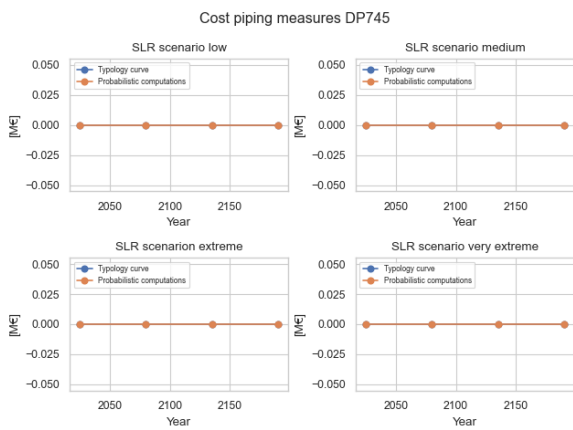
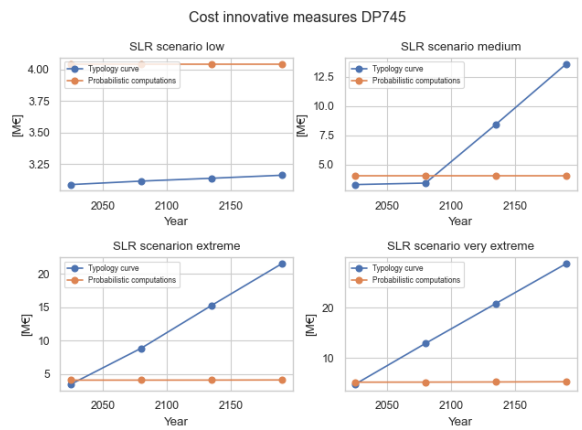
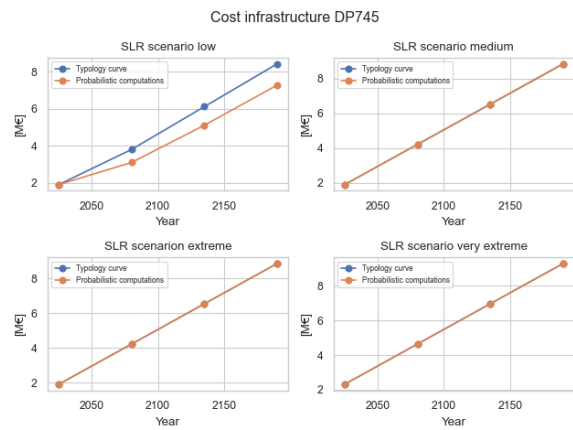
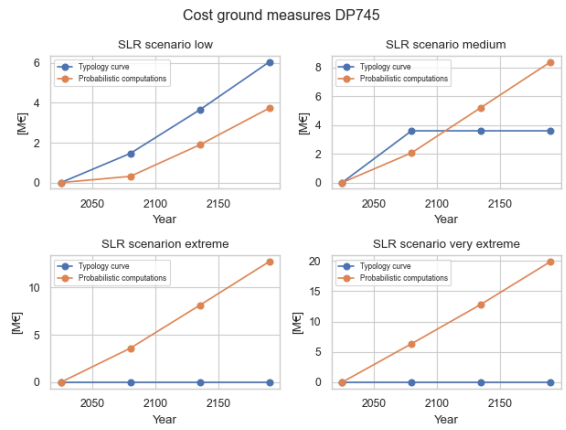
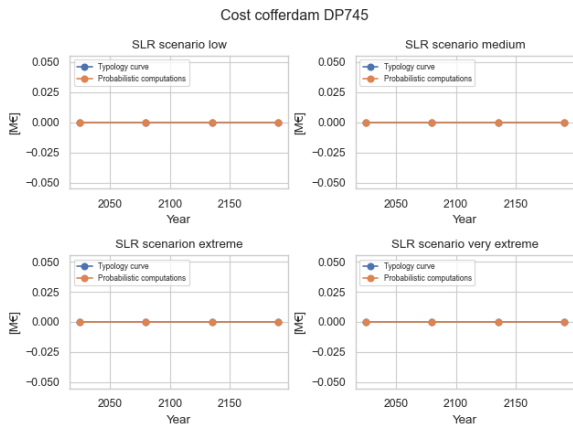


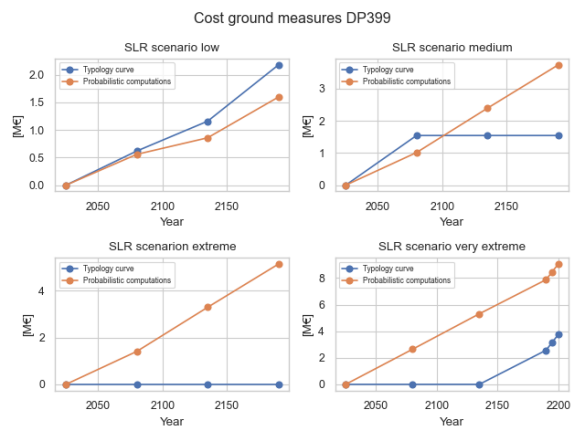
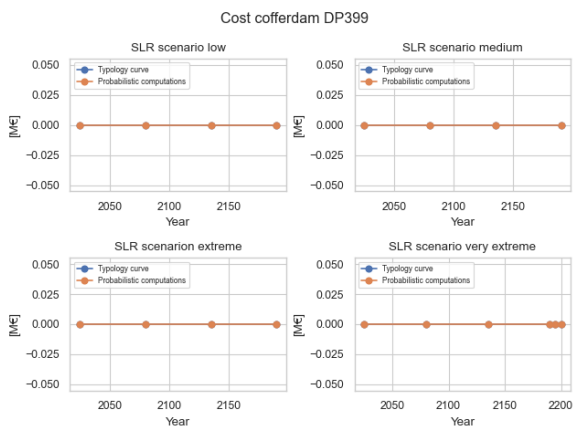
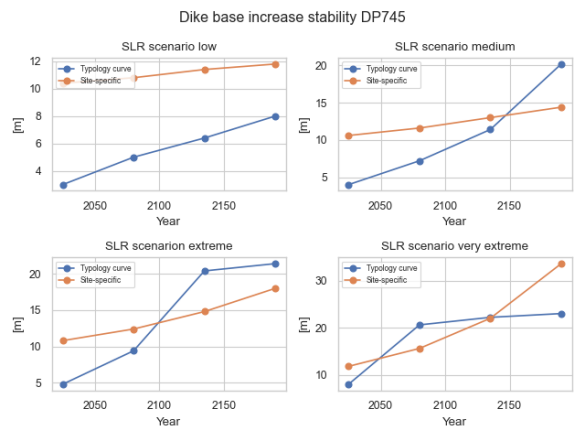
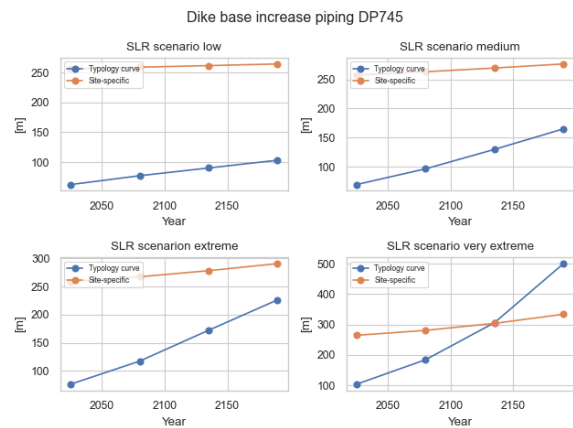
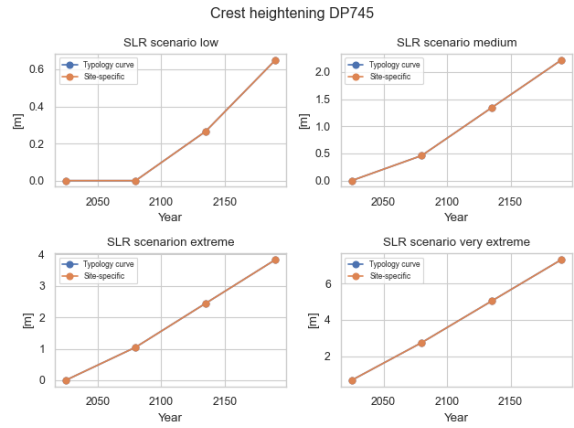
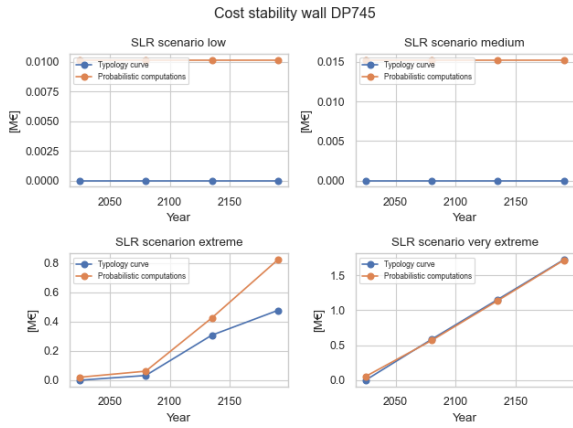


Cost using KP-ZSS increase in strength

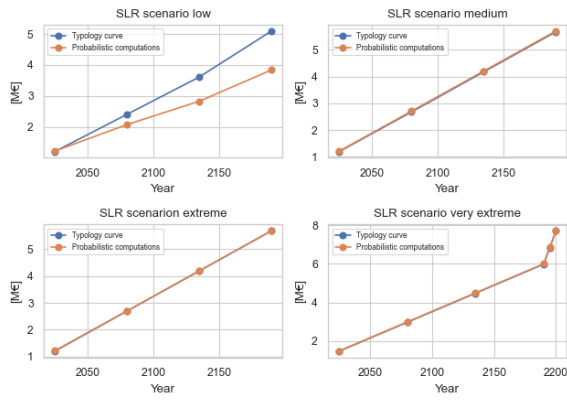
The following figures present the reinforcement cost under the four different sea level rise scenario but now using the increase in strength as determined by Kennisprogramma Zeespiegelstijging (KP-ZSS) and include the height requirement. In every figure OR stands for OKADER reinforcement, meaning the shift of the fragility curve due to a berm from KP-ZSS is used.



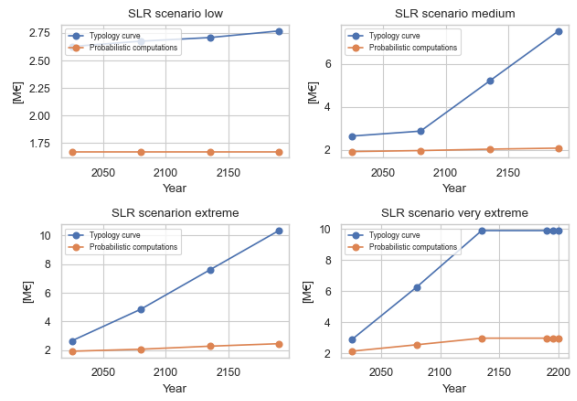




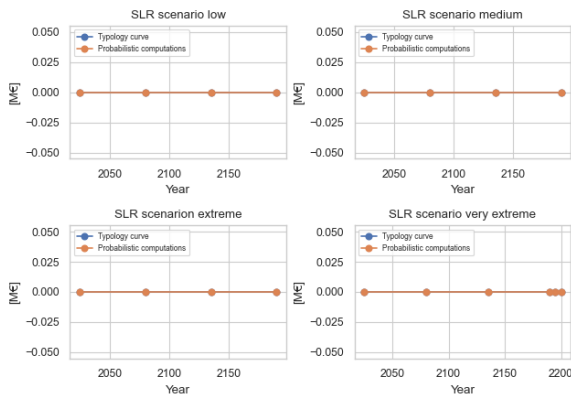
Cost infrastructure DP399



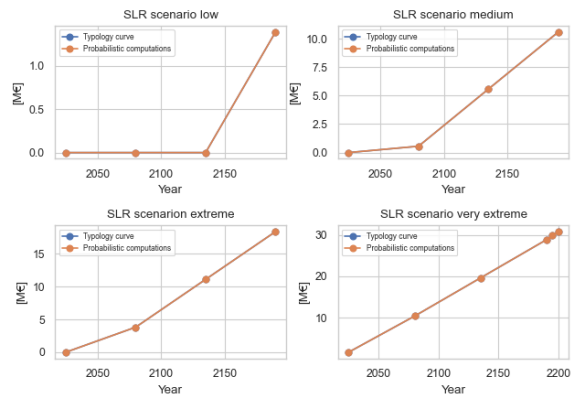
Cost innovative measures DP399



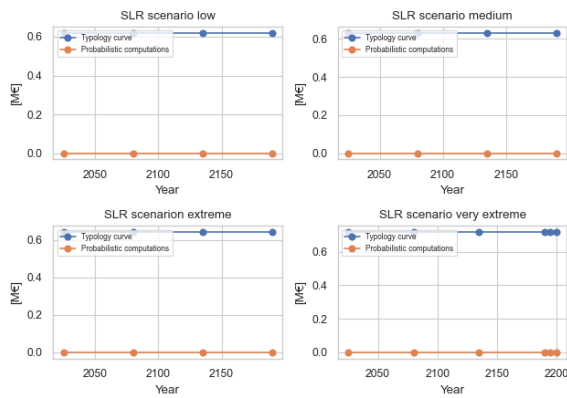
Cost piping measures DP399



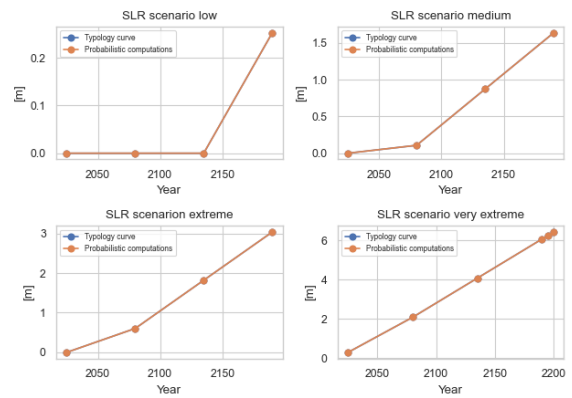
Cost revetment DP399



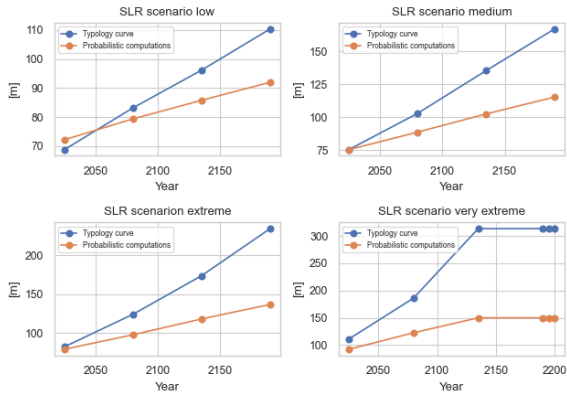
Cost stability wall DP399



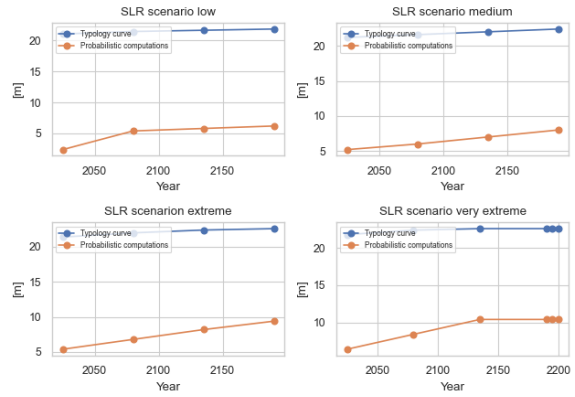
Crest heightening DP399



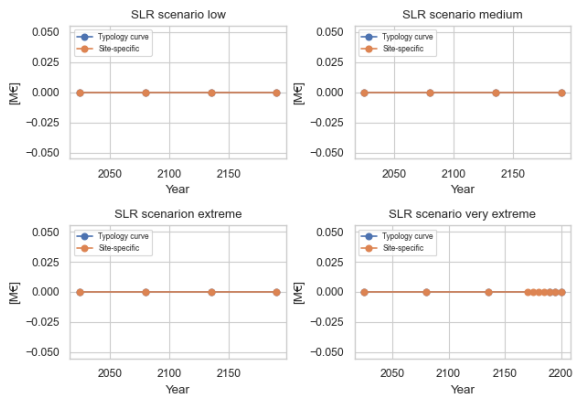
Dike base increase piping DP399



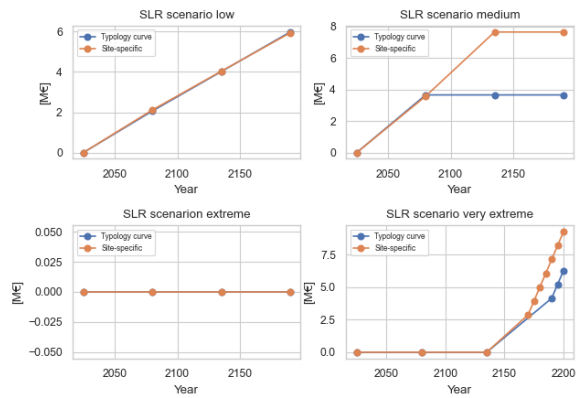
Dike base increase stability DP399



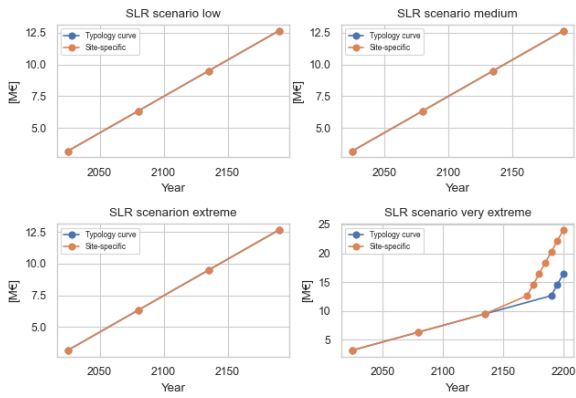
Cost cofferdam DP167



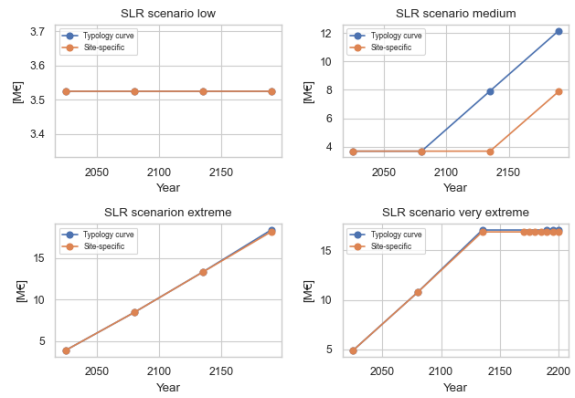
Cost ground measures DP167



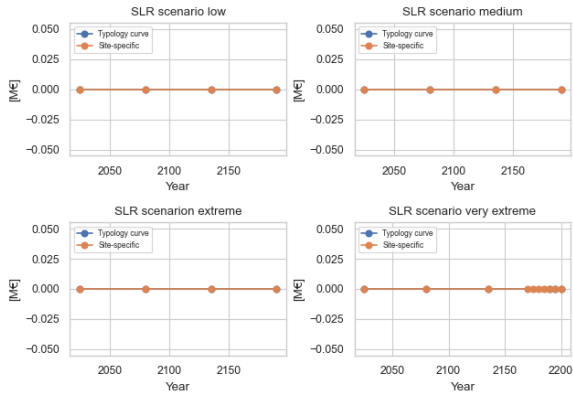
Cost infrastructure DP167



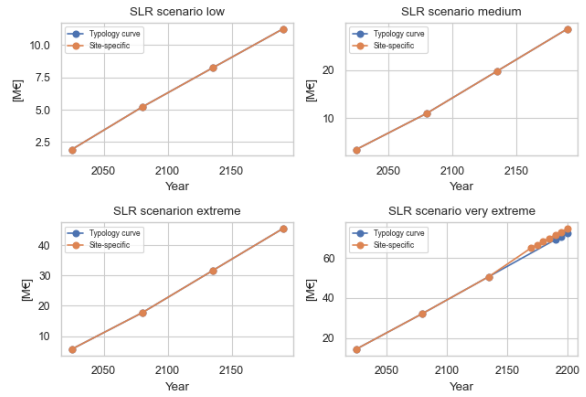
Cost innovative measures DP167



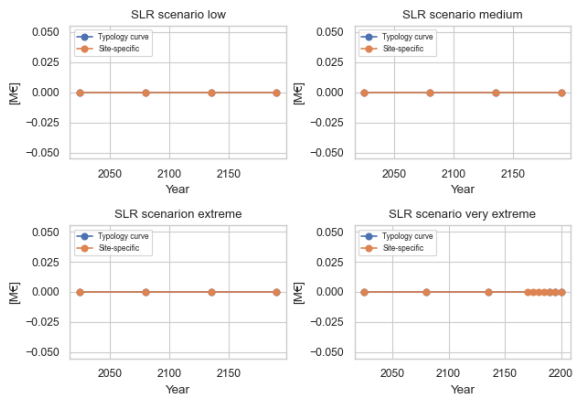
Cost piping measures DP167



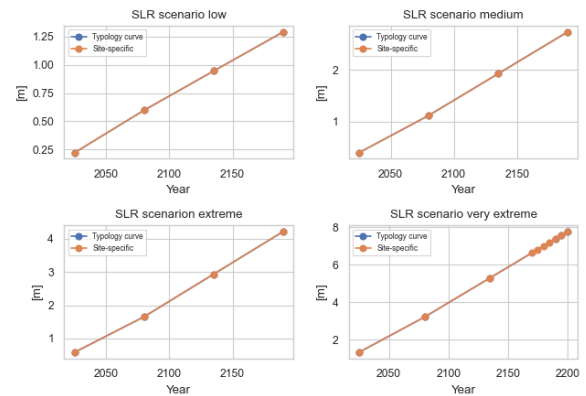
Cost revetment DP167



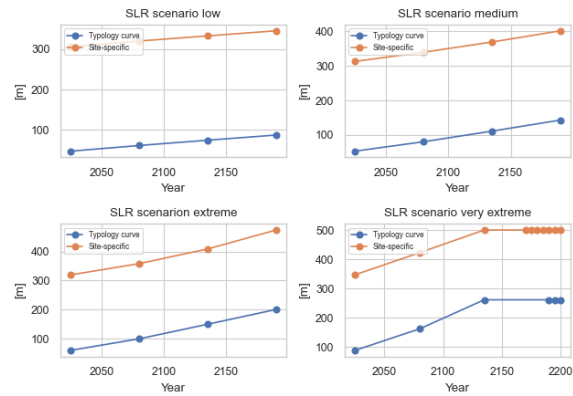
Cost stability wall DP167



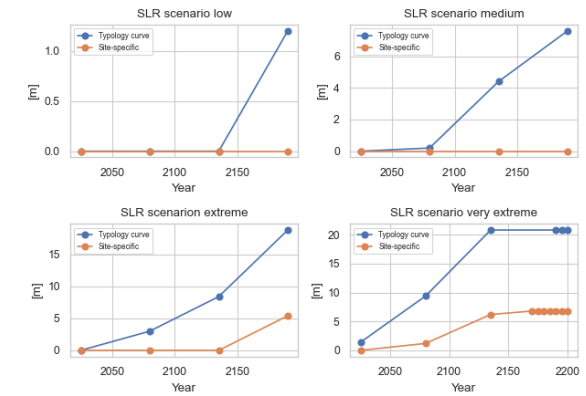
Crest heightening DP167



Dike base increase piping DP167



Dike base increase stability DP167



H.2. Discount rate

As discussed in Section 5.1.2, net present value is often used for economic decisions. To discount future costs, a discount rate is employed. The discount rate is a percentage used to convert expected future costs and benefits back to the base year of the project. The use of the discount rate is explained in section 5.2.

In the cost calculation, a discount rate of 1.6% is used to convert the costs to net present value. However, Rijkswaterstaat often advises using a standard discount rate of 2.25% (“Discontovoet”, 2023) for certain expenses. To gain insight into the effect of this choice, the costs have been recalculated using a discount rate of 2.25%.

The difference in the results is shown in Figure H.12. What stands out is that for section DP745, the costs are now higher for the probabilistic calculated fragility curve for the low and medium SLR scenarios. However, when looking at sections DP399 and DP167, there are minimal differences in cost between the two fragility curve methods. The mean of the difference in the two approaches is now 7.17% compared to the earlier reported 7.29% difference using the discount rate of 1.6%. This indicates that the choice of discount rate has little effect on the overall cost difference between these two approaches.

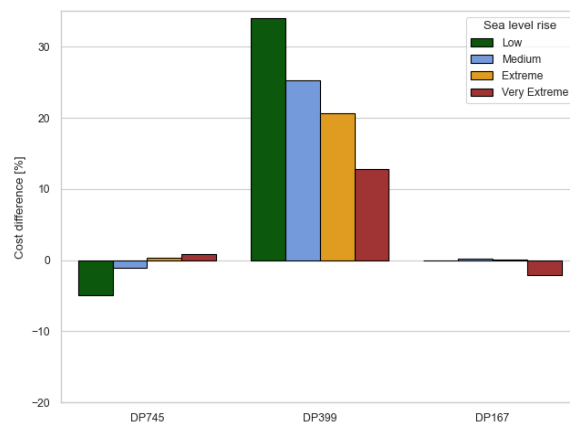


Figure H.12: Percentual cost difference for reinforcement between probabilistic calculated and typology-defined fragility curves in net present value with a discount rate of 2.25% for the year 2200

However, when examining the difference between the chosen discount rates, it is noticeable that they have a significant impact on the final reinforcement costs. This effect is depicted in Figure H.13. The calculated net present value with a discount rate of 2.25% is subtracted from the calculations with a discount rate of 1.6%. If the low SLR scenario is considered (the blue bars), the net present value decreases with 8% to 15% for both approaches. If the very extreme SLR scenario is regarded, the net present value decreases between 17.5% and 25% when the discount rate of 2.25% is applied.

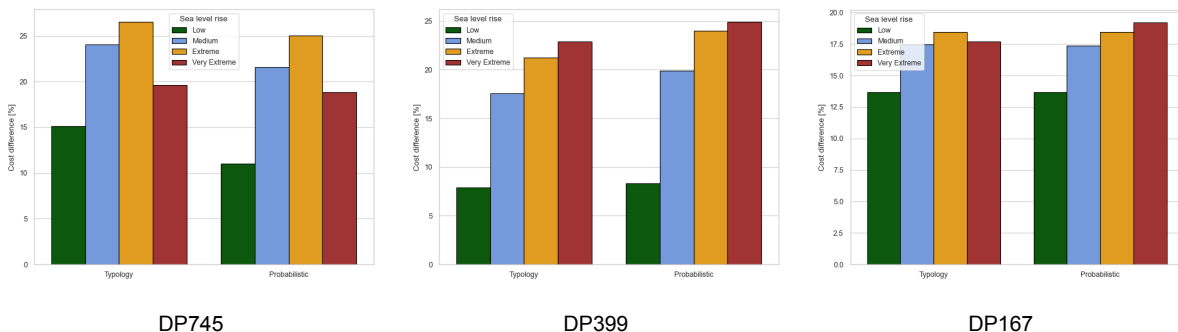


Figure H.13: Percentual difference net present value for a discount rate of 1.6% and 2.25%

If a different discount rate of 2.25% is applied, the difference between the fragility curve approaches



remains the same. But comparing both discount rates provides significantly different net present values. In the case of a low SLR scenario, the net present value decreases with 8% to 15% for both approaches. If the very extreme SLR scenario is regarded, the net present value decreases between 17.5% and 25%.

Initially, it was anticipated that the use of typology-defined fragility curves based on river dike sections would have a greater impact on the reinforcement cost. However, although the typology-defined fragility curves provide significantly different failure probabilities (both higher and lower compared to the site-specific computations), the resulting reinforcement cost does not differ that much. The results provide new insight into the driving cost factors for reinforcements under sea level rise, consisting of the revetment and SLR scenario. However, “Discontovoet” (2023) states the following: “Investments in public physical infrastructure often, but not always, involve fixed, sunk costs. Examples include the construction of roads, waterways, dikes, railway infrastructure, ports and locks, and the energy transmission and distribution infrastructure. The discount rate for these costs should be 1.6%”. Meaning the rate of 2.25% for further research is rejected.

H.3. Time step

Also, an analysis has been conducted on the influence of the chosen time step. As expected, a smaller time step leads to higher reinforcement costs, as more frequent visits are required for reinforcement. A comparison has been made for time steps of 1 year, 5 years, and 10 years. The results are displayed in Figure H.14 and Figure H.15.

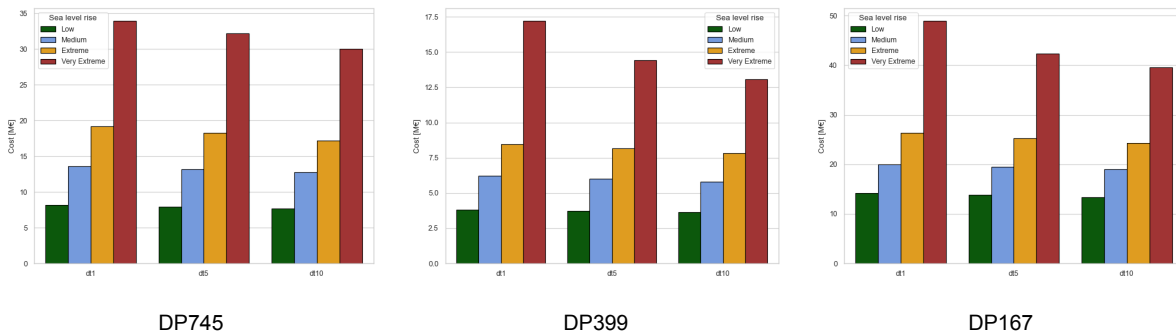


Figure H.14: Time step analysis site-specific fragility curves

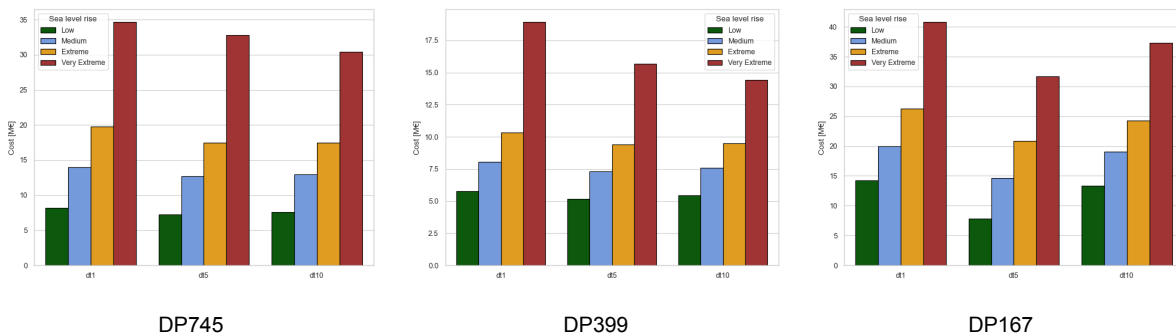


Figure H.15: Time step analysis typology-defined fragility curves